Peripheral alloantigen expression directs the organ specific T cell infiltration after hematopoietic cell transplantation

Die Expression von Alloantigenen im peripheren Gewebe beeinflusst die selektive Organinfiltration durch T Zellen nach hämatopoetischer Stammzelltransplantation

Doctoral thesis for a doctoral degree at the Graduate School of Life Sciences,
Julius-Maximilians-Universität Würzburg,
Experimentelle Stammzelltransplantation

submitted by
Christian Brede
from
Kassel, Germany

Würzburg, 2013

Submitted on: …………………………………………………………..……..

Members of the *Promotionskomitee*:

Chairperson: Prof. Dr. Ulrike Holzgrabe

Primary Supervisor: Dr. Andreas Beilhack

Supervisor (Second):   Prof. Dr. Thomas Hünig

Supervisor (Third):   Prof. Dr. Hermann Einsele

Supervisor (Fourth):   Prof. Dr. Robert Negrin

Date of Public Defence: …………………………………….…………

Date of Receipt of Certificates: …………………………………………

Für meine Familie

Table of Contents

List of Figures

List of Tables

Introductory statement on contributions and previous publication

This thesis was conducted in the research laboratory of Andreas Beilhack (Department of Medicine II, Würzburg University Hospital). Experimental procedures of this PhD project were performed by myself, with technical assistance from Ana-Laura Jordán-Garrote, Simone S. Riedel, Carina A. Bäuerlein, Carolin Kiesel, Katharina Mattenheimer, Miriam Ritz and Viktoria von Krosigk and Andreas Beilhack (all from Beilhack group). Gregory Harms, Mike Friedrich and Katrin G. Heinze (all from Rudolf Virchow Center, Research Center for Experimental Biomedicine, Würzburg) constructed the LSFM and helped performing LSFM, MPM and confocal imaging. Tobias Bopp (Institute for Immunology, University Medical Center, Mainz), Christian Linden (Institute for Virology and Immunobiology, University of Würzburg) and myself performed FACS-Sorting. Stephan Schulz (Institute of Pathology, Charité Berlin), Marina Grether (Institute of Pathology, Munich University Hospital), Anja Mottok and Andreas Rosenwald (both from Institute of Pathology, Würzburg University) performed histopathological grading, assisted for immunofluorescence and conventional microscopy, and contributed human samples. Parts of this thesis were originally published in "The Journal of Clinical Investigation".

Authors: Christian Brede, Mike Friedrich, Ana-Laura Jordán-Garrote, Simone S. Riedel, Carina A. Bäuerlein, Katrin G. Heinze, Tobias Bopp, Stephan Schulz, Anja Mottok, Carolin Kiesel, Katharina Mattenheimer, Miriam Ritz, Viktoria von Krosigk, Andreas Rosenwald, Hermann Einsele, Robert S. Negrin, Gregory S. Harms and Andreas Beilhack (2012). Title: Mapping immune processes in intact organs at cellular resolution. The Journal of Clinical Investigation 122 (12), 4439-4446. doi:10.1172/JCI65100. Copyright © 2013 American Society for Clinical Investigation. Reuse permission license ID 3067551118730.

Abstract

In acute graft-versus-host disease (GVHD) alloreactive donor T cells selectively damage skin, liver, and the gastrointestinal tract while other organs are rarely affected. The mechanism of this selective target tissue infiltration is not well understood. We investigated the importance of alloantigen expression for the selective organ manifestation by examining spatiotemporal changes of cellular and molecular events after allogeneic hematopoietic cell transplantation (allo-HCT).

To accomplish this we established a novel multicolor light sheet fluorescence microscopy (LSFM) approach for deciphering immune processes in large tissue specimens on a single-cell level in 3 dimensions. We combined and optimized protocols for antibody penetration, tissue clearing, and triple-color illumination to create a method for analyzing intact mouse and human tissues. This approach allowed us to successfully quantify changes in expression patterns of mucosal vascular addressin cell adhesion molecule–1 (MAdCAM-1) and T cell responses in Peyer's patches following allo-HCT. In addition, we proofed that LSFM is suitable to map individual T cell subsets after HCT and detected rare cellular events. We employed this versatile technique to study the role of alloantigen expression for the selective organ manifestation after allo-HCT. Therefore, we used a T cell receptor (TCR) transgenic mouse model of GVHD that targets a single peptide antigen and thereby mimics a major histocompatibility complex (MHC)-matched single antigen mismatched (miHAg-mismatched) HCT. We transplanted TCR transgenic (OT-I) T cells into myeloablatively conditioned hosts that either express the peptide antigen ovalbumin ubiquitously (βa-Ova) or selectively in the pancreas (RIP-mOva), an organ that is normally not affected by acute GVHD. Of note, at day+6 after HCT we observed that OT-I T cell infiltration occurred in an alloantigen dependent manner. In βa-Ova recipients, where antigen was ubiquitously expressed, OT-I T cells infiltrated all organs and were not restricted to gastrointestinal tract, liver, and skin. In RIP-mOva recipients, where cognate antigen was only expressed in the pancreas, OT-I T cells selectively infiltrated this organ that is usually spared in acute GVHD. In conditioned RIP-mOva the transfer of 100 OT-I T cells sufficed to effectively infiltrate and destroy pancreatic islets resulting in 100% mortality. By employing intact tissue LSFM in RIP-mOva recipients, we identified very low numbers of initial islet infiltrating T cells on day+4 after HCT followed by a massive T cell migration to the pancreas within the following 24 hours. This suggested an effective mechanism of effector T cell recruitment to the tissue of alloantigen expression after initial antigen specific T cell encounter. In chimeras that either expressed the model antigen ovalbumin selectively in hematopoietic or in parenchymal cells only, transplanted

OT-I T cells infiltrated target tissues irrespective of which compartment expressed the alloantigen. As IFN-γ could be detected in the serum of transplanted ovalbumin expressing recipients (βa-Ova, βa-Ova-chimeras and RIP-mOva) at day+6 after HCT, we hypothesized that this cytokine may be functionally involved in antigen specific OT-I T cell mediated pathology. *In vitro* activated OT-I T cells responded with the production of IFN-γ upon antigen re-encounter suggesting that IFN-γ might be relevant in the alloantigen dependent organ infiltration of antigen specific CD8$^+$ T cell infiltration after HCT. Based on these data we propose that alloantigen expression plays an important role in organ specific T cell infiltration during acute GVHD and that initial alloreactive T cells recognizing the cognate antigen propagate a vicious cycle of enhanced T cell recruitment that subsequently culminates in the exacerbation of tissue restricted GVHD.

Zusammenfassung

In der akuten Graft-Versus-Host Disease (GVHD) infiltrieren allogene Spender T Zellen Haut, Leber und den Magen-Darm-Trakt des Empfängers und attackieren das Gewebe. Andere Organe sind dagegen interessanterweise nur selten betroffen. Die Mechanismen dieser selektiven Organinfliltration sind bisher weitestgehend unbekannt. In meiner Dissertationsarbeit untersuchte ich den Einfluss der Alloantigenexpression auf die selektive Organmanifestation während der GVHD.

Um komplexe Immunprozesse die nach allogener Stammzelltransplantation auftreten, besser zu verstehen, entwickelten wir eine Lichtblattmikroskopietechnik (LSFM) die zelluläre und molekulare Veränderungen im intakten Gewebe detektieren kann. Wir etablierten eine neuartigen mehrfarben LSFM-Methodik, die es ermöglicht, Immunprozesse in großen Gewebsstücken von Maus und Mensch in Einzelzellauflösung dreidimensional darzustellen. Dazu kombinierten und optimierten wir Protokolle, um eine Penetration von Antikörpern tief in das Gewebe sowie die Aufklärung und die dreifache Beleuchtung des Gewebes zu ermöglichen. Diese Methode erlaubte uns die erfolgreiche Quantifizierung der Proteinexpression des Adressins mucosal vascular addressin cell adhesion molecule–1 (MAdCAM-1) als auch die Quantifizierung der T Zell Antwort im intakten Peyer's Plaque nach allogener hämatopoetischer Transplantation (HCT). Weiterhin konnten wir die Methode zur Untersuchung der Migration unterschiedlicher T Zell-Subpopulationen nach HCT erfolgreich einsetzen und konnten einzelne, organinfiltrierende Zellen detektierten und quantifizieren. Wir benutzten die LSFM Methode um den Einfluss der Alloantigenexpression auf die selektive Organmanifestation zu studieren. Dazu verwendeten wir ein Transplantationsmodell, in dem der Haupthistokompatibilitätskomplex übereinstimmt (MHC-matched) und eine Diskrepanz nur in einem einzelnen Peptid Antigen (miHAG-mismatch) zwischen Spender und Empfänger bestand. Wir transplantierten T Zell Rezeptor (TCR) transgene (OT-I) T Zellen in myeloablativ bestrahlte Empfänger, die das Peptidantigen Ovalbumin entweder in allen Geweben (βa-Ova) oder selektiv in der Bauchspeicheldrüse (RIP-mOva) exprimieren. Die Bauchspeicheldrüse ist ein Organ, das normalerweise nicht von der akuten GVHD betroffen ist. An Tag 6 nach allogener HCT waren alle Organe die das Alloantigen exprimieren auch von Spender T Zellen infiltriert. In myeloablativ bestrahlten RIP-mOva Empfängern reichten bereits 100 transferierte OT-I T Zellen aus, um Alloantigen-exprimierende pankreatische Inselzellen zu zerstören. Dies führte zu einer Mortalität von 100% der Empfänger und spricht für eine sehr effiziente Alloantigendetektion und Gewebsinfiltration durch die Spender T Zellen. Um die Kinetik der Organinfiltration der Spender T Zellen detailliert zu untersuchen, verwendeten wir die neue

Lichtblattmikroskopietechnik, welche die Analyse intakter Organe ermöglicht. In RIP-mOva Empfängern identifizierten wir erste wenige Spender T Zellen im Pankreas an Tag 4 nach Transplantation, gefolgt von einer massiven Pankreasinfiltration durch Spender T Zellen innerhalb von 24 Stunden. Dies deutet auf eine gezielte Rekrutierung der Spender T Zellen nach erstem Antigenkontakt in das Gewebe mit Alloantigenexpression. Um zu untersuchen, ob die Alloantigenexpression vom parenchymalen Gewebe oder aber durch hämatopoetische Zellen zur spezifischen Organinfiltration führt, transplantierten wir OT-I T Zellen in chimäre Empfänger, in denen das Alloantigen entweder nur im Gewebsparenchym oder ausschließlich von hämatopoetischen Zellen exprimiert wird. An Tag 6 nach der allogenen HCT fanden wir Spender T Zellen in allen Geweben, unabhängig davon welches Empfängerzellkompartment das Alloantigen präsentierte. Wir detektierten hohe IFN-γ-Werte im Serum von Ovalbumin exprimierenden Empfänger (βa-Ova, βa- Ova-Chimären und RIP-mOva). Weiterhin fanden wir, dass nach erneutem Kontakt mit dem spezifischen Alloantigen, OT-I T Zellen die *in vitro* aktiviert wurden, IFN-γ produzierten. Wir schließen aus diesen Beobachtungen, dass für die antigenabhängige Gewebeinfiltration IFN-γ wichtig ist. Zusammenfassend postulieren wir, dass die Alloantigenexpression im Gewebe eine wichtige Rolle in der organspezifischen Infiltration durch Spender T Zellen spielt, und dass T Zellen die Alloantigen spezifisch erkennen, dafür verantwortlich sind, dass weitere Effektor-T Zellen in das Gewebe rekrutiert werden.

1 Introduction

1.1 Selective organ manifestation in Graft-versus-Host Disease

1.1.1 Hematopoietic cell transplantation and complications in the clinic

Hematopoietic cell transplantation (HCT) is a potentially curative therapy that is used for numerous hematological and lymphoid cancers as well as for inherited disorders of blood cells. Based on the source of the donated stem cells, the graft is categorized as autologous (from the same patient) or as allogeneic (from a foreign donor). In an allogeneic HCT (allo-HCT), donor T cells are critical for reconstituting T cell immunity in the host and mediate an antitumor effect called graft-versus-leukemia (GVL). The source of graft that is used normally depends on the availability and on the indication. The degree of human leukocyte antigen (HLA, human) match between the donor and the recipient is an important factor to assess the risk of acute Graft-versus-Host Disease (GVHD). GVHD is a life-threatening complication that generally occurs after allo-HCT and is a reaction of donor immune cells against host tissues. The syndrome is mediated by donor T cells that recognize the recipient as 'non-self' and attack host tissues by employing a wide range of immune mechanisms. Mainly three tissues are affected by acute GVHD: skin, liver, and the gastrointestinal tract. Bone marrow transplantation usually requires a preparatory conditioning regimen of the recipient, either by immunosuppressive medications, irradiation or a combination of both, to suppress immune reactions and prevent the rejection of the graft. The immunosuppressed patient is highly susceptible to viral, fungal and bacterial infections up to several months after HCT until the complete engraftment of the transplanted cells. Hence, besides acute GVHD as the major complication following HCT (Ferrara and Reddy, 2006) infections and leukemia relapse are further sources of morbidity and mortality following HCT, limiting the treatment of a broader spectrum of diseases.

About 60,000 patients are treated with hematopoietic stem cells per year worldwide (Gyurkocza et al., 2010) and the number of treatments are increasing. The incidence of acute GVHD in patients who receive allogeneic donor cells without previous depletion of T cells range from 10% to 80%, dependent on the risk factors and prophylaxis (Sullivan, 2004). The risk of acute GVHD can be significantly reduced by T cell depletion of the graft, but this generally results in an increased relapse risk, higher infectious morbidity and a reduced GVL effect. Because of this, it is attempted to balance the risk by giving sufficient immune

suppression to prevent most severe acute GVHD whilst preserving the positive effects of GVL and immune reconstitution.

1.1.2   Target antigen recognition

The pathogenesis of acute GVHD is currently understood to occur in three sequential phases (Ferrara et al., 1999): In the first phase, the antigen-presenting cells (APCs) are activated due to the conditioning regimen that also leads to damage of host tissues. In the second phase activation and proliferation of donor T cells takes place. Upon interaction with host APCs donor T cells that have recognized an alloantigen become activated, and differentiate into effector cells. The third phase is the effector phase of GVHD. Activated effector T cells are recruited to peripheral tissues such as the skin and gut (Beilhack et al., 2005) where they cause profound tissue damage that characterizes GVHD. The cause of the selective GVHD organ manifestation still remains elusive. However, understanding the tissue-specific infiltration of GVHD target organs appears of fundamental importance as the anatomical separation of GVHD and the desired anti tumor effect poses an attractive mechanism to discern GVHD from graft-versus-tumor responses that could be exploited therapeutically.

Secondary lymphoid organs (SLOs), such as spleen, lymph nodes or Peyer's patches (Figure 1.1), enable interactions between activated APCs and antigen-specific T cells that, upon contact, get activated proliferate and differentiate into effector T cells that migrate to the selective target tissues. Hence, SLOs were demonstrated to be essential for the priming of alloreactive T cells, but the lack of certain priming sites resulted neither in reduced, nor in delayed acute GVHD (Beilhack et al., 2008). For example previous studies have been demonstrated the importance of Peyer's patches in the induction of GVHD because recipients lacking these lymphoid organs did not develop acute GVHD under certain experimental conditions (Murai et al., 2003). However, by using a myeloablative conditioning mouse model, T-cell activation and proliferation was shown to occur in several SLOs including Peyer's patches and that animals that lacked Peyer's patches still developed acute GVHD (Welniak et al., 2006; Beilhack et al., 2008).

Another fundamental aspect in GVHD is the identity of the target antigen that is recognized by the T cells after HCT. In MHC-matched transplantations, T cells can recognize minor histocompatibility antigens (miHAgs), which are the distinct peptide products of polymorphic genes that are present in the recipient but not in the donor (Figure 1.2A). For the recognition of MHC-bound miHAgs the T cell receptor (TCR) has to be in contact with both the peptide
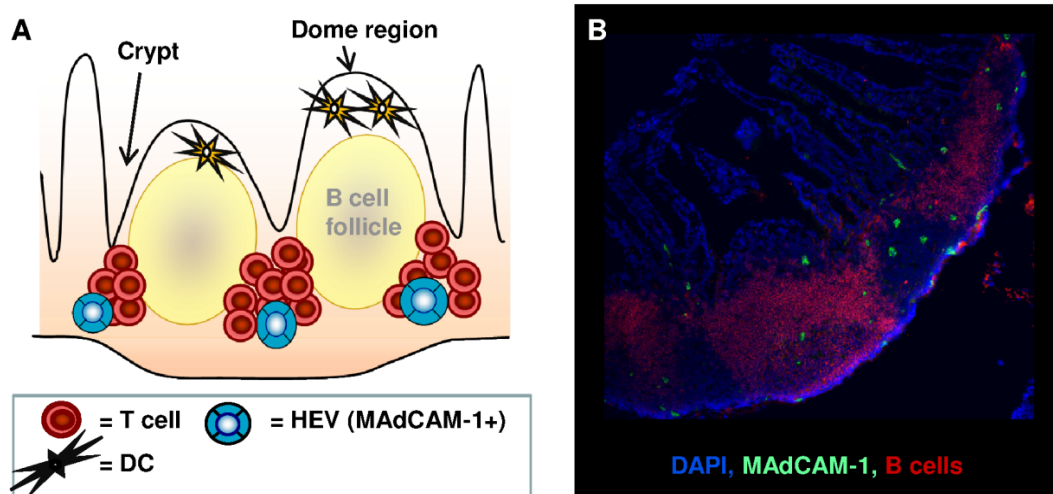
Figure 1.1: Peyer's patches (PPs) are important sites of adaptive immune responses. PPs are aggregations of lymphoid tissue located in the small bowel. (A) Scheme illustrates important structures and organization of a PP. The follicular areas mainly consist of B-lymphocytes, follicular dendritic cells and macrophages and the interfollicular structures are populated by T cells, macrophages and dendritic cells. PPs are connected to the body via lymphatic vessels and endothelial venules. Naïve lymphocytes immigrate into the PP via specialized high endothelial venules that express MAdCAM-1. (B) Immunufluorescence microscopy of a PP from an untreated wt mouse. Nuclei, stained with DAPI, MAdCAM-1 (green) B cells (red). PPs are the interface between bacterial environment and immune response having a pivotal role in alloresponse and inflammation.

and the MHC molecule. In MHC-mismatched transplantations the TCR primarily recognizes intact epitopes on MHC molecules as foreign (Figure 1.2B). The precursor frequency of T cells that can recognize a mismatched MHC molecule in an allo-HCT is very high (Shlomchik, 2007).
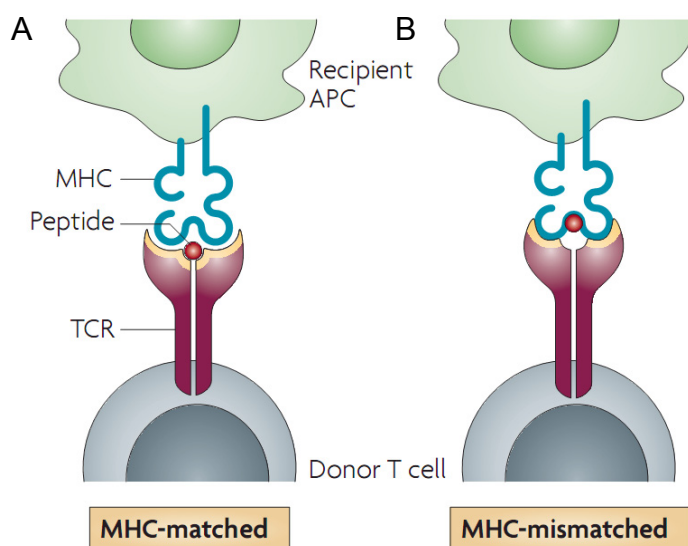
Figure 1.2: Antigen recognition by donor T-cells after allo-HCT. A) In MHC-matched minor histocompatibility antigens (miHAgs) mismatched transplants, T-cell receptors (TCRs) of donor T cells can recognize foreign peptides presented by allogeneic MHC molecules. This TCR-peptide recognition resembles the recognition of pathogen-derived antigens. B) In MHC-mismatched transplants, the TCR of the donor T cell bind the allogeneic MHC molecule, independent of the loaded peptide. Sketch taken from (Shlomchik, 2007).

13

1.1.3   CD4 versus CD8 T cell mediated immune responses

The T cell co-receptors CD4 and CD8 bind the constant regions of the major histocompatibility complex (MHC) class II and class I molecules, respectively (Csencsits and Bishop, 2003). Foreign peptides presented by MHC class I stimulate CD8^{+} T cells, while CD4^{+} T cells recognize peptides presented by MHC class II. CD4^{+} T helper cells are well known for their importance in providing critical signals during priming of cytotoxic T cell (CTL) responses *in vivo*. T cell help is required for the generation of primary CTL responses as well as in promoting memory CD8^{+} T cell development (Williams and Bevan, 2007). Generally CD4^{+} T cells provide help for CD8^{+} CTL expansion and development via IL-2 production or enhancing the stimulatory capacity of APC to CD8^{+} CTLs by CD40L-CD40 interactions. The route of antigen delivery (Bour et al., 1998), the avidity of the TCR-antigen binding (Heath et al., 1993) and the frequency of the CD8^{+} effector cells (Wang et al., 2001) may influence an CD4 helper independent development of CD8 responses.

In a model of viral infections, the generation of primary CD8^{+} T cell responses to herpes simplex virus (HSV) required help from CD4^{+} T cell (Jennings et al., 1991), whereas primary CTL responses to acute infection with Listeria monocytogenes and lymphocytic choriomeningitis virus can occur in the absence of CD4^{+} T cells. Recently, it was shown that CD4^{+} T cell help was not only necessary for effector CTL stimulation, but also provided the necessary cue for an effective CD8^{+} T cell migration to HSV infected tissue (Nakanishi et al., 2009).

In models of immune-mediated disease, CD4-independent CD8^{+} T cell responses have been reported to be common, like in autoimmune diabetes (Graser et al., 2000), tumor rejection (Yamazaki et al., 1999) or xenograft rejection (YI et al., 2000). In GVHD, the roles of individual CD4^{+} and CD8^{+} T cells have been intensively studied by employing various mouse models (Reviewed in Reddy and Ferrara, 2009; Schroeder and DiPersio, 2011). In MHC mismatched HCT both, CD4^{+} or CD8^{+} T cells are capable to induce GVHD. Allogeneic CD4^{+} T cells precede the increase of donor CD8^{+} T cells in lymphoid organs during GVHD initiation and also appeared earlier in the small intestines after HCT followed by infiltrating cytotoxic T cells (Beilhack et al., 2005). Also in miHAg-mismatched mouse models, either CD8^{+} T cells, CD4^{+} T cells, or both can contribute to GVHD dependent on the strain combination of donor and recipient (examples listed in: Reddy and Ferrara, 2009; Schroeder and DiPersio, 2011). CD8^{+} T cells induce GVHD primarily by cytolytic activity, which requires the engagement of the T cell receptor (TCR) with the MHC on target tissue (Reddy et al., 2009). Proliferating CD4^{+} T cells may differentiate into type 1, type 2 or type 17 helper cells (Th1, Th2 or Th17). Th1 cells produce cytokines, such as IFN-γ, TNF-α and IL-2 that have been implicated in the pathophysiology of acute GVHD (Ferrara and Krenger, 1998; Reddy and Ferrara, 2003). Th2

cells can migrate to the lung, where they secrete IL-4 and IL-13 causing inflammation on lung epithelium (Coghill et al., 2011). Th17 T cells have been demonstrated to contribute to acute GVHD by augmenting Th1 cell differentiation (Yi et al., 2008; Zhao et al., 2011).

Finally, different CD4+ and CD8+ T cell subsets, such as naive, effector memory, central memory and regulatory T (Treg) cells either separately or together have been shown to influence the outcome after HCT dramatically (reviewed in Leventhal et al., 2012).

1.1.4   Direct and cross-presentation of alloantigens in GVHD

In GVHD, antigen presenting cells (APCs) take up antigen in peripheral tissues, migrate to the draining lymph nodes (LNs), and present the tissue-derived MHC-peptide complexes to T lymphocytes. Dendritic cells (DCs) can take up antigen using different mechanisms and are very well equipped to form class II and class I peptide-MHC complexes. The presentation of peptide-MHC class II complexes to CD4+ T cells is called direct presentation and can be mediated by all APCs, including DCs, macrophages, and B cells (Banchereau et al., 2000). In contrast, CD8+ T cells recognize peptides associated with MHC class I molecules, which are expressed on the surface of all cells. The peptides presented on MHC class I molecules of most cells are normally derived from endogenous proteins. Exclusively DCs have the ability to load peptides derived from exogenous antigens onto MHC class I molecules (Guermonprez et al., 2003). This mechanism is called cross-presentation and can lead to the initiation of an immunogenic CD8+ cell response. Cross-priming is an important mechanism to activate cytotoxic T lymphocytes (CTLs) for immune defense against viruses that do not infect APCs and tumors. Furthermore cross-priming is involved in immune-mediated diseases such as type 1 diabetes. CTLs are the main effector cells of type 1 diabetes in humans. In transgenic mouse models of diabetes cross-priming is necessary and sufficient for an efficient islet infiltration and destruction (Carbone et al., 1998).

The role of cross-presentation and –priming after allo-HCT has been investigated in miHAg mismatched CD8+ T cell-dependent models of GVHD, with different outcomes. The study of Shlomshik et al. (1999) demonstrated the requirement of host APCs expressing MHC class I to initiate GVHD, suggesting cross-priming via donor APCs is not sufficient for GVHD induction. In contrast, it could be shown that cross-priming of MHC-I-presented miHAgs can significantly contribute to GVHD (Wang et al., 2011). In this study non-hematopoietic and hematopoietic antigens were cross-presented and targeted by alloreactive CD8+ T cells. Exclusively donor CD11c+ DCs were found to cross-prime CD8+ T cells. However, in most mouse models progenitors of donor APCs are transferred with the graft and have to develop from hematopoietic stem cells, too late to contribute to the initiation of GVHD. Nevertheless,

when host APCs are largely replaced by donor-derived cells they may drive further tissue injury by cross-presentation of host antigens. Thus, in experiments in which donor APCs are selectively prevented from cross-presenting host antigens, GVHD still occurs, but its incidence and severity are sharply diminished (Matte et al., 2004). Importantly, in a model of single minor MHC mismatched T cells it could be shown that the antigen can be efficiently cross-presented by either host or donor APCs to initiate GVHD (Toubai et al., 2012).

1.1.5   T cell trafficking in GVHD

Understanding the T cell trafficking after HCT to specific sites is an important aspect in GVHD, and has become the focus of a growing body of research. Generally, donor T cells are infused intravenously into the recipient and have to migrate to and within secondary lymphoid tissues, where they recognize alloantigens on either host or donor APCs and become activated. After 3 to 4 days, large numbers of T cells exit the lymphoid tissues and migrate to the target organs causing tissue damage (Beilhack et al., 2005; Wysocki et al., 2005).

Transplanted T cells are homing to lymphoid tissues within hours after administration (Panoskaltsis-Mortari et al., 2004; Beilhack et al., 2005). It is well established, that chemokines and the expression of selectins and integrins and their ligands play an important role in T cell trafficking to secondary lymphoid organs, as well as to the target tissues (Cyster, 2005). For example, the expression of CD62L by T cells is critical for their homing into secondary lymphoid tissues (Beilhack et al., 2008). The interaction between α4β7 integrin and its ligand MAdCAM-1, which is expressed by high endothelial venules (HEV), was shown to be important for homing of donor T cells to Peyer's patches (Murai et al., 2003). Furthermore T cell homing to lymphoid tissues might depend on other factors induced by the conditioning regimen or the inflammatory milieu (Murai et al., 2003; Welniak et al., 2006). Chemokines that are constitutively expressed and control cell movement during homeostasis are CCL19 and CCL21 that bind to the receptor CCR7, which is expressed by various subsets of immune cells (Gunn et al., 1998; Rot and von Andrian, 2004). CCR7 and its ligands, functioning on HEVs, are essentially involved in the homing of T cells into lymph nodes. T cell access to and the priming within secondary lymphoid organs is essential for initialization of GVHD and blocking completely the T cell entry to secondary lymphoid organs prevented acute GHVD (Beilhack et al., 2008).

Although the migration of T cells into lymphoid tissues is well characterized, the migration into the selective target organs during GVHD is less well understood. One possible explanation for the selective organ manifestation in acute GVHD is that alloreactive effector T

cells are instructed within the lymphoid organs to migrate to corresponding target tissues. For example, T cells encountering antigen in a skin draining LN would be imprinted to migrate to the skin (Campbell and Butcher, 2002). Several studies support this concept, suggesting that homing properties of T cells are imprinted during the initiation of an immune response (Campbell and Butcher, 2002; Mora et al., 2003; Stenstad et al., 2006) and once activated, effector T cells can target organs independently of antigen recognition (Teshima et al., 2002). In accordance with prior studies, Beilhack et al. (2008) found that, although homing receptor acquisition in SLOs is nonstochastic, alloreactive T cells infiltrated GVHD target tissues irrespective of their initial priming site. In this regard, local imprinting of alloreactive T cell trafficking in GVHD initiation sites appears to play a minor role. Instead, GVHD target tissues appear to selectively attract alloreactive T cells (Davenport et al., 2000). Unlike specific pathogen–induced tissue inflammation, that supports T cell migration into affected tissues via vascular endothelial changes and chemokine gradients, in GVHD all tissues are initially damaged from total body irradiation or chemotherapy. Anyway, the severity of damage caused by conditioning might depend on the tissues susceptibility, causing a selective tissue manifestation. Inflammation induced by host conditioning plays an important role in the initial recruitment of T cells, which induce an inflammatory cascade promoting further recruitment of T cells to GVHD target organs (Chakraverty et al., 2006). However, GVHD can also occur without irradiation (Murai et al., 2003), and therefore other mechanisms must be sufficient for target organ infiltration. Allogeneic transplantations in germ free mice have a greatly reduced incidence of acute GVHD (Van Bekkum and Knaan, 1977) and led to the hypothesis of the involvement of microbial vicinity to explain the selective organ manifestation. In fact, all target organs have in common to be barriers to microorganisms and might have a greater propensity to recruit activated T cells. Especially skin and gut are regularly exposed to microorganisms and also the liver functions as a barrier to endotoxin and gram-negative bacteria that pass through the intestinal mucosa (Ferrara et al., 1999). Also the bronchial epithelium of the lung, as being discussed to be a GVHD target organ, is likewise an important barrier to infection. Thus bacterial products like lipopolysaccharides (LPS) might be released into circulation and peripheral tissues by the conditioning regimen, with activating macrophages and subsequently releasing high levels of pro-inflammatory cytokines (Cooke et al., 2001). Indeed, many experimental studies have shown that the conditioning of the host activate the production of cytokines, such as IFN-γ, TNF-α IL-1, IL-2, that are important in the pathogenesis of acute GVHD (e.g. Hill et al., 1997; Mapara et al., 2006; Kittan and Hildebrandt, 2010). For example, IL-2 promotes T cell activation and expansion (Jaksch and Mattsson, 2005). During the initial phase of GVHD, especially IFN-γ and TNF-α are considered to induce the production of chemokines in target organs (Schroeder and DiPersio, 2011).

Further molecular mechanisms that have been shown to be involved in directing T cell migration to GVHD target tissues are interactions between chemokines and chemokine receptors, integrins and selectins with adhesion molecules (reviewed in Wysocki et al., 2005). Chemokines play an important role in recruiting cells of the innate and adaptive immune system to sites of inflammation (Rollins, 1997; Moser et al., 2004) and the expression of chemokines can be enhanced by inflammatory cytokines (Mackay, 2001). The expression profile of chemokine and chemokine receptor during GVHD greatly differs between the target organs of GVHD. Several chemokines such as CCL2–5, CXCL2, CXCL9–11, CCL17 and CCL27 were found to play a role in target infiltration during acute GVHD (Cyster, 2005; Mapara et al., 2006). The production of CCL3 during acute GVHD is critical for the recruitment of CD8$^+$ but not CD4$^+$ T cells to the liver, lung, and spleen (Serody et al., 2000). In studies of conditioned mouse models CXCR3$^+$ T cells and CCR5$^+$ T cells caused acute GVHD in the liver, gastrointestinal tract, and lung (Murai et al., 1999; Hildebrandt et al., 2004; Wysocki et al., 2004). *In vivo* administration of CCR5 or CXCR3 neutralizing antibody reduced the infiltration of alloreactive CD8$^+$ T cells into GVHD target organs (Murai et al., 1999; He et al., 2008). The selectin ICAM-1 and its interaction to α4β1 have been shown to be important for T cell homing to the lung (Panoskaltsis-Mortari et al., 2001) and the liver (Harning et al., 1991). For example, the homing of alloreactive T cells to the gastrointestinal tract during GVHD, especially the interaction between MAdCAM-1 and α4β7 integrin, is important (Petrovic et al., 2004).

1.1.6 Importance of alloantigen expression in GVHD

Already 40 years ago, Billingham proposed the requirement of alloantigen expression within the recipient tissue to be crucial for the development of GVHD (Billingham, 1966). More recently, it became clear that alloantigen expression is essential for the activation phase of acute GVHD (Shlomchik et al., 1999). For a long time it was believed that also the effector phase of GVHD is antigen-specific and requires alloantigen expression on the host target epithelium (Lampert et al., 1981). However, in the last decade several studies either confirmed or challenged this assumption raising some unresolved controversies in the field.

Teshima et al. (2002) suggested that the damage to GVHD target organs does not require alloantigen expression on epithelial target cells and alloantigen expression by hematopoietic cells alone was sufficient for both, CD4-dependent and CD8-dependent GVHD. However, this conclusion was drawn from experiments of a MHC-mismatched GVHD model that led to rapid death that was, at least partly, mediated by inflammatory cytokines. In contrast to MHC-mismatched HCT, recipients of miHAg-mismatched HCT, typically survive the early cytokine-storm and instead, GVHD primarily manifests by T cell infiltration of target tissues. This

phenomenon might be explained by the fact that precursor frequency of alloreactive T cells targeting the foreign MHC complex is approximate 100 – 1000 fold greater than in miHAg mismatched transplantations. Employing miHAg mismatch models, it could be shown that hematopoietic expression of miHAgs is not enough to elicit a CD4-mediated lethal GVHD, implicating that non-hematopoietic host cells are critical targets in acute GVHD of miHAg-mismatched transplantations (Jones et al., 2003).

In contrast, in a MHC-matched, multiple miHAg-mismatched model CD8$^+$ but not CD4$^+$ T cells required cognate interactions with target tissues to mediate GVHD (Matte-Martone et al., 2008) and thus the expression of miHAg could theoretically dictate which organs are involved in the disease. In accordance with this, it could be demonstrated that different miHAgs determine the phenotype, target organ involvement and the kinetics of GVHD (Kaplan et al., 2004). MiHAgs are widely expressed, but can differ in their tissue expression (De Bueger et al., 1992; Bleakley and Riddell, 2004) and therefore might explain the selective organ damage in GVHD. Nevertheless, some identified miHAgs that can cause GVHD, such as H-Y antigens (Toubai et al., 2012), are expressed ubiquitously. Taken together, the importance of alloantigen expression on epithelial target cells for GVHD still remains elusive.

Yet, if T cells migrate to selective organs (like intestinal tract and skin) although alloantigens are expressed and presented ubiquitously, the organ infiltration should be considered as antigen independent (Figure 1.3A). Similarly, if T cells selectively infiltrate organs that do not express alloantigen, while organs expressing alloantigens remain unaffected, the organ infiltration should be considered antigen independent. In contrast, if ubiquitously alloantigen expression and presentation would result in a systemic organ infiltration or organ specific alloantigen expression would result in the selective infiltration of these organs, might indicate that acute GVHD organ infiltration is determined by antigen recognition (Figure 1.3B).
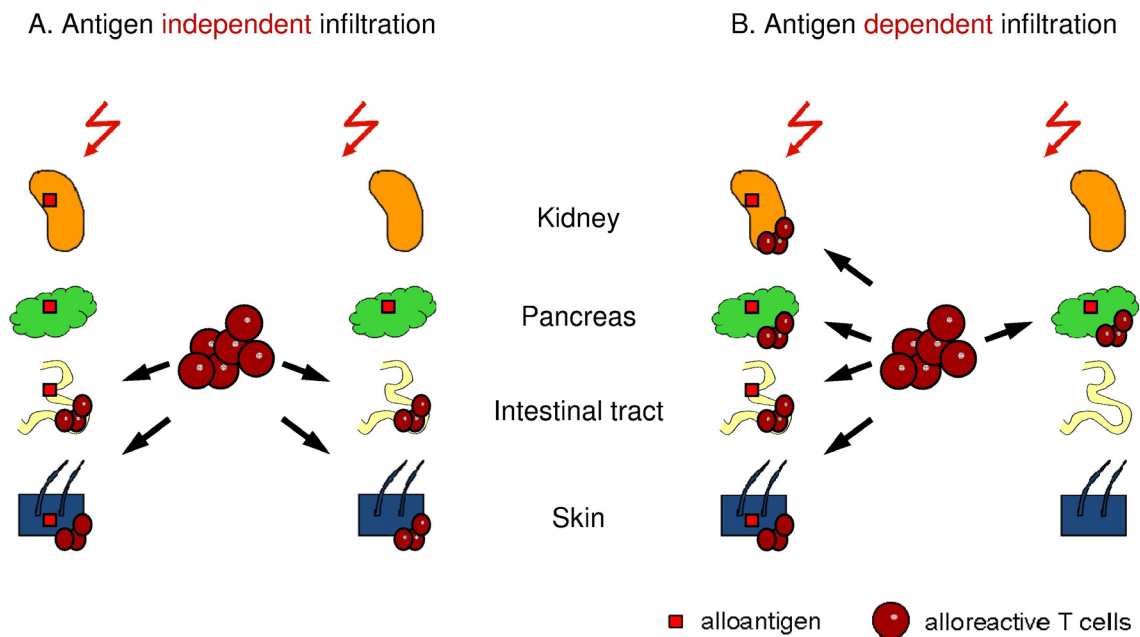
Figure 1.3: Does the tissue alloantigen expression and presentation influence the alloreactive T cell migration in acute GVHD? (A, B) Different scenarios of T cell migration after total body irradiation might rule out the importance of alloantigen presentation in the host tissues. Both scenarios in (A) reflect an antigen independent organ infiltration while T cell distribution in sketch (B) describes an antigen dependent organ infiltration.

1.1.7 Antigen-specific transgenic TCR models of GVHD

Studies from mouse models have been instrumental for the understanding of the cellular interactions and development of GVHD. Mouse models of bone marrow transplantation involve the transfer of either MHC- or miHAg-mismatched T cells and the GVHD mainly affects the skin, gastrointestinal tract, and liver and thereby resembles the tissue tropism and further GVHD clinical aspects in humans. The most common conditioning method in mouse models of GVHD is total body irradiation. The conditioning ablates the recipient's bone marrow, facilitates the donor stem cell engraftment and prevents the rejection of the grafted cells by diminishing recipient T cells and natural killer (NK) cells. The induction of GVHD, either to full MHC disparity or to the clinically more relevant miHAg, results in a disease that is dependent on either $CD8^+$ T cells, $CD4^+$ T cells, or both. Generally, mouse models of GVHD thereby suffer from the difficulty to identify the specific alloantigen that is recognized by the responding T cells. This obstacle limits the investigation of antigen-specific donor T cell responses within the host. To overcome this limitation, the use of identifiable T cells with specificity to a defined antigen causing acute GVHD might be helpful.

In TCR transgenic mice the specificity of the T cells is restricted to a single peptide epitope and therefore allows visualizing antigen specific T cells *in vivo*. To provoke an antigen specific T cell response in the host, the antigen can be either expressed by the recipient or it

has to be administered exogenously. TCR-transgenic mice, including H-Y, TEa, 2C, DO11.10, and OT-II, were initially generated to study thymic selection, but have recently been used studying diverse aspects of GVHD such as the role of antigen affinity (Yu et al., 2006), T_{REG} function (Damdinsuren et al., 2010) or cross presentation of antigens in GVHD (Wang et al., 2011). More recently, using CD8^{+} T cells from MataHari TCR transgenic mice and CD4^{+} T cells from "Marylin" or "Rachel" transgenic mice, Toubai et al. (2012) demonstrate that the recognition of a clinically relevant single H-Y antigen epitope is sufficient to initiate acute GVHD. Furthermore, they identified that H-Y expression on recipient stroma, but not on recipient hematopoietic cells are critical for GVHD severity (Toubai et al., 2012). TCR transgenic Models of GVHD are listed in Table 1.

Table 1: T cell receptor transgenic Models of GVHD.

TCR (tg)	Recipient strain	Antigens	T cell dependence	Purpose	Reference
TEa, 2C	(BALB/c x C57BL/6)F1	2C, TEa	CD4 + CD8	Define effect of host conditioning	Gonzalez et al., 2002
2C	(BALB/c x C57BL/6)F1	2C	CD8	Limited repertoire of Ag might elict GVHD	Dey et al. 1999; Yu et al. 1999
B6.H60	B6.H60.Kb-/-	H60	CD8	To study cross presentation	Wang et al. 2011
OT-I	B6 actOVA.Kb-/-	SIINFEKL	CD8		
MataHari	C57Bl/6		CD8	To define role of host APCs in GVHD initiation	Toubai et al. 2012
Rachel	C57Bl/6	H-Y	CD4		
Marylin	C57Bl/6		CD4		
TS1	HA104 Tg	S1	CD4	To define role of CD4^{+} T_{EM} after HCT	Juchem et al. 2011
D10	(B6 x C3H)F1	D10	CD4	To determine alloantigen affinity for allo-response	Yu et al. 2006

An extensively studied model antigen in mice is the chicken ovalbumin (OVA) that has been widely used in allergy research (Kumar et al., 2010), diabetes (Hänninen et al., 2007) and kidney disease (Heymann et al., 2009). TCR transgenic, OVA-specific CD4^{+} (OT-II) and CD8^{+} (OT-I) T cells recognize the peptides presented respectively by MHC I or II (H-2K[b], C57Bl/6). To model type 1 diabetes for example, rat insulin promoter–mOVA (RIP-mOVA) mice expressing the model antigen OVA in pancreatic islets have been used to study T cell involvement in disease progression. Further transgenic mice exist that express ovalbumin tissue specific promotors, such as under the control of a keratin 5 promotor (K5-mOVA), or keratin 14 promoter (K14-mOVA) in skin epithelia (Azukizawa et al., 2003; Shibaki et al., 2004) or under the control of intestinal fatty acid binding promoter (iFABP-OVA) in the small intestine (Vezys et al., 2000). Thus, transgenic mouse models have become powerful tools,

presenting tissue-specific cognate antigens and T cells with well-defined antigen-specific TCRs.

1.2 Mapping immune processes in intact organs with light sheet fluorescence microscopy (LSFM)

1.2.1 Imaging immune processes

A variety of different imaging strategies have been utilized to study immune cell activity and migration in animal models of human disease. Imaging techniques such as magnetic resonance imaging (MRI), positron emission tomography (PET) and single photon emission tomography (SPECT) are particularly attractive since they can be readily translated from preclinical animal models to clinical application in humans (Gross et al., 2007). Another effective method to visualize immune responses in larger specimen is bioluminescence imaging (BLI), as 100 – 1000 immune cells can be assessed *in vivo*. Especially for studies of GVHD, where luciferase-expressing T cells can be transplanted, BLI has been proven to provide valuable new insights in cell migration and proliferation and *ex vivo* BLI permitted even more precise localization of donor cell infiltrates. However, these techniques generally do not provide sufficient resolution to visualize individual cells and in many cases lack sensitivity to detect rare biological events in different areas throughout the body. Other imaging techniques like confocal microscopy or multi-photon-laser-scanning microscopy (MPM) are instructive focusing on pre-selected tissues, but limited in the scope of the areas that can be imaged.

So far, enormous efforts have been undertaken to visualize single immune cells throughout the body in murine models of human disease, particularly by high-precision cryosectioning of entire organs and subsequent compilation of consecutive images (Reinhardt et al., 2001; Machnik et al., 2009). This laborious approach provided valuable insights, however, was prone to tissue distortions and artifacts. Recently, several 3D microscopy techniques for morphological and functional imaging have been developed to visualize mesoscopic specimens such as optical projection tomography (OPT) (Sharpe et al., 2002), optical coherence tomography (OCT) (Boppart et al., 1996), and light sheet based techniques such as selective plane illumination microscopy (SPIM) (Huisken et al., 2004) or ultramicroscopy (Dodt et al., 2007). So far, LSFM has only been employed in very few intact adult mouse organs such as the brain (Ermolayev et al., 2009b), spinal cord (Ertürk et al., 2011), or the middle ear, (Santi et al., 2009) using single color illumination. Other microscopy techniques like OPT and OCT do not achieve cellular resolution (Kumar et al., 2010) or do not allow a

multicolor application (Drexler and Fujimoto, 2008). In light-sheet microscopy, a tissue clearing procedure (replacement of water by a higher refractive index substance) is typically used to make the specimen transparent. Here, to investigate alloreactive T cell trafficking we combined deep tissue staining protocols with optimized clearing procedures and advanced LSFM for the first time to be used as a quantitative triple-color technique investigating intact murine and human samples. Complex immune processes, as for instance in hematopoietic cell transplantation or in anti-tumor responses, can now be analyzed on a single cell level in large tissues specimens or even entire organs.

1.2.2   Principal of light sheet fluorescence microscopy

The principal idea of light sheet based techniques dates back to 1903 and was developed by Siedentopf and Zygmondi to observe single gold particles in glasses (Siedentopf and Zsigmondy, 1903). In light sheet microscopy a thin light sheet, shaped by a cylindrical lens is created to illuminate only a single plane of a specimen. The illumination is established orthogonal to the detection axis and thus illumination and detection light paths are completely separated from each other. The light sheet is a focused elliptically Gaussian beam that is centered and aligned to the focal plane of the detection objective. As all parts above or below the light sheet are in the dark, no out-of-focus light contributes to the image and an optical sectioning effect is generated. This optical sectioning, in contrast to physical sectioning, allows for imaging an intact sample. The dimensions of the light-sheet can be adapted from ~ 2 µm - 10 µm, depending on sample sizes and employed objective. Images are collected by using an objective lens and are finally detected with an electron multiplication CCD (EMCCD) camera. To gather three dimensional image stacks the sample is moved stepwise through the light sheet in small increments.

Light sheet fluorescence microscopy has several advantages over other commonly used epifluorescence microscopy methods. LSFM profits from a good signal-to-noise-ratio, since the thin light sheet generates no out-of-focus illumination. In comparison to raster scanning microscopy techniques, such as confocal microscopy or multi-photon microscopy, where point or line-scanning is time consuming, LSFM allows imaging the complete field-of-view at once, making data acquisition extremely fast. Furthermore, in confocal microscopy the laser beam is scanned across the sample to acquire an image, thereby exposing not only the focal plane to light, increasing photo-bleaching and photo-toxicity of the sample. Another advantage of light sheet microscopy is that it achieves excellent resolution at high penetration depths.

1.2.3   Modifications and applications of LSFM

Light sheet fluorescence microscopy techniques already have been used for several different biological and biomedical applications. Accordingly, many implementations exist to adapt either the mode of light sheet generation, or the sample preparation to improve the imaging performance.

Selective plane illumination microscopy (SPIM) is a light sheet based technique that has been used for many applications, especially for developmental research (Figure 1.4, (Huisken et al., 2004). This implementation of fluorescence light sheet microscopy is optimized for imaging small, live specimens *in vivo* such as developing embryos of Medaka and Drosophila (Figure 1.4C). Especially the high speed image acquisition became important for high-resolution fluorescence imaging of live biological specimens (Figure 1.4D). The embryos can be kept alive and imaged in a medium-filled chamber for a few days. A unique feature of SPIM is the ability to rotate the sample and acquire multiple views that are then combined by image processing (multiview fusion) (Swoger et al., 2003, 2007). However, in SPIM the parallel light sheet illumination from the side results in shadows and fluorescence attenuation caused by the interaction of the excitation light with the biological sample. The scattering and absorption in dense life tissue make it difficult to accurately analyze images. To overcome such artifacts multidirectional SPIM (mSPIM) has been developed (Huisken and Stainier, 2007). In mSPIM the sample is illuminated from two sides with a thinner pivoting light sheet created by a laser beam that is scanned over an angle of 10° at a frequency of 1 kHz using a mirror. Thus, artifacts, such as shadows and stripes, are markedly reduced.

Ultramicroscopy is another modified light sheet technique that has been developed to image large and opaque specimens like adult *Drosophila melanogaster*, mouse embryos or adult mouse brains that are few millimeter in size (Figure 1.3B,E,F, Dodt et al., 2007). Therefore the specimen has to be fixed and requires a clearing procedure to become optically transparent. During imaging, the sample is retained in the clearing solution. Furthermore, in this microscopy set-up two light-sheets are used to illuminate the sample from opposing directions, compensating the excitation light attenuation caused by penetrating the sample. Providing a more even illumination, this implementation is ideal for the imaging of larger, cleared specimens.

1.2.4   Development of light sheet generation

An alternative method to create a light sheet with a cylindrical lens is by rapidly scanning a single line focused laser beam during the exposure time. Similar to the pivoting light sheet, used in mSPIM, in digital scanned laser light-sheet fluorescence microscopy (DSLM) the laser beam is moved up and down to create a plane illumination, as shown by Keller et al. 2008. The benefit of this technique is the uniformity of the light sheet intensity profile, higher illumination efficiency and increased contrast. This modification leads to an improved quality of the complex morphology and optical properties of live specimens (Keller et al., 2008) and of fixed and cleared tissues. Additional alterations in generating a light sheet promise to further increase contrast, generate less image artifacts, and provide even higher resolution, such as structured-illumination (Keller et al., 2010), Bessel beam plane illumination (Planchon et al., 2011) or even combination of LSFM with STED microscopy (Friedrich et al., 2011).
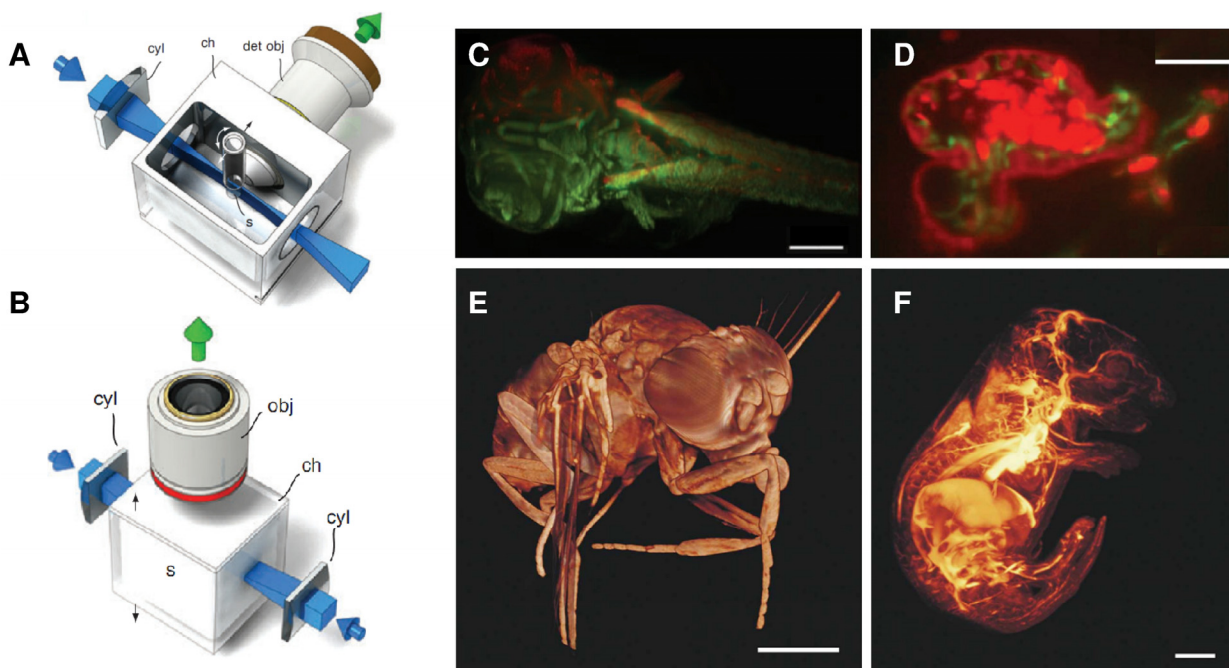
Figure 1.4: Modifications and applications of LSFM.
(A) Selective plane illumination microscopy (SPIM) and (B) ultramicroscopy are implementations of light sheet fluorescence microscopy (LSFM) techniques. Both methods using similar setups (cylindrical lens (cyl), sample chamber (ch), objective lens (obj), sample (s), light sheet (side of generation indicated with blue arrows), emission (indicated with a green arrow), but light sheet generation and sample preparation are adopted to achieve best imaging performance. (C,D) Fish embryos can be imaged with SPIM and revealed (C) different tissues of a Medaka embryo after multiview reconstruction (z-Projection, scale 200 µm). (D) High-speed imaging with SPIM revealed the heart beats of a Zebrafish expressing fluorescent proteins in myocardium, endocardium and blood (Scale 50 µm). (E,F) Ultramicroscopy allows for visualization of (E) whole adult Drosophila (z-Projection, scale 400 µm) and (F) autofluorescence of the blood vessel system in a mouse embryo (z-Projection, scale 2 mm). Sketches and pictures A-F taken from (Huisken et al., 2004; Dodt et al., 2007; Huisken and Stainier, 2009).

1.2.5 Sample preparation and adoptions

Light sheet based microscopy was initially developed for optically transparent objects. However, different protocols have been developed to render opaque specimens transparent, allowing the successful imaging even deep into adult mouse organs.

The principle idea of making biological samples transparent is to replace the water of the specimen with a liquid of the same refractive index as proteins and lipids (Spalteholz, 1914). Typically, differences in the refractive index of bordering components in cells and whole organs lead to an opaque appearance, resulting in light scattering effects. For the clearing procedure the specimen is classically dehydrated in ethanol and subsequently immersed in a solution consisting of a mixture of 1 part benzyl alcohol and two parts benzyl benzoate (BABB). This chemical clearing reagent has the same refractive index of proteins. Now intra- and extracellular compartments of a specimen have the same refractive indices and light can traverse the specimen unhindered, allowing optical imaging deep inside the tissue. Pigment bleaching with hydrogen peroxide (Korytowski and Sarna, 1990) or the removing of opaque substances, as calcium in bones by EDTA chelation, might further increase the imaging quality of certain specimens. Importantly, LSFM is a fluorescent method and therefore, the incorporation of fluorescent-labeled molecules (i.e. antibodies) deep within the tissue is required to specifically label tissue structures. Optimized protocols are needed to obtain a sufficient penetration of fluorescent molecules.

Further improvements to optimize clearing procedures rendering organs transparent will assist to reduce background fluorescence and enhance fluorescent protein stability. For some organs, as the murine spinal cord, a tetrahydrofuran-based dehydration procedure was shown to be more effective than the use of ethanol (Ertürk et al., 2011). Hama et al. (2011) reported about an aqueous reagent, named Sca*l*e that rendered biological samples optically transparent and completely preserved fluorescent signals in the clarified structures, compared to BABB.

2 Questions and specific aims

To understand the mechanisms of T cell migration to selective GVHD target organs appears crucial for developing novel strategies to minimize GVHD and to maximize immune reconstitution and the GVL effect after allo-HCT. Therefore, this thesis addresses the question whether tissue specific alloantigen expression determines T cell migration patterns to certain tissues in GVHD. We postulated that if selective organ manifestation in GVHD would be dependent on alloantigen expression and presentation, the selective expression of alloantigen in different GHVD target and non-target organs would influence the migration of alloantigen specific T cells after HCT. To experimentally test this hypothesis, we transplanted bone marrow and antigen specific T cells in myeloablative conditioned transgenic mice that expressed ovalbumin (OVA) as a model antigen in a tissue-specific manner in GVHD-non-target organs or expressed OVA ubiquitously in all organs.

For the detection of first organ infiltrating T cells we set the goal to establish a novel microscopy set-up, termed light-sheet fluorescence microscopy (LSFM) a sensitive method to visualize and quantify single cells in its biological context by imaging large tissue specimens. LSFM emerged as a versatile technique that proved particularly instructive when combined with other methods.

The specific aims of my thesis project were:

1. To study whether tissue alloantigen expression determines the selective target organ manifestation during acute GVHD.
2. To investigate donor T cell migration patterns after allo-HCT.
3. To establish an imaging technique that allows for analyzing single cells in large and intact tissue specimens.

3 Material and Methods

3.1 **Material**

3.1.1 Chemical reagents

Aceton	Sigma (Deisenhofen, Germany)
Baytril	Bayer (Leverkusen, Germany)
Benzyl alcohol	Sigma (Deisenhofen, Germany)
Benzyl benzoat	Sigma (Deisenhofen, Germany)
D-Luciferin	Biosynth (Staad, Switzerland)
Entellan	Merck (Darmstadt, Germany)
Ethanol	Sigma (Deisenhofen, Germany)
Fetal Calf Serum (FCS)	Invitrogen (Darmstadt, Germany)
Hexane	Sigma (Deisenhofen, Germany)
Hydrogen peroxide 30%	Sigma (Deisenhofen, Germany)
Ketamine	Pfizer (Berlin, Germany)
Methanol	Sigma (Deisenhofen, Germany)
Normal Rat Serum (NRS)	Invitrogen (Darmstadt, Germany)
O.C.T.	Sakura (Staufen, Germany)
Paraformaldehyde	Roth (Karlsruhe, Germany)
Triton X 100	Roth (Karlsruhe, Germany)
Trypan blue	Sigma (Deisenhofen, Germany)
Xylazine 2%	CP-Pharma (Burgdorf, Germany)

3.1.2 Buffers and solutions

- Lysis buffer (10x): NH_4Cl (89.9 g), $KHCO_3$ (10 g), EDTA (0.37 g) in 1000 ml distilled water, sterile filtered

- PBS (10x): NaCl (80 g), Na_2HPO_4-$2H_2O$ (14,2 g), KCL (2 g), KH_2PO_4 (2 g) in 1000 ml distilled water, pH: 6,8

- Dynal buffer: BSA (0.5 g), EDTA 0.5 M (0.2 ml) in 500 ml (1x) PBS

- PFA (4%): 4 g PFA in 100 ml (1x) PBS, dissolved at 65°C, pH: 7.4

- Anesthetics: 8 ml Ketamine (25 mg/ml, Ketanest, Pfizer Pharma, Berlin, Germany), 2 ml Xylazin (2%) (Rompun, CP-Pharma, Burgdorf, Germany), 15 ml (1x) PBS

- cRPMI-1640: RPMI-1640 medium supplemented with 10% FCS, Penicillin (100 U/ml), Streptomycin (100 µg/ml), L-glutamine (2 mM) and β-mercaptoethanol (50 µM) (all Invitrogen, Darmstadt, Germany)

3.1.3 Antibodies and secondary reagents

Table 2: Murine primary antibodies used for FACS staining and fluorescence microscopy.

Antibody	Clone	Conjugation	Isotype	Purchased from
CD11c	N418	Alexa488 or PE	armenian hamster	Biolegend
CD19	6D5	APC, biotin, PE	rat	Biolegend
CD21/35	7E9	APC	rat	Biolegend
CD31	MEC13.3	biotin	rat	Biolegend
CD31	390	biotin	rat	Biolegend
CD3ε	145-2C11	purified	armenian hamster	BD Pharming
CD4	RM4-5	Alexa488, APC, APC-CY7 or PE	rat	Biolegend
CD4	GK1.5	Alexa647	rat	Biolegend
CD44	IM7	Pacific Blue	rat	Biolegend
CD45.1	A20	Alexa647, APC-Cy7, PE	mouse	Biolegend
CD45.2	104	Alexa647, APC-Cy7, FITC	mouse	Biolegend
CD62L	MEL-14	APC-CY7	rat	Biolegend
CD8α	53-6.7	Alexa488, APC, APC-CY7, biotin or PE-CY7	rat	Biolegend
CD8α	53-6.7	FITC or PE	rat	eBioscience
CD90.1	OX-7	Alexa488, Alexa647 or FITC	mouse	Biolegend
CD90.1	HIS51	APC or biotin	mouse	eBioscience
CD90.2	30-H12	biotin, FITC or PE	rat	Biolegend
IL2	JES6-5H4	Alexa647	rat	eBioscience
IFN-γ	XMG1.2	Brilliant Violet 412	rat	Biolegend
Insulin	polyclonal	unconjugated	Guinea Pig	Dako
Lyve-1	ALY7	eFluor 660	rat	eBioscience
MAdCAM-1	MECA-367	Alexa488, biotin	rat	Biolegend
OVA257-264 peptide bound to H-2K^b	25-D1.16	biotin	mouse	eBioscience

Secondary antibodies: Donkey anti goat CY3 purchased from Dianova (Hamburg, Germany), goat anti mouse IgG AlexaFluor® 568 purchased from Invitrogen (Karlsruhe, Germany).

Secondary reagents: Streptavidin-conjugated AlexaFluor® 488, AlexaFluor® 532, AlexaFluor® 546, AlexaFluor® 568 or AlexaFluor® 647 all purchased from Invitrogen (Karlsruhe, Germany).

3.1.4   Commercially available kits

CFSE Cell Proliferation Kit	Invitrogen (Karlsruhe, Germany)
Avidin-Biotin blocking Kit	Vector Laboratories (Burlingame, CA)
Vektashield mounting medium	Vector Laboratories (Burlingame, CA)
Dynabeads® Magnetic Beads	Invitrogen (Karlsruhe, Germany)
Cytometric Bead Array	BD Bioscience (Heidelberg, Germany)

3.1.5   Consumables

6 well flat bottom culture plates	Greiner Bio-One (Frickenhausen, Germany) or Sarstedt (Newton, USA)
96 well flat bottom culture plates	Sarstedt (Newton, USA)
96 well U bottom culture plates	Sarstedt (Newton, USA)
96 well V bottom culture plates	Sarstedt (Newton, USA)
5, 15 and 25 ml single use pipettes	Greiner Bio-One (Frickenhausen, Germany)
10 µl tips	Sarstedt (Newton, USA)
200 µl tips	Sarstedt (Newton, USA)
1000 µl tips	Sarstedt (Newton, USA)
15 ml and 50 ml centrifuge tube	Greiner Bio-One (Germany)
Cell strainer 70 µm	BD Biosciences (CA, USA)
Cryomolds	Sakura (Staufen, Germany)
SuperFrost Microscope Slides	R. Langenbrinck (Emmendingen, Germany)
U-100 Insulin Syringes	BD Bioscience (Heidelberg, Germany)
5, 10 and 15 ml Syringes	BD Bioscience (Heidelberg, Germany)
Glucose test stripes FreeStyle Lite®	Abbott (Wiesbaden, Germany)

3.1.6 Mice

BALB/C and C57BL/6 mice between 8 and 12 weeks old were purchased from Charles River Laboratories (Sulzfeld, Germany).

Following (transgenic) mice included in the study were bred in our own mouse colony at the Center for Experimental Molecular Medicine (ZEMM) Würzburg:

Table 3: Mice

Scientific name	Transgene	Coat color	Short name
C57Bl/6.L2G85.CD90.1	Luciferase	black	B6.L2G85.CD90.1
C57Bl/6.L2G85.CD45.1	Luciferase	black	B6.L2G85.CD45.1
C57Bl/6.L2G85.DsRed	Luciferase, Ds Red	black	B6.L2G85.DsRed
C57BL/6.L2G85.OT-I.Ragko.CD45.1	OT-I TCR, Luciferase	black	B6.L2G85.OT-I.Ragko.CD45.1
C57BL/6.L2G85.OT-I.Ragko.CD90.1	OT-I TCR, Luciferase	black	B6.L2G85.OT-I.Ragko.CD90.1
C57BL/6.L2G85.OT-II.Ragko	OT-II TCR, Luciferase	black	B6.L2G85.OT-II.Ragko
C57BL/6.L2G85.OT-II.Ragko.CD45.1	OT-II TCR, Luciferase	black	B6.L2G85.OT-II.Ragko.CD45.1
C57BL/6-Tg(ACTB-OVA)916Jen/J	beta actin OVA	albino, black	B6a.βa-Ova or βa-Ova
C57BL/6-Tg(Ins2-TFRC/OV)296Wehi/WehiJ	RIP-mOVA	albino, black	B6a.ins.ova or RIP-mOva
C57BL/6J-Tyr^{c-2J}/J	none	albino	B6.a

Briefly, transgenic mice B6.L2G85.CD90.1 expressing firefly luciferase (luciferase[+]) were generated by backcrossing the luciferase[+] FVB/N-L2G85 founder line (Cao et al., 2004; Beilhack et al., 2005) with the C57Bl/6 mice for more than 12 generations. Further transgenic mice expressing luciferase B6.L2G85.CD45.1 and B6.L2G85.DsRed, which additionally express the fluorescent protein DsRed, were bred in our colony. B6.L2G85.OT-I.Ragko.CD45.1 and B6.L2G85.OT-I.Ragko.CD90.1 mice were generated by crossing B6.L2G85.CD45.1 or B6.L2G85.CD90.1 with OT-I mice purchased from Jackson Laboratory (Jackson laboratory reference: C57BL/6-Tg(TcraTcrb)1100Mjb/J) and B6.Rag deficient mice (B6.129S7-Rag1[tm1Mom]/J). OT-I mice carry a transgenic CD8^{+} T cell receptor specific for the ovalbumin derived peptide 257-264 (SIINFEKL) in the context of H-2K[b]. B6.L2G85.OT-II.Ragko and B6.L2G85.OT-II.Ragko.CD45.1 were created by crossing B6.L2G85 or B6.L2G85.CD45.1 with OT-II mice purchased from Jackson Laboratory (Jackson laboratory reference: C57BL/6-Tg(TcraTcrb)425Cbn/J and B6.Rag deficient mice (B6.129S7-Rag1[tm1Mom]/J). OT-II mice have a transgenic CD4^{+} T cell receptor specific for the ovalbumin derived peptide 323-339 presented in the context of the MHC class II. The transgenic strain B6a.βa-Ova (Jackson laboratory reference: C57BL/6-Tg(ACTB-OVA)916Jen/J expresses ubiquitously the membrane bound chicken ovalbumin (OVA) gene under the chicken beta

actin promoter. B6a.ins.ova mice express membrane bound OVA under the control of the rat insulin promoter (Ins2) (Jackson laboratory reference: C57BL/6-Tg(Ins2-TFRC/OV)296Wehi/WehiJ also termed "RIP-mOVA"). OVA expression is detectable in pancreatic beta cells, kidney proximal tubular cells and a weak expression in the testis. For improved *in vivo* bioluminescence imaging of luciferase transgenic OT-1 and OT-2 T cells we backcrossed both OVA expressing mouse strains to the B6 albino background (C57BL/6J-Tyr<c-2J>).

Before each experiment, all transgenic animals were genotyped with PCR or phenotyped by flow cytometry (exclusion of existing B cells in the peripheral blood of B6.L2G85.OT-I.Ragko.CD45.1, B6.L2G85.OT-I.Ragko.CD90.1, B6.L2G85.OT-II.Ragko and B6.L2G85.OT-II.Ragko.CD45.1 mice. All studies were performed under institutional approval according to specific animal use protocols.

3.2 Methods

3.2.1   Single cell suspension from spleen and lymph nodes

Organs were removed from mice, cut into pieces and homogenized by gently smashing through a cell strainer. The cell strainer was rinsed with 8 ml Lysisbuffer into a 50 ml centrifuge tube. Erythrocytes were lysed by incubating the cells in Lysisbuffer for 2 minutes (min) at room temperature. After adding 10 ml PBS the cells were centrifuged at 1500 rpm for 5 min at 4ºC. The supernatant was removed and the pellet was resuspended in PBS. If required (e.g. for transplantation or FACS sorting) the cells were again passed through a cell strainer before counting.

3.2.2   Single cell suspension from organs using enzymatic digestion

Organs were removed from mice and kept in cold PBS. Subsequently, tissues were cut mechanically in small pieces followed by an enzymatic digestion in PBS (Mg+, Ca+) with 2 mg/ml collagenase D and 0.1 mg/ml DNaseI at 37°C for 30 min. The cell suspension was smashed through a cell strainer, and rinsed with PBS + 0.5% BSA.

3.2.3 Multicolor flow cytometry

Fluorescence activated cell sorting (FACS) analysis was performed on single-cell suspensions using a BD FACSCantoII flow cytometer (BD Bioscience, Heidelberg, Germany).

For analysis of primary mouse cells the single cell solution was transferred to a 96 well plate or FACS tubes. To block unspecific binding to Fc receptor cells were incubated with NRS (1:10) for 5 min in the fridge. The cells were stained with primary fluorochrome labeled antibodies for 30 min in the fridge and subsequently centrifuged for 5 min at 1500 rpm. The pellet was resuspended in PBS and dead cells were excluded by propidium iodide staining approximate 5 min before FACS. A maximum of 8 colors was analyzed at a single sample. To compensate for the spillover in the emission spectrums for each fluorochrome, a control cell suspension or antibody capture beads were individually stained with single fluorochrome labeled antibody also used in the multiple staining. This compensation procedure (Tung et al., 2004) allowed calculating and subtracting the appropriate overlap to yield the specific signal intensity for each fluorochrome. To set gates in multicolor stained samples the fluorescence minus one (FMO) method (Herzenberg et al., 2006) was performed. In this gating control strategy the samples were stained with all fluorochromes, but one fluorochrome at a time. All antibodies were titrated for optimal performance before their application. Used antibodies are listed (see antibodies 3.1.3). Acquired FACS data was analyzed with FlowJo software (Tree Star, Ashland, OR).

3.2.4 Magnetic bead-based cell separation

Dynabeads® Magnetic Beads CD8 or CD4 positive, CD8 or CD4 negative or T cell negative Isolation Kits (Invitrogen Karlsruhe, Germany) were used either to deplete or to enrich T cells from a single cell suspension. Sample preparation was according to the manufacturer instructions. The purity of the enrichment was analyzed with FACS.

3.2.5 FACS based cell separation

Magnetic bead pre-enriched T cells were further sorted to pure $CD8^+$ or $CD4^+$ T cells or further into $CD4^+CD44^{hi}CD62L^{lo}$ effector memory, $CD4^+CD44^{hi}CD62L^{hi}$ central memory and $CD4^+CD44^{lo}CD62L^{hi}$ naïve T cell subsets using a FACSAria III cell sorter (BD Bioscience, Heidelberg, Germany). The post sort purity is given in the respective experiment.

3.2.6 Hematopoietic cell transplantation

Recipient mice were conditioned with a single total body irradiation dose of 8 Gy (BALB/C) or 9 Gy (C57BL/6) using a Primus1 (Siemens, Erlangen, Germany) or a MX20 LX60 irradiator (Faxitron Bioptics, Much, Germany). For hematopoietic reconstitution, mice were intravenously injected (into the orbital cavity) with 5 x 10^6 sex- and age-matched bone marrow (BM) cells within 2 hours (h) after radiation. To induce acute GVHD allogeneic enriched T cells or splenocytes were coinjected intravenously. The specific numbers of transferred T cells are stated for each experiment. Preferably mice at the age of 8 to 12 weeks were used for hematopoietic stem cell transplantation experiments.

3.2.7 Blood glucose

One small drop of blood was gained by carefully cutting the tail vein of the mouse with a scalpel. Blood glucose was measured in mg/dl using a FreeStyle Freedom Lite® (Abbott, Wiesbaden, Germany) blood glucose monitoring system with the appropriate FreeStyle Lite® diagnostic medical dipsticks. The test stripes were dipped into the drop of blood until an acoustic sound signaled the end of the measurement. Monitoring of the different groups was always to the same time of day and mostly before 12 a.m. The systems measurement range of glucose levels is between 20 - 500 mg/dL (1.1 - 27.8 mmol/L). Consequently, values stated as low (lo) had to be listed with 20 mg/dl and values stated as high (hi) were listed with 500 mg/dl.

3.2.8 Chimeras

Chimeras were created by hematopoietic reconstitution with 10 x 10^6 T cell depleted BM cells injected i.v. within 2 h after radiation. Reconstituted mice were analyzed for chimerism by flow cytometry analysis of the blood and used for experiments after 1-3 months. All animal studies were performed under institutional approval according to specific animal use protocols.

3.2.9 Bioluminescence imaging (BLI)

In vivo bioluminescence imaging was performed using an IVIS Spectrum CCD-imaging system (Caliper Xenogen, Alameda, CA). Mice were anesthesized with an intraperitoneally injected mixture of Ketamine (50 µg/g body weight) and Xylazine (5 µg/g body weight) in 0.1 M Phosphate-Buffered Saline (PBS) in a total volume of 10 µl/g body weight. D-Luciferin was

injected in a concentration of 150 μg/g body weight and images were taken 10 min after injection and allowed identification of cell proliferation and migration (Figure 3.1).

To perform *ex vivo* imaging mice were either injected with the same mixture of anaesthetic and luciferin or directly after *in vivo* BLI with an additional dose of luciferin (150 μg/g body weight) only. Accordingly, 10 or 5 minutes after injection, mice were euthanized and organs were removed within 3 min. *Ex vivo* bioluminescence images provided higher resolution of selective organ signal distribution. Samples were stored in PFA or embedded in TissueTec or for further histological analyses. Imaging data were analyzed with Living Image ® 4.0 (Caliper, Xenogen).
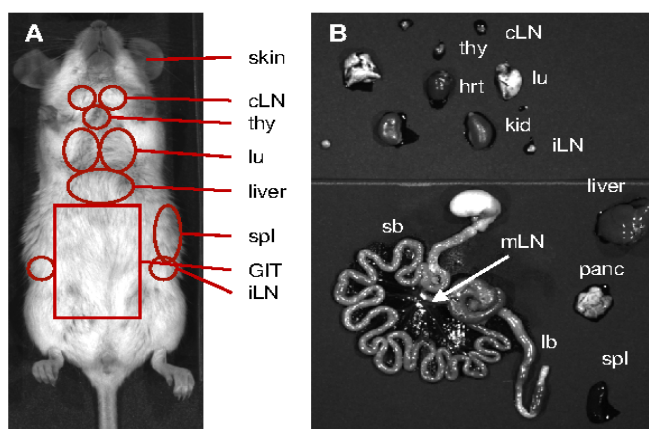
Figure 3.1: Scheme for set regions of interest (ROIs) to quantify BLI measurements (*in vivo* and *ex vivo*). (A) Photograph of a mouse with arrows roughly indicating the location of selected organs. In combination with the BLI image the photo allows to identify the localization of transplanted luciferase^{+} cells *in vivo*. **(B)** Arrangement of explanted organs for *ex vivo* BLI. Cervical lymph node (cLN), thymus (thy), heart (hrt), lung (lu), kidney (kid), inguinal lymph node (iLN), liver, gastrointestinal tract (GIT), small bowel (sb), mesenteric lymph nodes (mLN), large bowel (lb), pancreas (panc), and spleen (spl).

3.2.10 Immunofluorescence microscopy (IFM)

Tissue samples were embedded in O.C.T. within cryomolds and cryopreserved at -20°C. Frozen sections of 5 μm thickness were mounted on microscope slides and stored at -20°C. The sections were initially thawed for 10 min at room temperature (RT). After acetone fixation (7 min at RT) and air drying (2 min), sections were washed in PBS (3x 5 min) and incubated with blocking solution (PBS + 2% FCS) for 15 min. If required samples were incubated with an Avidin-Biotin blocking Kit for 15 min each. Incubations with primary antibodies were performed for 1 h at RT and samples were washed in PBS (3x 5 min). Samples were incubated with secondary antibodies or streptavidin labeled fluorophores for 30 min at RT and washed in PBS (3 x 5 min). Used antibodies are listed (antibodies section). Nuclei were stained with DAPI (4',6-diamidino-2-phenylindole) in a dilution of 1:3000 for 5 min at RT and washed again in PBS (3 x 5 min). Samples were coated with mounting medium for fluorescence (Vectashield, Vector Laboratories, Burlingame, CA), covered with cover slips and sealed. Fluorescence microscopic evaluation was performed on a Zeiss microscope (Axio Imager.M1, Zeiss, Jena, Germany). Standard objectives were 10x with numerical

aperature (NA) 0.25, 20x with NA 0.8 or 40x with NA 1.3 oil. Images were processed using AxioVision 4.8 (Zeiss, Jena, Germany) or ImageJ (US National Institutes of Health, Maryland, USA).

3.2.11 Confocal microscopy

Tissue samples prepared for LSFM were placed into a three-dimensional self-constructed chamber filled with clearing solution. The chamber consisted of high quality steel threaded rings (diameter 3.5 mm) separating two round cover slides (approx. 500 µm in height and 300 – 400 µl volume). Serial confocal Z-stacks were taken with an increment of 2 µm on a Leica SP5 laser-scanning confocal microscope (Leica, Mannheim, Germany) with a 20x (NA 0.7) immersion objective. The fluorescence emission resulted from excitation from a 633 nm laser and was detected with 680-720 nm spectral bandwidth on Leica TCS SP5 scanner and LAS AF software (Leica, Mannheim, Germany).

3.2.12 Multi-photon-laser-scanning microscopy (MPM)

Samples were embedded into a self-constructed chamber for MPM. MPM was equipped with an optical parametric oscillator (OPO, APE) for two-photon excitation at 1100 nm. The excitation beam was focused with a 20x NA 0.95 water objective (Olympus). Emission was detected with HQ535/50nm, HQ605/70nm and HQ710/75nm filter. Sequential 3D stacks were obtained for up to 1 mm penetration depth at a step size of 5 µm. Single color image stacks (overlap 16%) were stitched together, image size was reduced from 5566 x 3768 pixel to 756 x 512 pixels and photomultiplier tube (PMT) induced noise outliers were removed with ImageJ (processing package Fiji, US National Institutes of Health) before 3D image processing with Volocity (PerkinElmer).

3.2.13 Light sheet fluorescence microscopy setup

We used a LSFM setup similar to a previously described setup (Ermolayev et al., 2009b), however the sample was illuminated from one side by various laser sources: 405 nm diode Laser (56ICS025 Melles Griot), 473 nm DPSS laser (MBL-473 100 mW, CNI), 532 nm DPSS laser (MGL-W532 500 mW, CNI) and 639 nm diode laser (Cube 640-40, Coherent). An objective inverter (LSM Tech, Stewartstown) on a commercial inverted microscope (Axiovert 200, Zeiss) allowed a flexible horizontal positioning of the objective at a greater distance and range than typically possible on an inverted microscope. The laser excitation beams (3-4 mm diameter) were expanded 3-fold with a telescope (Thorlabs). With focus

beam waist of 4 to 9 µm a ca. 1 cm tall light sheet was created by focusing the beam in a cylindrical lens (f=5 cm and f=3.6 cm, Newport) depending on the detecting objective lens (Apochromat 5x with 0.16 NA and LD Achroplan 20x with 0.4 NA objectives (Zeiss)). The beam light sheet was adjusted exactly along the focus plane of a microscope. Fine focusing of the light sheet on the specimen was performed by moving the cylindrical lens mounted on a translation stage (Standa).

After sample fixation and clearing (see *Sample Preparation*), the specimen was affixed with Pattex acryl amide glue (Henkel) to a home made glass rod and placed in a home made cover glass chamber filled with clearing solution. The sample was positioned with a stepper motor-controlled stage (Standa). The stage with a feedback-memory system enabled translational and rotational step motion with accuracy of 0.1 µm and 0.1 degrees, respectively.

The fluorescence emission light was filtered using a motorized filter wheel (Standa) according to the excitation wavelength: DAPI 405 nm HQ440/40, Alexa Fluor[®] 488 (Invitrogen) 488 nm HQ525/50, Alexa Fluor[®] 532 (Invitrogen) HQ605/75; Alexa Fluor[®] 647 (Invitrogen) 640nm HQ695/55 (all Chroma). Fluorescence was detected by a back-illuminated electron multiplying charge-coupled device (EMCCD) camera (512 x 512 pixels, 16 µm/pixel Cascade II, Photometrics). Exposure times for image acquisition were 200 – 500 ms per frame. To acquire the complete image stack each excitation wavelength and emission filter combination were used sequentially plane by plane. We used the software package LabView (National Instruments, Austin, TA, USA) to control all hardware including the synchronization with data acquisition software MetaMorph 7.1 (Molecular Devices, Downingtown, PA, USA). Finally, the individual color stacks were overlaid via image processing using Volocity Software package (Improvision, Coventry, Great Britain).

3.2.14 Alterations of the primary LSFM setup

To further improve LSFM a resonant optical scanner SC10 (Electro Optical Products Crp., New York, USA) was implemented allowing for scanning the light sheet (Huisken and Stainier, 2007; Keller et al., 2010) with an angel of 20 degree and a frequency of 1 kHz. This method successfully reduced shadowing effects in the pictures.

3.2.15 Image acquisition by LSFM

Multiplexed and multicolor images were acquired in two different steps. First, each color channel was acquired separately. The individual color stacks were superimposed using

Volocity Software package (Improvision, Coventry, Great Britain). Between each stack the appropriate laser wavelength was triggered by the camera. The emission filter turret position in the microscope was manually adjusted. Second, each plane of a stack was imaged sequentially by each wavelength and emission filter combination. Resulting multi-color stacks were processed on Volocity software. Exposure times for image acquisition were 200 or 500 ms per frame. The excitation wavelengths, emission filter colors and camera acquisition were synchronized by LabView Software (National Instruments, Austin, TA, USA) via TTL pulses provided by I/O board (ME-RedLab, Meilhaus GmbH, Puchheim, Germany) to the CCD camera and to the motorized filter wheel. Data acquisition and storage were synchronized as well by LabView and administered using the software package MetaMorph 7.1 (Molecular Devices, Downingtown, PA, USA).

3.2.16 Image processing

Resulting multicolor stacks were processed, if necessary (e.g. cropped, reduced), with ImageJ (US National Institutes of Health). Subsequently, we used the 3D image processing software Volocity (Improvision, Coventry, Great Britain) to prepare the individual images and videos and developed algorithms to automate cell counting and volume calculations.

3.2.17 Volume calculations and automated cell counting

Multicolor stacks were processed on Volocity software (Improvision, Coventry, Great Britain) for 3D rendering and subsequently volume quantification and cell counting. We calculated volumes of autofluorescence, MAdCAM-1 and clustered donor T cells (Volocity Measurements: Find objects using intensity > Clip objects to ROI) within a 3D ROI fitted to border the whole Peyer's patch. Lower limit of specific threshold intensity was calculated with ImageJ by the mean of 10 individual threshold measurements for each individual sample. For automated cell counting we used following algorithm (Volocity Measurements: Find objects using intensity > Exclude objects touching edge of image > Exclude objects by size > Filter Measurements: Standard deviation). The lower limit of the object size was set to 400 μm^2 as calculated before. We used a lower limit of the standard deviation ranging from 250-500 to ensure automated event identification. Mathematical analysis was performed with Excel (Microsoft) and statistical analysis with Prism 5 (GraphPad Software, San Diego, CA, USA).

3.2.18 Preparation and clearing of mouse specimens for LSFM

Organs were prepared for LSFM by modified protocols of previously described procedures (Spalteholz, 1914; Dodt et al., 2007). Briefly, mice were anesthetized by intraperitoneal injection of Ketamine-Xylazine and transcardially perfused with 20 ml ice-cold PBS followed by 40 ml of 4% paraformaldehyde (pH 7.4). Following the perfusion, organs were removed. The samples were placed and stored in paraformaldehyde for at least 2 h at 4°C until further procedure. Hemoglobin rich organs were bleached for 30 min in 15% hydrogen peroxide/methanol to brighten optically dark structures. For homogenous immuno-fluorescence of large specimens *ex situ*, the tissue samples were blocked for 18-24 h with 2% FCS/PBS in 0.1% Triton-X and afterwards incubated with the respective antibodies for 24 h at 4°C on a shaker. Samples were washed 3 times in PBS for 1 h and if required incubated with streptavidin or secondary antibodies labeled with fluorochromes for another 24 h and washed again 3 times in PBS for 1 h. To clear specimens the tissue was dehydrated in a graded ethanol series (30%, 50%, 70%, 80%, 90%, 96% and in 100% for 2 h each) at room temperature. After rinsing the samples for 2 h in 100% n-hexane (Sigma, Munich, Germany), the n-hexane was replaced stepwise by a clearing solution consisting of 1 part benzyl alcohol in 2 parts benzyl benzoate (Sigma, Munich, Germany). Air exposure was strictly avoided at this step. Tissue specimens became optically transparent and suitable for the LSFM imaging after incubation in the clearing solution for at least 2 h at room temperature.

3.2.19 Antibody intravenous staining

Alternatively to *ex situ* antibody staining fluorochrome labeled antibodies were injected intravenously (i.v.) 2.5 h (300 µg CD4, CD45.1, CD90.1 or CD11c) or 0.5 h (50 µg MAdCAM-1) before euthanizing the mice. Organs were removed and prepared for 3D microscopy. To confirm distribution and specificity of i.v. antibody staining additional post-section staining was performed with the same antibody. To demonstrate antibody distribution and specificity of inflamed and non-inflamed tissues, CD4-Alexa647 antibody was injected in untreated mice or in mice at day+6 after allo-HCT. 2.5 h later mice were euthanized and spleens and PPs were harvested and digested according to a previously described protocol (32) with slight modifications. Briefly, organs were digested (2 mg/ml collagenase D and 0.1 mg/ml DNaseI) at 37°C for 30 min in the presence of saturating amounts of CD4-FITC antibody (30 µg/ml) to prevent an ex post staining of remaining unbound CD4-Alexa647. Thus, CD4-FITC single positive cells indicated *ex situ* stained cells. If not specifically indicated as antibody i.v. staining, fluorescence staining was performed according to the *ex situ* staining protocol.

3.2.20 Preparation of human tissue for LSFM

The preparation of human samples was similar to mouse tissue preparation with important modifications for dense human specimen. Fresh biopsy tissue was fixed for 2-4 h in PFA washed in PBS, bleached in 15% hydrogen peroxide/methanol and again washed in PBS. Subsequently the sample was pretreated with 0.1% Triton-X/PBS for 24 h before adding 2% FCS for another 8 h. To allow for homogenous staining of deeper tissue layers antibody incubation was performed for 4-6 d in 0.1% Triton-X/PBS. After washing again in PBS the sample was dehydrated in a graded ethanol series for 4 h each. The clearing procedure was performed exactly to the preparation of mouse tissue. All biopsies were obtained for diagnostic purposes and the study was approved by the Ethics Committee of the Medical Faculty, University of Würzburg, Germany.

3.2.21 Mixed lymphocyte reaction (MLR)

To analyze proliferation capacity and cytokine production of OT-I T cells in vitro, cells were either stimulated by irradiated ovalbumin expressing cells or by TCR stimulation. Effector cells (OT-I) were mixed with irradiated (20 Gray) splenocytes from βa-Ova mice in a ratio of 1:4. For maximal T cell stimulation, TCRs were stimulated by adding CD3ε (30 ng/ml) and IL-2 (26.5 IU/ml) to cRPMI medium. Cells were maintained in 200 µl cRPMI medium in a 96-well round-bottom plate. After 96 h, T cell proliferation and cytokine production was analyzed by flow cytometry.

4 Results

4.1 Mapping immunological processes in intact organs using LSFM

4.1.1 A virtual journey through intact tissues by advanced multicolor LSFM

Using LSFM we imaged Peyer's patches (PPs) that are initiation sites for adaptive immune responses as they occur in infections and autoimmune diseases and in GVHD. We visualized intact PPs of adult mice after specific deep-tissue antibody staining and clearing of the tissue specimens (Figure 4.1A,B).

Three spectrally distinct light sheets were created for a one-sided illumination and images were detected sequentially (Figure 4.1C). Intrinsic autofluorescence in the green color channel provided microanatomical details of the intestinal mucosa and submucosa. Even subepithelial dome regions and B cell follicles of PPs could be visualized and clearly differentiated from adjacent crypts and villi. To highlight T lymphocytes we stained with red labeled anti-CD4-Alexa647. High endothelial venules (HEVs), that play an important role for lymphocyte entry to PPs, were labeled with mucosal addressin cell adhesion molecule-1 (MAdCAM-1-Alexa546, measured in the yellow color channel). High precision optical z-stacks provided 1800 optical sections (5x objective) with an increment of 5 μm and allowed for scanning of whole PPs and lymph nodes (LNs) (size > 18 mm^3) in three color channels within minutes. The resulting z-stack required no further image processing and could be directly used for 3D tissue reconstruction (Figure 4.1D,E), volume measurements and quantification of protein expression. This precise 3D tissue reconstruction additionally allowed a virtual journey through the small intestine, which offers unique insights into the whole PP including adjacent areas (Supplemental Video 1,2). Using a 20x objective enabled us to visualize single CD4$^+$ cells (Figure 4.1F) and even subcellular components, such as individual nuclei (Figure 4.1G), deep within the tissue. In our hands, LSFM has proven to have a major acquisition speed advantage over Multi-photon microscopy (MPM) in imaging whole transparent PPs (LSFM < 12 min, MPM approx. 6 h) and reached a higher penetration depth (LSFM > 2 mm). In our hands, LSFM has proven to have a major acquisition speed advantage over MPM in imaging whole transparent PPs (LSFM < 12 min, MPM approx. 6 h) and reached a higher penetration depth (LSFM > 2 mm).
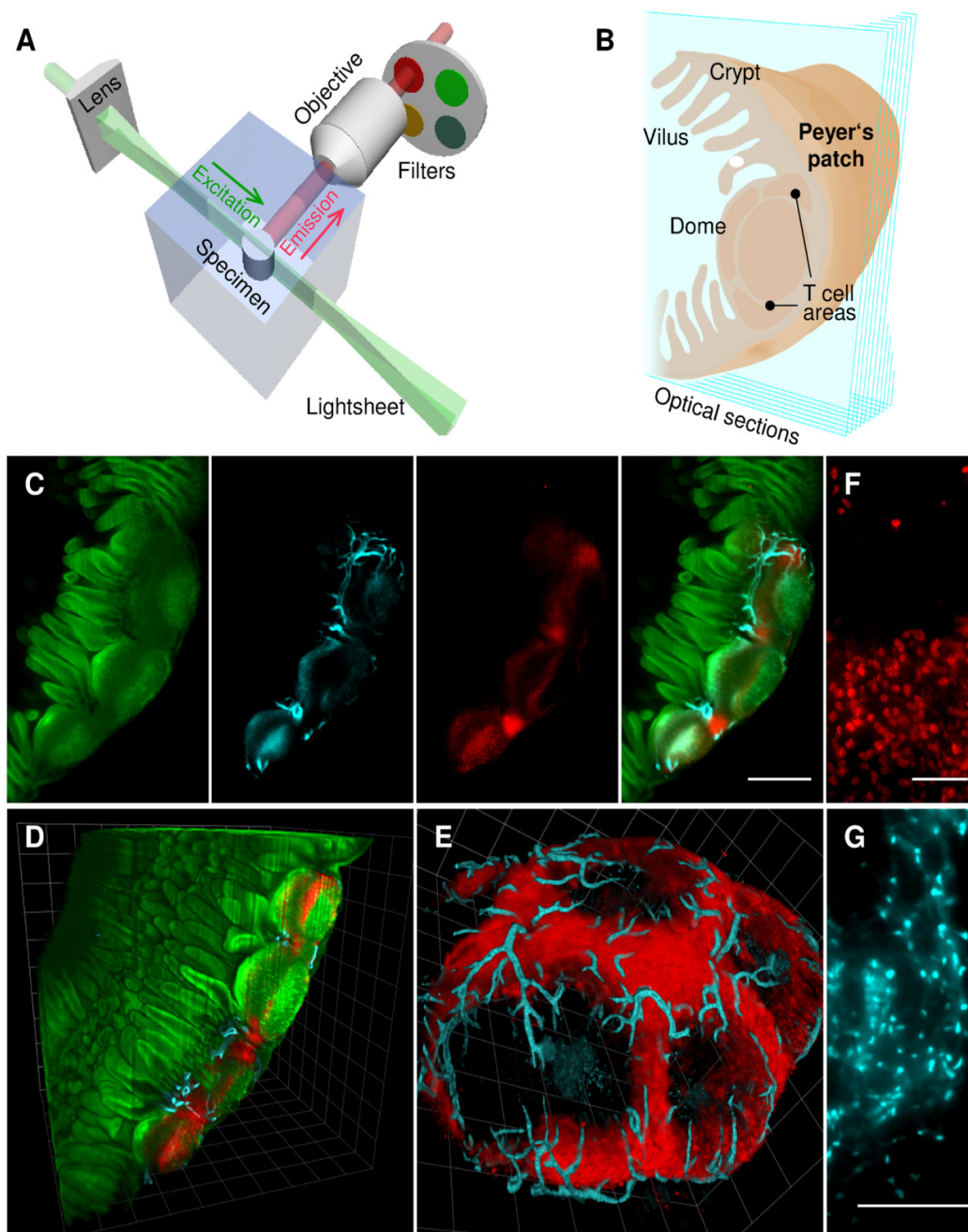
Figure 4.1: Principal of optical sectioning and computational 3D reconstruction by multicolor LSFM. (A) The sample is placed into the chamber with clearing solution and illuminated by laser light-sheets of different wavelengths to excite and detect fluorescence (beam path of emission and excitation is indicated by an arrow) in the labeled specimen in three detection channels by turning an optical filter wheel. To create optical z-stacks, the sample is moved by 1-5 µm increments through the light-sheet. Assembling X-Y-Z planes allows computational 3-dimensional reconstruction; (B) gut associated PPs are important sites of mucosal immune reactions. (C) Imaging of tissue autofluorescence (green) allows for visualization of micro-anatomical features of intact organs such as the small intestine containing a PP with high endothelial venules (MAdCAM-1, cyan) and CD4$^+$ T cells (red) as single and color-merged single optical sections; objective, 5x; scale bar, 100 µm, and (D) after computational 3D reconstruction; (E) 3D reconstruction of the whole organ reveals co-localization of MAdCAM-1 expression and CD4$^+$ T cells in a PP. Using a 20x objective allowed a higher magnification of (F) single CD4$^+$ T cells (z-Projection Scale bar, 100 µm) and (G) subcellular precision imaging single cell nuclei (stained with DAPI) within lymph nodes (z-Projection Scale bar, 100 µm).

4.1.2   Application of LSFM in multiple murine and human tissues

Labeling of intact tissues with multiple fluorescent antibodies for 3D imaging opens a broad range of biomedical applications because any molecule of interest can be stained. For optimal analysis of whole organs a homogeneous and specific antibody staining deep into the tissue is required. To this end two strategies turned out to be efficient. We injected fluorochrome labeled antibodies intravenously (i.v.) and shortly thereafter, euthanized animals for microscopic analysis. We confirmed the specificity of antibody binding and distribution with immunofluorescence microscopy on frozen sections and by flow cytometry (see section 3.1.2.1 Deep tissue antibody staining). Alternatively, we optimized a protocol to stain fixed intact organs that allowed for deep tissue staining. Only the combination of deep tissue antibody staining with sample clearing procedures allows visualizing any individual fluorescently labeled cell type within various mouse tissues such as the heart, testicle, skin and lymph nodes (Figure 4.2A-C). After the clearing procedure, most tissue specimens became optically transparent and suitable for the imaging with LSFM. The successful imaging of hemoglobin rich heart and optical dense liver required extra tissue brightening by peroxidase treatment before sample clearing. In addition to studies in the mouse we applied LSFM to analyze human specimens such as tonsils and colon cancer biopsies. Here, we successfully stained and displayed CD8$^+$ T cells in relation to CD31$^+$ endothelial cells in tonsils (Figure 4.2D) and tumor infiltrating CD4$^+$ and CD8$^+$ T cells in colon cancer (Figure 4.2E). Of note, the desmoplastic stroma reaction that is often present in cancer samples required to modify the processing procedure to allow antibody access into these very dense tissues.

4.1.2.1   Deep tissue antibody staining

For deep tissue antibody staining in fixed organs several critical steps turned out to be important to achieve good results. We avoided over-fixation of the tissues, as the PFA increases the antigen masking we performed short timed post fixation, if possible. The pretreatment of the fixed organs up to 24 h with Triton-X, turned out to enhance antibody penetration. Specimens were processed in pieces of max. 1.5–2 cm. Normally, for mouse tissues an antibody staining of 1d was sufficient to fully penetrate the specimen. To guarantee antibody access into dense human tissues, antibody incubation was performed for 4-6 d. The long time staining was performed on a shaker to avoid antibody sedimentation.
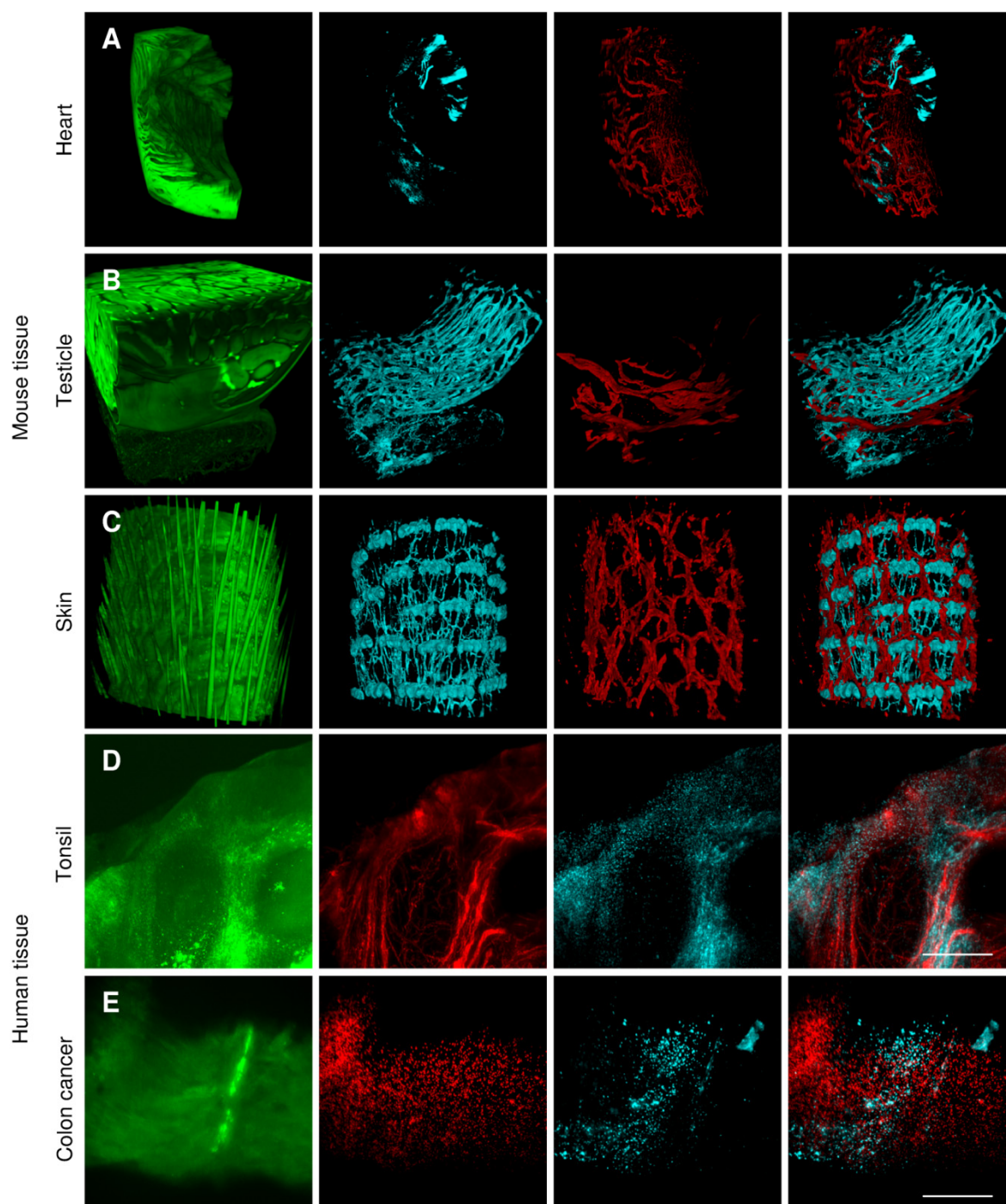
Figure 4.2: Multicolor LSFM of diverse murine and human tissues.
(A-C) A C57Bl/6 mouse was injected i.v. with fluorescent labeled antibodies CD31 (cyan) and LYVE-1 (red). Organs such as (A) heart, (B) testicle and (C) skin were removed 1 h after injection and prepared for LSFM. Shown are 3D reconstructions from optical sections imaged with a 5x objective. (D,E) LSFM allowed imaging of whole human tissue biopsies after modifying the processing procedures. (D) z-Projection of a human tonsil biopsy (autofluorescence, green) shows the co-localization of CD31 (red) and CD8 (cyan) (Scale bar: 500 μm). (E) A moderate differentiated human colon adenocarcinoma specimen with tumor infiltrating CD8$^+$ T cells (red) and CD4$^+$ T cells (cyan) (Scale bar: 500 μm).

Some antibodies did not work in the PFA fixed tissues, thus we established tissue staining protocols by injecting antibodies intravenously. Antibodies were injected i.v. 2.5 h (CD4, CD11c) or 0.5 h (MAdCAM-1) before perfusion. After injection, antibodies should distribute via the bloodstream and diffuse to peripheral tissues. To confirm distribution and specificity of

44

antibody injected intravenously (i.v) staining sections of several organs from an untreated mouse were compared to sections from mouse intravenously injected with fluorescent labeled antibodies (MAdCAM-1, CD11c and CD4) by conventional immunofluorescence microscopy (Figure 4.3). The detected antibody distribution by immunofluorescence microscopy indicated that defined cell populations and structures were labeled by this method.
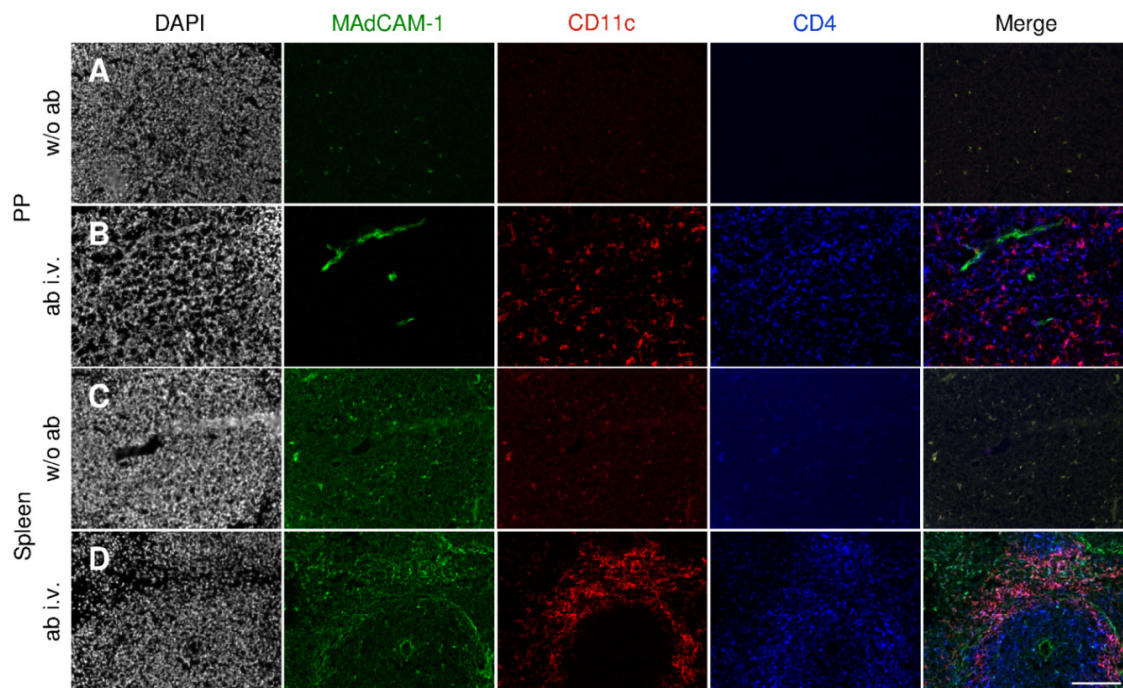
Figure 4.3: Antibody *in vivo* staining. Antibodies were injected i.v. 2.5 h (CD4, CD11c) or 0.5 h (MAdCAM-1) before perfusion. Specific antibody distribution was confirmed by conventional immunofluorescence microscopy. PP of (**A**) an untreated mouse and (**B**) of a mouse intravenously injected with fluorescent-labeled antibodies (MAdCAM-1 (green), CD11c (red) and CD4 (blue). Spleen of (**C**) an untreated mouse (w/o antibody) and (**D**) a mouse injected with antibodies. Sections were stained with DAPI *ex situ* (Scale bar: 100 µm).

To further demonstrate that all the cells and target molecules in the tissues are stained specifically and none of the cellular events were missed with this particular staining protocol, we compared i.v. staining followed by traditional post-sectioning staining. Again we injected antibody i.v. (CD4 and MAdCAM-1) in an untreated BALB/c mouse 2.5 h or 30 min before it was euthanized. For post-section staining we used the same antibodies respectively, either CD4 or MAdCAM-1 labeled with a different fluorochrome than the antibody we had injected intravenously. All post-section staining were negative, indicating that the antibodies had efficiently entered the tissues (Figure 4.4A,B) and labeled CD4 or MAdCAM-1 proteins specifically. Furthermore, to demonstrate antibody distribution and specificity of inflamed tissues, CD4-Alexa647 antibody was injected in untreated mice or in mice at day+6 after allogeneic HCT. 2.5 h after antibody injection organs were digested in the presence of CD4-FITC to prevent an ex post staining of remaining unbound CD4-Alexa647. Less than 2%

CD4-FITC single positive cells could be identified demonstrating an effective i.v. staining also under inflammatory conditions (Figure 3.4D).
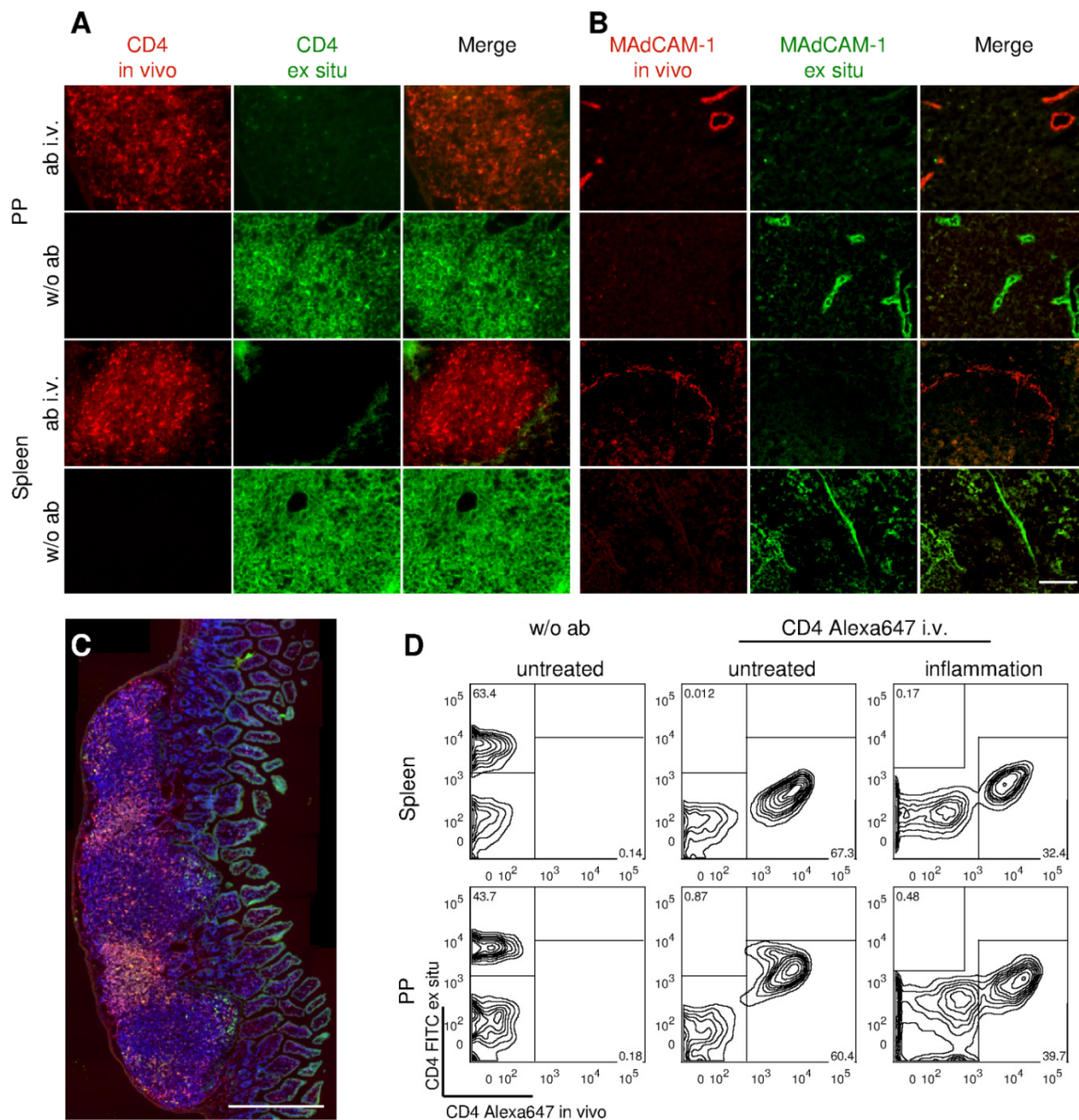
Figure 4.4: Distribution and specificity of i.v. antibody labeling procedure. To confirm antibody i.v. staining in an untreated BALB/c mouse (**A**) CD4 (red) was injected 2.5 h and (**B**) MAdCAM-1 (red) was injected 0.5 h before perfusion and post-section staining was performed with DAPI and respectively either with CD4 (green) or MAdCAM-1 (green) (20x, scale bar: 100 μm). Sections from mice injected with antibody (ab i.v.) were compared to sections from mice that did not receive antibody injection (w/o antibody). (**C**) Tiling of a whole PP cross-section with surrounding mucosal tissue indicates a specific whole tissue distribution of i.v. injected CD4 (red) antibody (20x, stitched from 30 images, scale bar: 500 μm). (**D**) FACS confirmation of i.v. antibody staining in inflamed and untreated tissues. CD4Alexa647 antibody was injected in untreated mice or in mice at day+6 after allo-HCT (inflammation). 2.5 h after injection spleen and PPs were digested in presence of CD4FITC antibody and subsequently analyzed with FACS. Cell frequency within the gate demonstrate an i.v. staining efficiency of > 98% of cellular events.

4.1.3 Quantification of immune processes in entire organs in a murine GVHD model

As LSFM proved valuable to map individual immune cells in murine and human tissues, we consequently applied this technique to investigate evolving immune processes by repeated sampling. Consequently, we employed a model of acute GVHD to study T cell interactions with HEVs in whole PPs after allo-HCT (Beilhack et al., 2008). We induced acute GVHD in myeloablative conditioned BALB/c mice by transplanting bone marrow cells from C57Bl/6 (CD90.2$^+$, CD45.2$^+$) donors and luciferase transgenic C57Bl/6 CD45.1$^+$ or CD90.1$^+$ T cells. We followed the *in vivo* progression of GVHD on a macroscopic level by non-invasive bioluminescence imaging (BLI) that pinpointed organs of donor T cell infiltration (Figure 4.5).
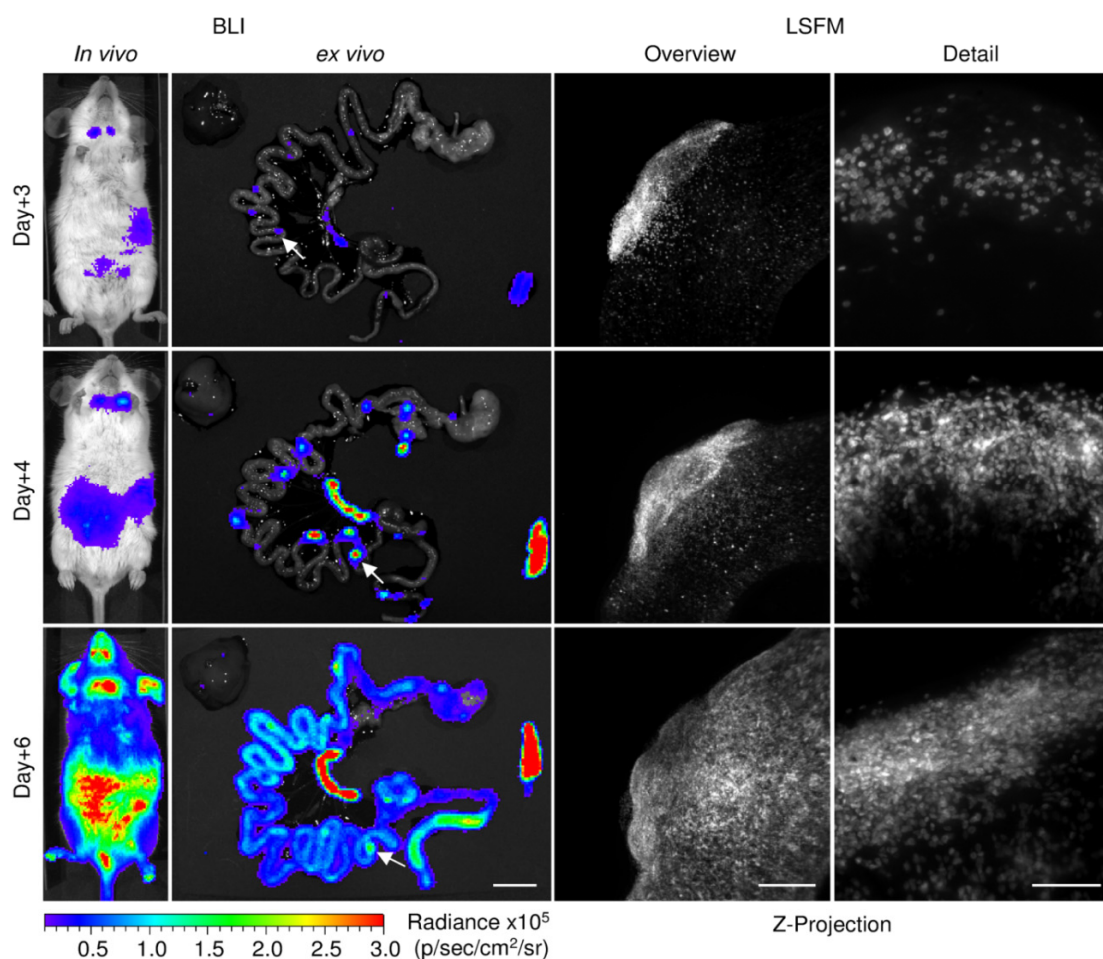
Figure 4.5: From whole body bioluminescence to single cell LSFM imaging. Bone marrow together with luciferase$^+$ CD45.1$^+$ transgenic T cells were transplanted into irradiated allogeneic recipients to induce acute GVHD. Organs (indicated by arrows) were removed at the transition from GVHD initiation phase to effector phase (day+3 and day+4 after allo-HCT) and at the effector phase (day+6) and stained *ex situ* for donor T cells. Until day+3 the transplanted T cells proliferated within secondary lymphoid organs and started to egress by day+4. Scale bar: BLI 1 cm, LSFM overview 500 μm and detail 100 μm.

At the transition from GVHD initiation to effector phase (day+3 to day+4 as described by Beilhack et al., 2005) and at the first peak of the effector phase (day+6) we prepared PPs (Figure 4.5) and other tissues of recipients for subsequent whole organ microscopy. To identify donor T cells we injected anti-CD45.1 or anti-CD90.1 specific monoclonal antibodies

i.v. and stained for the adhesion molecule MAdCAM-1 *ex vivo* on the fixed tissue. Subsequently we mapped and quantified the expression of MAdCAM-1 in relation to T cell numbers within PPs in the course of GVHD (Figure 4.6). Whereas LSFM allows clearly identifying single cells from different T cell subsets, dense lymphocyte clustering challenged automated cell counting. As a solution we calculated absolute T cell numbers in whole PPs by using the mean value of the measured cell volume (see 4.1.3.1 Cell counting). The 3D reconstruction of small intestines in healthy mice revealed that the MAdCAM-1 expression averaged at approx. 6% of the entire PP and was predominantly restricted to HEVs (Figure 4.6A). During the GVHD initiation phase (day+3-4) the overall MAdCAM-1 expression in PPs
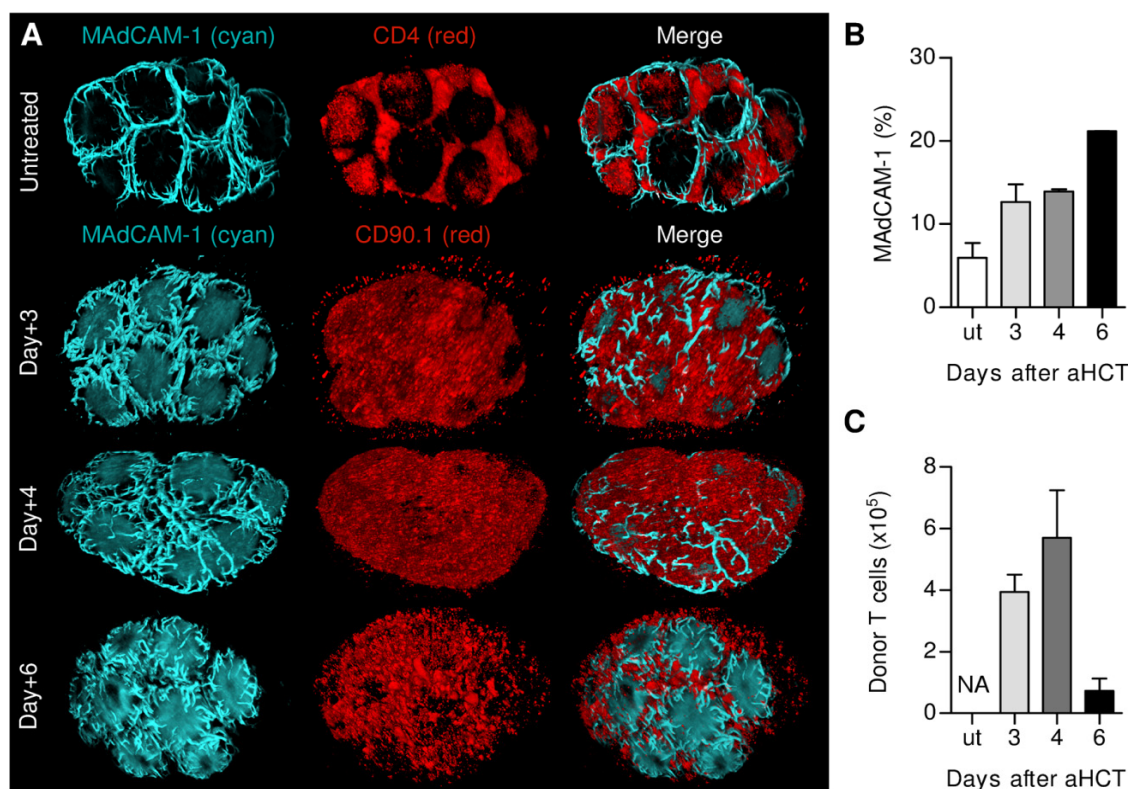
Figure 4.6: Visualizing and quantifying cellular changes after allo-HCT in 3D. Bone marrow together with CD90.1[+] transgenic T cells were transplanted into irradiated allogeneic recipients to induce acute GVHD. CD90.1 or CD4 antibody, respectively, was injected i.v. MAdCAM-1 was stained *ex situ*. (**A**) Representative PPs of untreated (upper line) and transplanted mice highlight differences in MAdCAM-1 expression and numbers of donor T cells. (**B**) After allo-HCT MAdCAM-1 is highly upregulated in the PPs, particularly in follicular areas. (**C**) Quantification of donor T cells in the entire PP demonstrate proliferation until day+4. By day+6 most donor T cells exit as confirmed by BLI. Shown is one representative experiment of two with 2-4 mice per time point.

increased by more than 50% and was even higher during the effector phase on day+6 after allo-HCT. At this point we found a massive MAdCAM-1 upregulation in follicular B cell areas (Figure 4.6B). Donor T cell numbers in the entire PP increased between day+3 and day+4 (Figure 3.6C), demonstrating active cell recruitment and proliferation. By day+6 most donor T cells disappeared from the PPs indicating migration to peripheral GVHD target organs as confirmed by immunofluorescence microscopy of PP cross-sections (see 4.1.3.2 Confirming cell quantification within Peyer's patches after HCT). On day+3 and day+4 high numbers of

donor T cells also located to MAdCAM-1 positive follicular areas which mostly disappeared by day+6.

4.1.3.1 Cell counting

Although we could clearly identify single T cells (stained for CD4, CD90.1 or CD45.1), dense lymphocyte clustering within PPs impeded automated counting. To overcome this limitation we measured T cells at less dense areas to quantify the mean volume per cell from the rendered voxel data (Figure 4.7A-F). The most frequent cell size was measured at 200-400µm^3 and averaged at 435.6 µm^3 ± 19.7 (n = 233). To confirm this measurement with a well-established method we used confocal microscopy and indeed detected similar values (most frequent cell size 200-400 µm^3, mean 561.1 µm³ ± 33.4, n = 195), supporting the volumes measured by LSFM. The size measurements may not reflect *in vivo* conditions of a CD4$^+$ T cell. However, we could use the mean volume of a cell to calculate absolute T cell numbers in whole PPs. Now, upon allo-HCT the volume of an alloreactive T cell can dramatically change during activation. In fact, we found a significant increase of mean T cell volume (826.9 µm^3 ± 17.2, n = 816) at day+3 after allo-HCT, that did not significantly differ to T cell volumes on day+4 and day+6. To avoid inexact enumeration caused by changing volume of donor T cells due to cell activation, we calculated mean values for day+3, day+4 and day+6 after allo-HCT, respectively (Figure 4.7G-J).

To further evaluate the approach of T cell number quantification via volume measurement, we compared three different ways to quantify absolute cell numbers by LSFM (Figure 4.8). First, we counted cells manually within a defined tissue volume and found 177 cells in total. Next, we counted 171 cells automatically within the same tissue via a Volocity software based computer algorithm described in the Methods section. Lastly, we quantified cell numbers by cell volume based calculation within the same tissue area and calculated 189 cells.
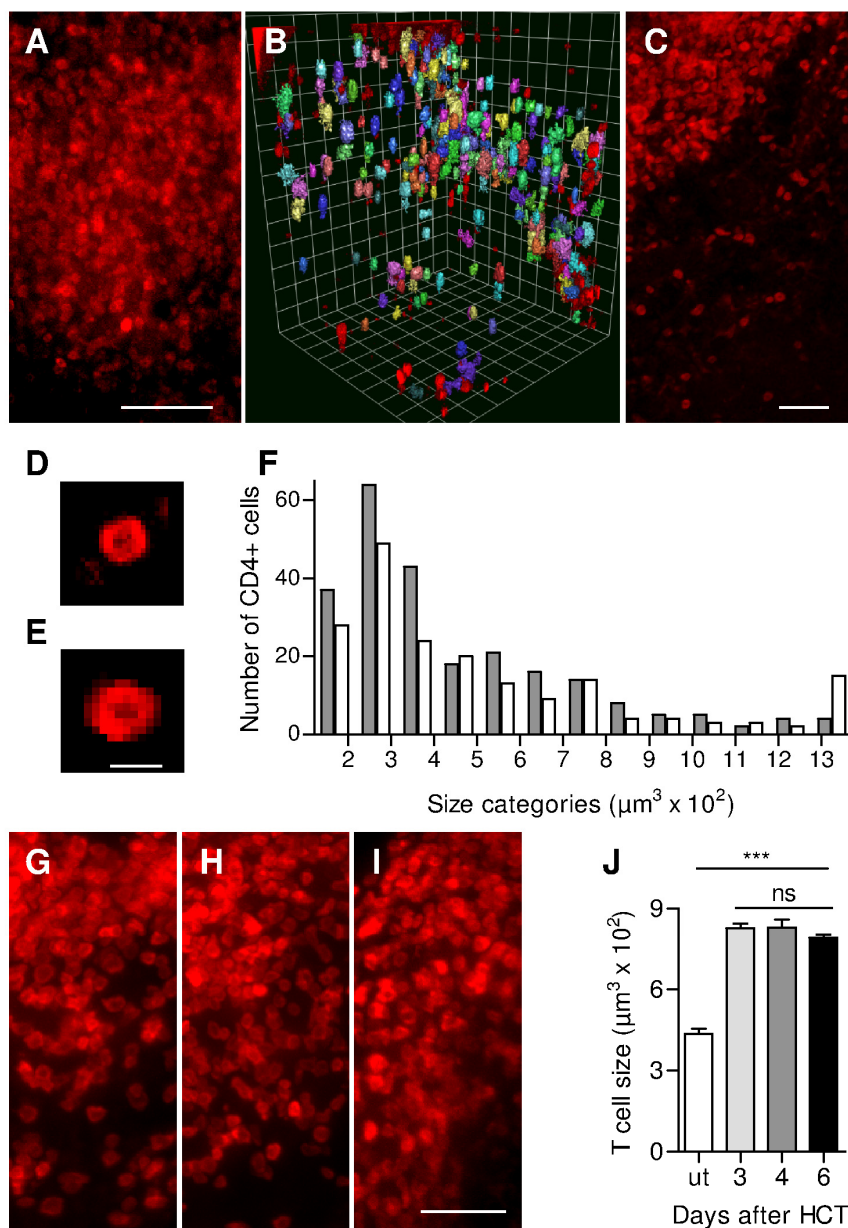
Figure 4.7: Quantification of T cells in intact PPs.
(A) Clustering of T cells within a PP (CD4, red) impede automated cell counting (z-Projection; scale bar: 50 μm).
(B) To calculate cell volumes, single CD4$^+$ cells are rendered (colored objects) and measured at less dense areas. (C) Comparison of cell imaging with confocal microscopy and LSFM measurements (z-Projection; scale bar: 50 μm). Representative single cells imaged with (D) LSFM and (E) confocal microscopy using a 20x objective (z-Projection; scale bar: 10 μm). (F) Size distribution of measured CD4$^+$ cells shown for LSFM (grey bars; mean volume 435.6 μm³ ± 19.7, n = 233) and confocal microscopy (white bars; mean volume 561.1 μm³ ± 33.4, n = 195). (G) Donor T cells on day+3, (H) day+4 (I) and day+6 after HCT (z-Projections; scale bar: 50 μm). (J) Mean T cell volume was increased during activation (day+3 mean volume 826.9 μm3 ± 17.2 n = 816; day+4 mean volume 830.2 μm3 ± 27.9 n = 301, day+6 mean volume 788.8 μm3 ± 15.2 n = 976). Statistics: ANOVA, Bonferroni corrected (ns = P>0.05, *** = P<0.001).
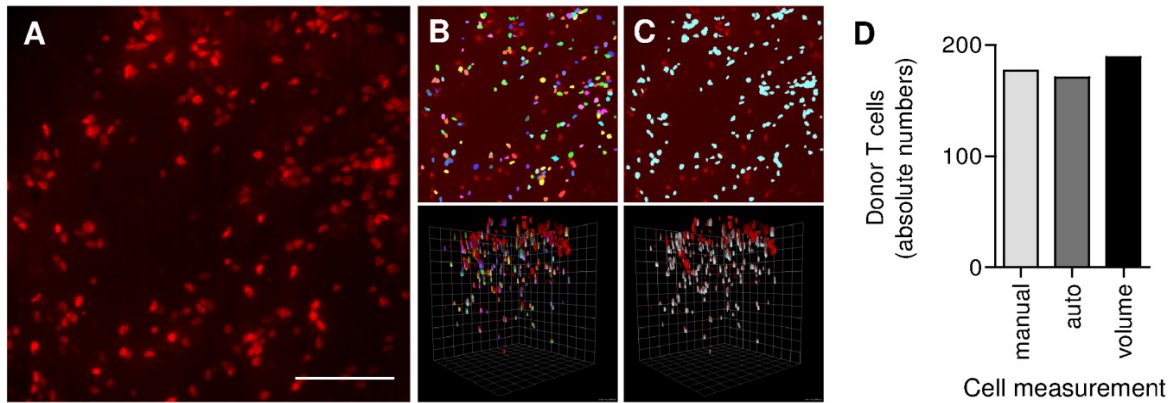
Figure 4.8: Comparison of T cell number quantification via volume measurement with manual or automated cell counting procedures. (**A**) Using LSFM we imaged several non-clustering donor T cells (red, CD45.1[+]) infiltrating the intestinal mucosa at day+4 after allo-HCT (20x objective, increment: 3 μm, z-Projection from 150 sections, Scale bar: 100μm). (**B**) Colored objects indicate cells after automatic counting based on a software algorithm (Volocity) described in the Methods section. Volume calculations and automated cell counting. Z-Projection (upper image) and 3D rendered image (below). (**C**) Cyan indicates volume rendered objects. Z-Projection (upper image) and 3D rendered image (below). (**D**) Comparison of T cell numbers counted manually, automatically with Volocity software or quantified by volumetric calculation based on the mean value of day+4 T cell volumes (830 μm^3) to assess absolute T cell numbers within tissues.

4.1.3.2 Confirming cell quantification within Peyer's patches after allo-HCT

In order to validate cellular quantification demonstrated by LSFM with another already established method we analyzed PPs after allo-HCT with flow cytometry. We transplanted 5 x 10^6 bone marrow cells together with 2 x 10^6 B6.L2G85.CD90.1 T cells into irradiated BALB/c to induce acute GVHD and analyzed PPs at day+3, day+4, and day+6. Although flow cytometry is perfectly suited to analyze the relative cellular distribution within various organs, for the purpose of analyzing absolute T cell numbers in PPs, two major limitations had to be accounted for. First, in contrast to lymph nodes the excision of PPs is inaccurate and the surrounding mucosal tissue is biasing the FACS analysis. This issue becomes critically important when many donor T cells have entered the intestinal mucosa as it occurred on day+6 after allo-HCT (compare Figure 4.5, day+6, *ex vivo* BLI and LSFM overview). Second, the massive loss of cells during the preparation of the single cell suspension from PPs (cutting, digestion, cell strainer, washing steps, etc) impedes the calculation of exact cell numbers. To circumvent a bias caused by mucosal T cell infiltration we analyzed donor T cell numbers from equivalent pieces (in number and size) of PPs and small bowel samples and subtracted the detected cell numbers as displayed in Figure 4.9. However, for the given reason we doubt that the cell numbers of PPs after allo-HCT determined by flow cytometry reflect the correct cell numbers.
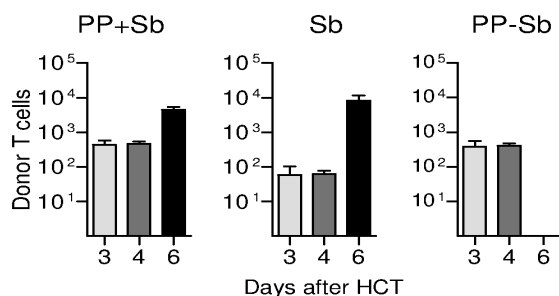
Figure 4.9: Flow cytometry analysis of PPs. Bone marrow cells together with CD90.1$^+$ transgenic T cells were transplanted into irradiated allogeneic recipients to induce acute GVHD. At day+3, day+4 and day+6 PPs and equivalent pieces (5-6 PPs/mouse) of small bowel (sb) were excised and digested (2 mg/ml collagenase D and 0.1 mg/ml DNaseI, at 37°C for 30 min) for FACS analysis. Cells were suspended in equal volumes and stained for CD90.1 and CD45.2 to identify donor T cells. Dead cells were excluded by PI staining. Shown is one representative experiment of two with 4 mice per time point.

Hence, we further validated the LSFM data by two alternative established approaches, namely BLI and IFM. We quantified the BLI signal of luciferase$^+$ donor cells projecting to PPs (Figure 4.10A,B). Importantly, again we subtracted background signal (measured in small bowel areas without PPs) enhanced by small bowel infiltrating T cells and obtained comparable results to quantification with LSFM. Additionally we quantified donor T cells from a whole PP cross-section and again found similar changes in cell numbers within PPs (Figure 4.10C,D). Taken together, both semi-quantitative methods underpin our cellular LSFM results (specifically the rapid decline of donor cells between day+4 and day+6 after allo-HCT).
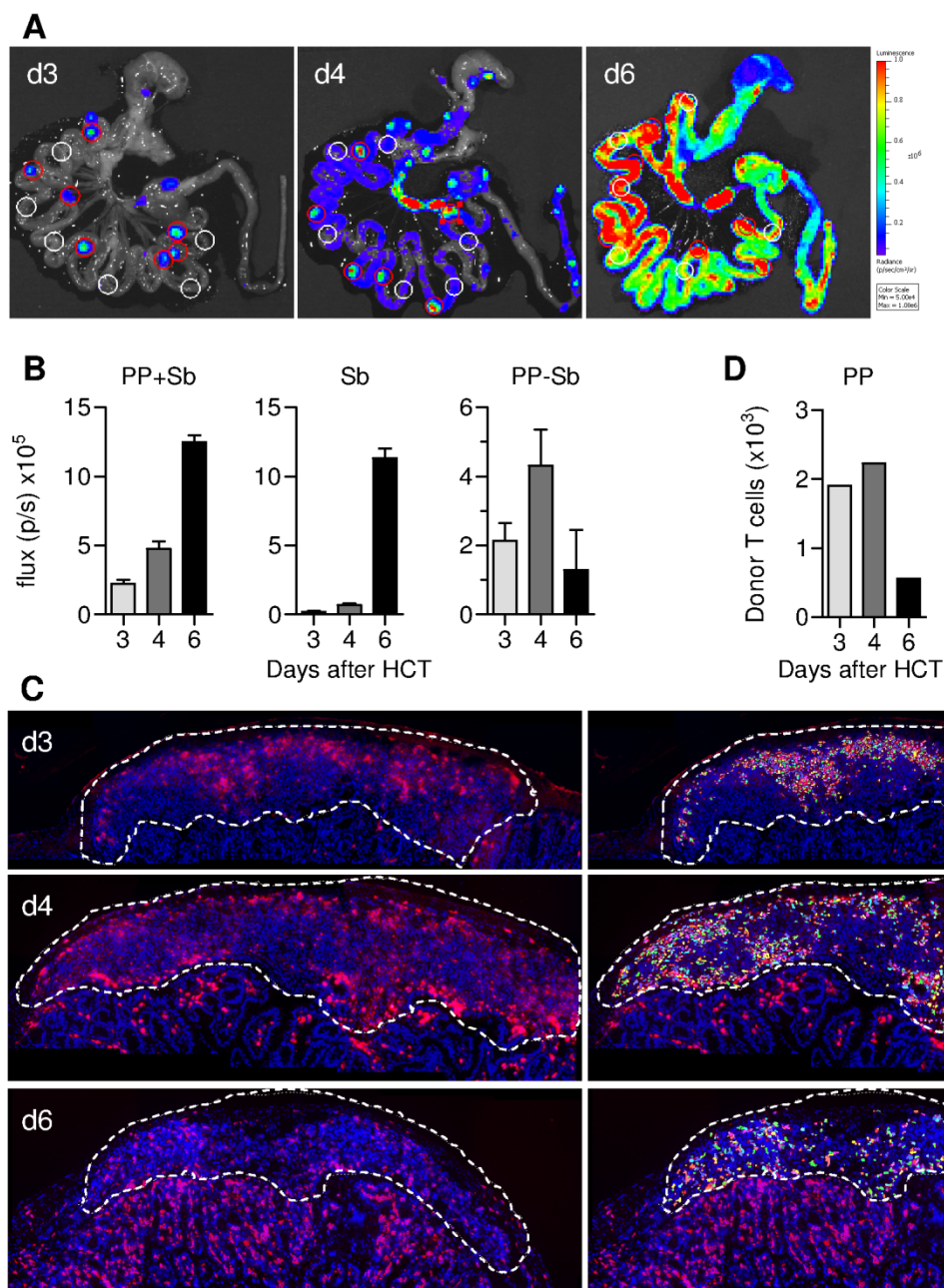
Figure 4.10: Visualizing and quantifying cellular changes within Peyer's patches after allo-HCT. Bone marrow together with CD90.1[+] luciferase[+] transgenic T cells were transplanted into irradiated allogeneic recipients to induce acute GVHD. (A) *Ex vivo* BLI was performed at the transition from GVHD initiation phase to effector phase (day+3 and day+4 after allo-HCT) and at the effector phase (day+6). (B) Emitted photons of donor T cells in PPs (red circles) or intestinal mucosa (Sb, white circles) were quantified respectively. (C) PPs from day+3, day+4 and day+6 were stained for donor T cells with CD90.1 (red) and DAPI (blue) and whole PP sections were imaged in high-resolution with IFM (20x) and stitched together. Donor T cells were automatically counted with the Software Volocity (colored objects) by determining nuclei with a high MFI in the red channel, indicating cellular staining. (D) Quantification of whole PP sections. (scale bar: 500 μm).

4.1.3.3   Imaging donor T cells

We analyzed the suitability of fluorescent proteins for the detection of donor T cells with LSFM. Therefore, either we transplanted 4 x 10^6 B6.L2G85.DsRed splenocytes together with

5 x 10^6 C57Bl/6 bone marrow cells into BALB/c recipients. Using *in vivo* BLI we followed the T cell proliferation until day+3, day+4 or day+6 and we prepared PPs of recipients for LSFM. Although donor T cells could be detected with BLI *ex vivo*, after fixation and clearing of the sample we could not detect any DsRed⁺ signal neither with LSFM, nor with confocal and MPM (Data not shown). However, in tissue sections that were not fixed and cleared, we detected DsRed⁺ donor cells using IFM (Figure 4.11A). This observation indicates a loss of fluorescent protein signal due to the sample preparation for LSFM (fixation and clearing). To rule out whether PFA fixation affects the fluorescent proteins, we analyzed single DsRed⁺ cells with FACS (Figure 4.11B). Untreated DsRed⁺ spleen cells were easily detectable with FACS (MFI: 441), already 1 h after PFA fixation the cells had a 4 fold decreased MFI (MFI: 129). After 7d the MFI of DsRed⁺ cells (MFI: 18.9) was comparable low to wt cells (MFI: 3.5). Hence, we found that PFA exposure can dramatically affect the brightness of DsRed⁺ cells even before tissue dehydration or BABB treatment maybe further affect the brightness of the fluorescent protein.
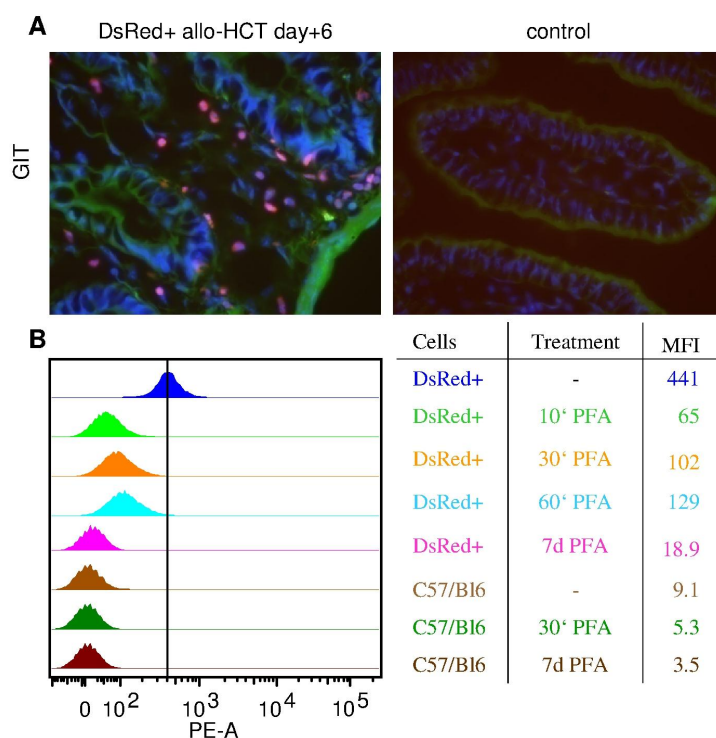
Figure 4.11: PFA treatment affects fluorescent proteins. (A) DsRed⁺ donor T cells were detectable in tissue samples of allogeneic recipients with IFM, but could not be detected in samples that were fixed and cleared for LSFM (not shown). (B) To evaluate the influence of PFA fixation to fluorescent proteins, we treated DsRed⁺ and C57Bl/6 cells with PFA before analyzing the MFI with FACS.

Cells	Treatment	MFI
DsRed+	-	441
DsRed+	10' PFA	65
DsRed+	30' PFA	102
DsRed+	60' PFA	129
DsRed+	7d PFA	18.9
C57/Bl6	-	9.1
C57/Bl6	30' PFA	5.3
C57/Bl6	7d PFA	3.5

Since in our hands the sample preparation for LSFM impeded the successful detection of DsRed or GFP marked T cells, we used congenic markers (CD45.1 or CD90.1) to label donor T cells. Although the CD90.1 staining as congenic marker was sufficient for detection and counting of donor T cells, the display of the cells suffered from inhomogeneous labeling (Figure 4.12). Most cells displayed spots with 2-3 agglomerates of antibody, giving a much higher signal than the surface staining by itself. This was observed for the commercial available clones OX-7 and HIS51 and suggested clustering of the CD90 surface protein in the T cell membrane. In comparison when we stained for CD4 we achieved a homogenous

surface staining without any antibody agglomerations. This phenomenon was not only observed when we imaged intact tissues with LSFM but as well with conventional fluorescence microscopy imaging of stained cells that were placed on microscope slides (Figure 4.12). To guarantee an accurate visualization of the donor T cells we stained for CD45.1 and found that this antibody also resulted in a homogenous cell surface staining. While CD90 is expressed on T cells only, CD45 is expressed on all hematopoietic cells but mature erythrocytes and platelets and can also be used as congenic marker. Hence, we decided to utilize T cells from donor CD45.1$^+$ mice for all subsequent experiments.
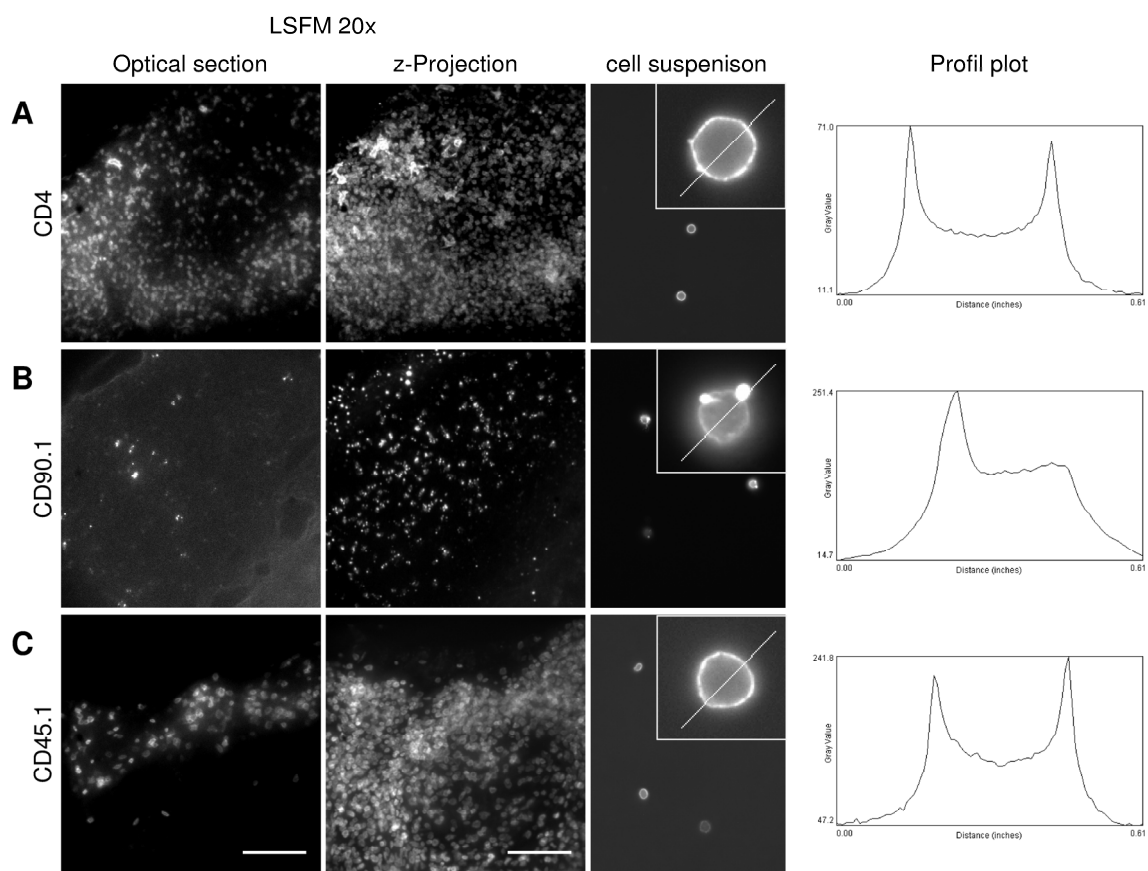
Figure 4.12: Assessment of donor T cell staining with congenic markers. (**A**) CD4 staining of intact tissues, as well as single cell suspensions resulted in a uniform membrane staining of CD4$^+$ cells. (**B**) When tissues of CD90.1$^+$ T cells recipients were stained for CD90.1, donor cells appeared heterogeneously labeled. Most T cells displayed one to three intense fluorescent surface clusters, resulting in a decreased image quality. These surface antibody agglomerations were also detectable in stained single cell suspensions. (**C**) Contrary, tissues of CD45.2$^+$ recipients stained for CD45.1 revealed uniformly labeled T cells. Scale bar: LSFM: 100 µm.

4.1.4   Visualizing and counting rare events with LSFM

As we were able to reliably visualize and quantify high numbers of donor T cells in PPs after HCT we tested whether multicolor LSFM is also capable of detecting rare cellular events. To this end we adoptively transferred FACS sorted CD4$^+$ T cell subsets (CD62L^{hi}CD44^{lo} naïve T$_N$ cells, CD62L^{hi}CD44^{hi} central memory T$_{CM}$ cells and CD62L^{lo}CD44^{hi} effector memory T$_{EM}$

cells) as defined by Sallusto et al. (1999) from CD45.1$^+$ donors (Figure 4.13A). Whole PPs and mLNs of the recipients were analyzed 20 h after T cell transfer. Using the software Volocity we established an algorithm (see section 2.2.15 Volume calculations and automated cell counting) that enabled us to automatically identify and count individual cells and found that T_N cells (mean 726 cells/PP) homed more efficiently than T_{CM} cells (mean 478 cells/PP) to PPs (Figure 4.13B,C) and to mLNs (Figure 4.14). Within the same experiment a similar homing trend to SLOs was confirmed by FACS analysis of the spleen (data not shown). T_{EM} cells are preferentially localized in non lymphoid tissues instead of SLOs (Masopust et al., 2001). In line with this, LSFM revealed low numbers of T_{EM} (mean = 81/PP) homing to PPs (Figure 4.13B,C). Most T_{EM} cells located in proximity to MAdCAM-1 expressing HEVs, indicating homing to the T cell zone.

Autofluorescence (grey) CD45.1 Donor T cells (red) MAdCAM-1 (cyan)
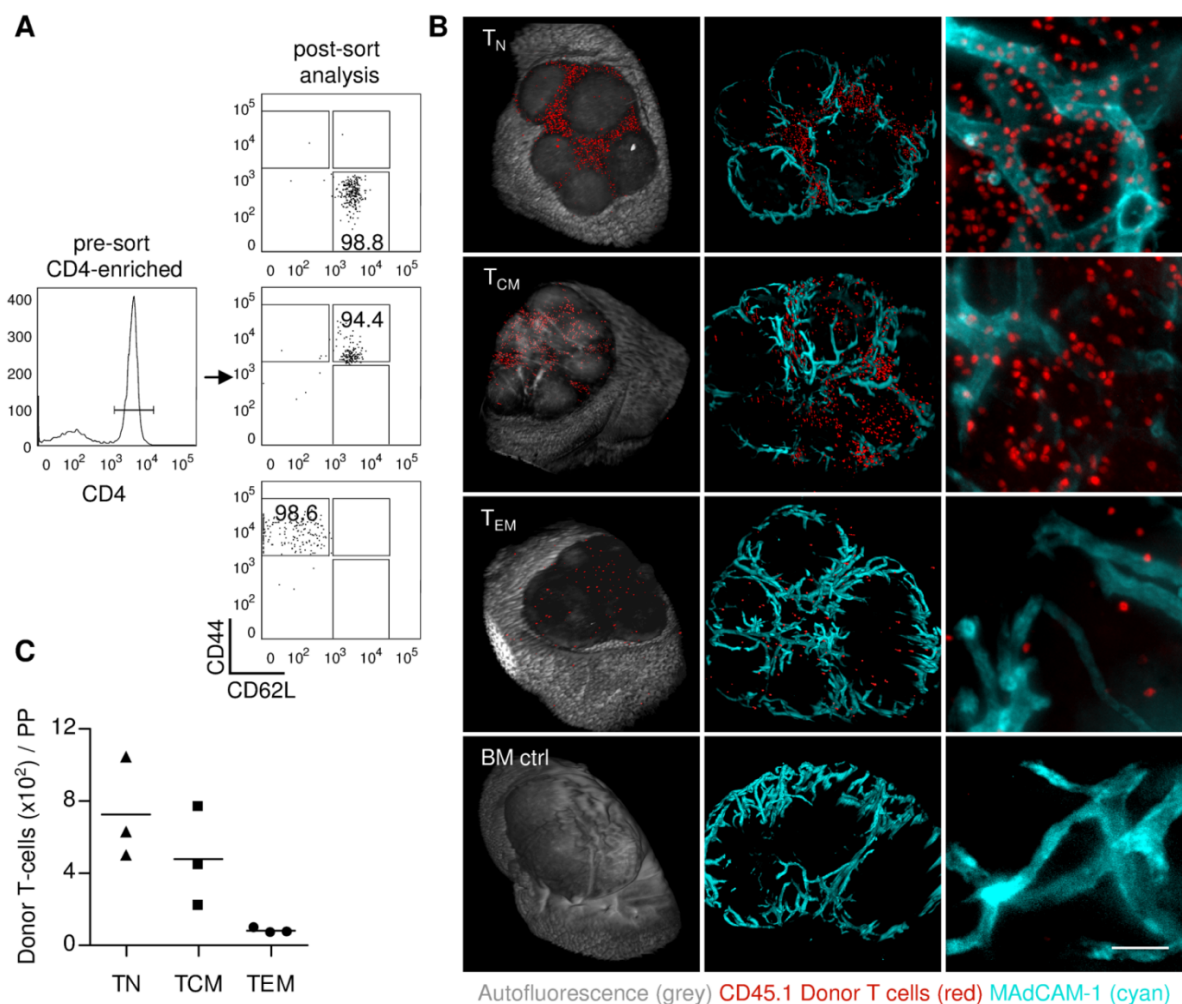
Figure 4.13: Detection of T cell homing by multicolor LSFM. (**A**) MACS-enriched CD4$^+$ T cells (C57Bl/6-L2G85 CD45.1$^+$) were sorted into T_N (CD44hiCD62Llo) T_{CM} (CD44hiCD62Lhi) and T_{EM} (CD44loCD62Lhi) and adoptively transferred into C57Bl/6 CD45.2$^+$ recipients. (**B**) LSFM imaging of whole PPs allowed the detection of donor T cells 20 h after transfer. Left panel: 3D reconstruction of PPs autofluorescence (grey) and isosurface of T cells included in the automated quantification. Central Panel: 3D reconstruction of MAdCAM-1$^+$ HEV (cyan) and isosurface of counted T cells (red). Right panel: representative section of the T cell area (20x, z-Projection, scale bar: 50 µm). (**C**) Quantification of transferred T cell numbers in the PPs (n = 3/group) revealed a better homing capacity of T_N and T_{CM} over T_{EM}. In contrast T_{EM} homed more efficiently to the liver (not shown). Antibody staining

was performed *ex situ*.
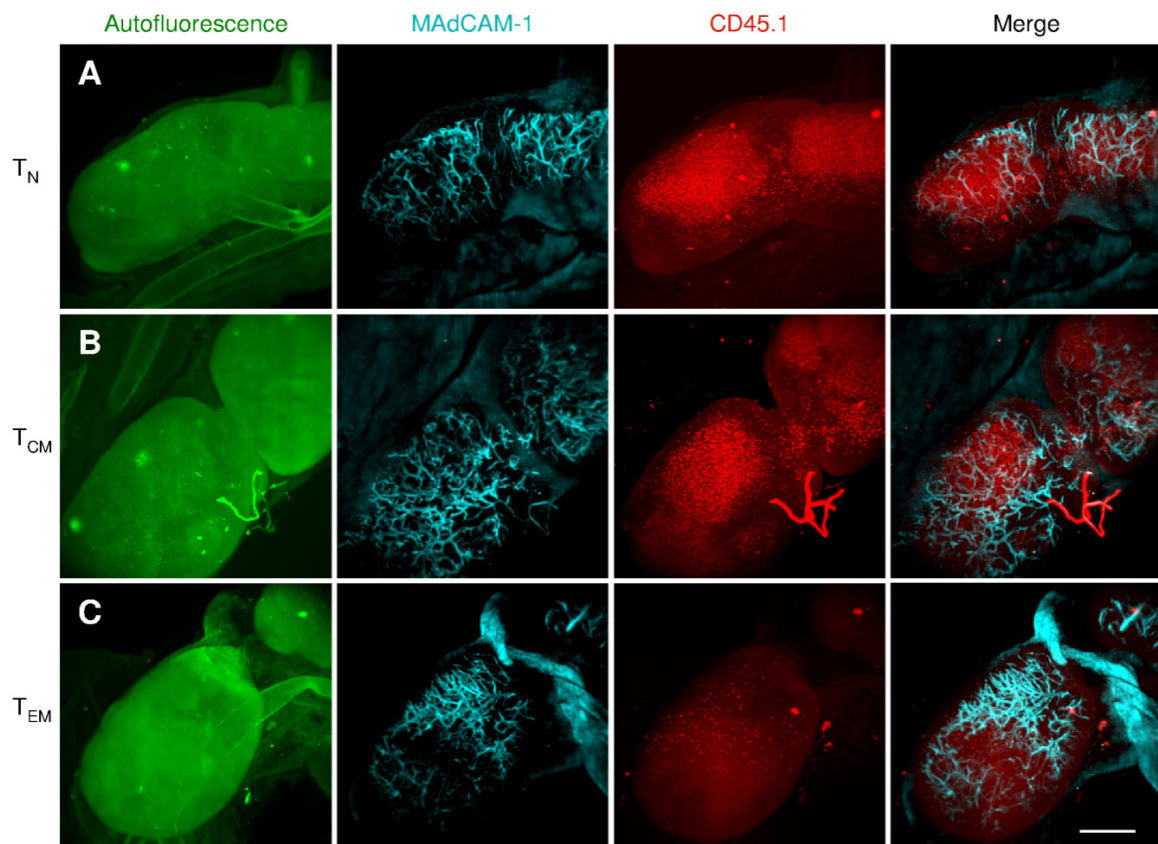
Figure 4.14: Homing capacity of individual T cell subsets to mesenteric lymph nodes. LSFM imaging of whole mLNs allowed the detection of donor T cell subsets 20 h after transfer. According to the homing capacity to PPs, T cell numbers in the mLNs revealed a better homing capacity of (**A**) T_N and (**B**) T_{CM} over (**C**) T_{EM} (z–Projections, scale bar: 500µm).

4.2 Relevance of tissue alloantigen expression for selective GVHD organ manifestation

4.2.1 Alloantigen tissue expression determines organ infiltration of TCR transgenic CD8^{+} T cells after allo-HCT

To overcome the limitation of MHC- and miHAg-mismatched transplant models of GVHD that face the difficulty in determining the specific alloantigen that the responding T cells recognize, we employed TCR-transgenic T cells. The specificity of the TCR-transgenic T cells is restricted to a single peptide epitope that is either constitutively expressed in all organs or only in selected organs of the recipient. By employing such a model system we aimed to establish a model of allo-HCT that would be defined by a single antigen-mismatch recognized by donor T cells.

To this end, we used TCR transgenic CD8^{+} T cells reactive with the OVA peptide SIINFEKL in the context of MHC class I H-2K^b (OT-I T cells) (Hogquist et al., 1994), to study antigen dependent T cell allo-responses after HCT (

Figure 4.15). Consequently we transplanted 2 x 10^6 splenocytes from B6.L2G85.OT-I.Ragko.CD90.1 (CD8$^+$ cell purity: > 80%) together with 5 x 10^6 BM cells from C57BL/6 into myloablative irradiated recipients (9 Gy) that matched in age and sex. The recipients expressed the cognate antigen either in all organs (βa-Ova), selectively in the pancreas (RIP-mOva), an organ that is normally unaffected by GVHD, or did not express ovalbumin at all (B6). We assessed weight change, and performed *in vivo*
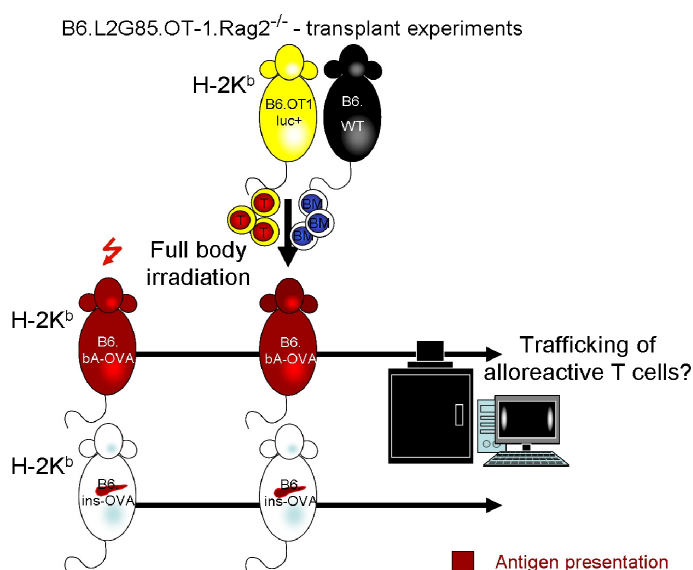
Figure 4.15: Scheme of T cell transplantation in a defined single antigen mismatch model. TCR-transgenic B6.L2G85.OT-1.CD45.1 T cells together with bone marrow of a C57Bl/6 were injected into lethal irradiated B6a.βa-Ova, B6a.ins.ova or B6a recipients. Trafficking of alloreactive T cells *in vivo* was performed using BLI and at selected time-points by *ex vivo* BLI, flow cytometry, immunofluorescence microscopy or LSFM to analyze T cell migration at higher resolution.
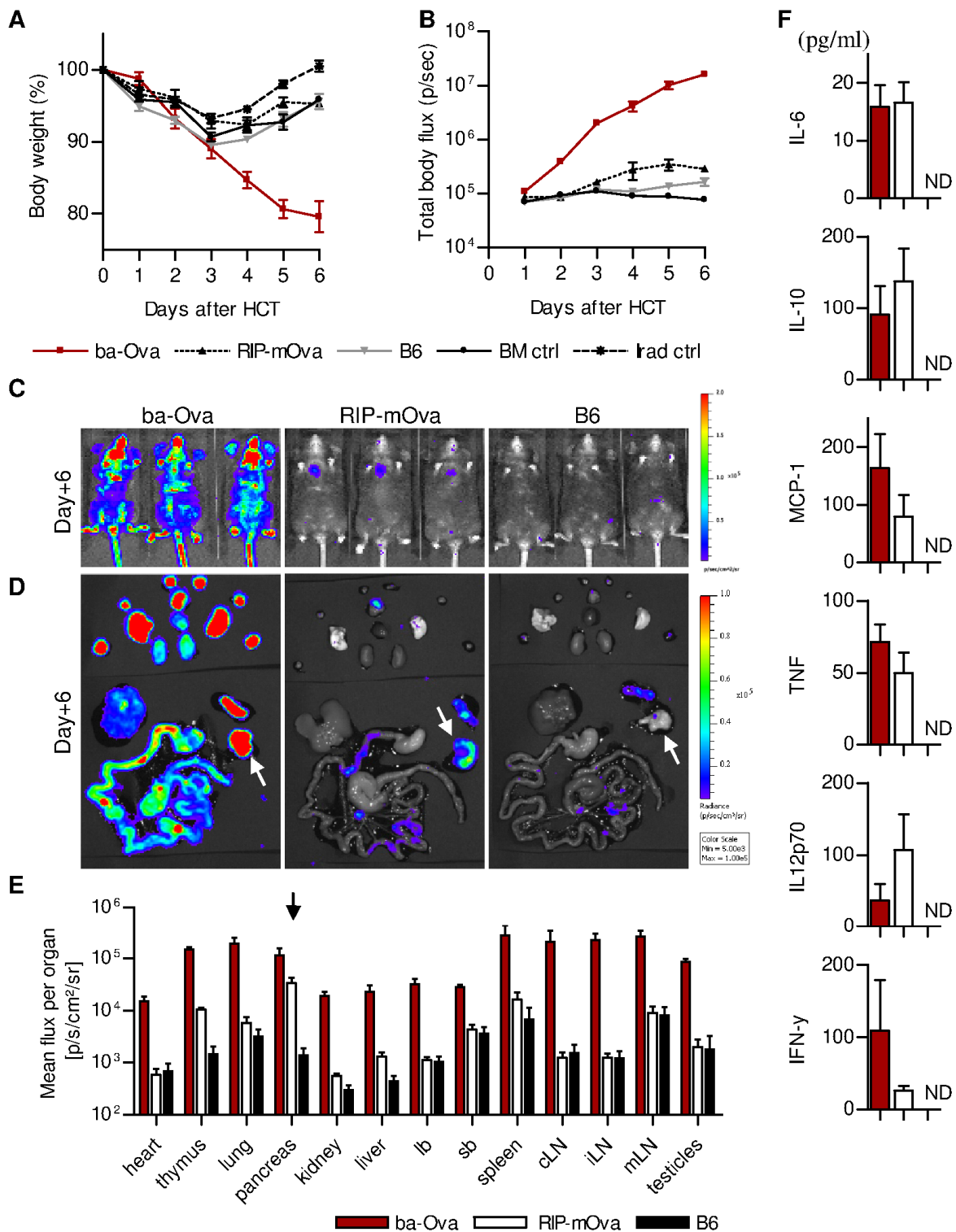
Figure 4.16: TCR transgenic CD8$^+$ T cell migration after HCT is influenced by single alloantigen expression in the tissue.
(A) Body weight change after allo-HCT of 2 x 10^6 luciferase$^+$ OT-I T cells together with 5 x 10^6 BM cells from a C57BL/6 donor into βa-Ova, RIP-mOva or B6 recipients. **(B,C)** *In vivo* BLI of recipients allowed a general assessment of T cell proliferation. **(D)** At day+6 after allo-HCT *ex vivo* BLI is pinpointing to specific T cell distribution (pancreas is indicated by an arrow) and **(E)** quantification of organ infiltration. (F) Serum levels of IL-6, IL-10, MCP-1, TNF, IL12p70 and IFN-y at day+6 after allo-HCT (ND indicates not detected).

BLI to analyze T cell proliferation and migration after allo-HCT. Until day+3 all OT-I T cell recipients as well as BM control and irradiation control lost about 10% of their initial body

weight (Figure 4.16A). While βa-Ova recipients lost up to 20% of weight until day+6 after HCT all other recipients regained weight. Unfortunately, the black fur of the recipient mice hindered the *in vivo* detection of photons from donor OT-I T cells and thus allowed only a general assessment of total flux. Allo-HCT of OT-I T cells into βa-Ova recipients resulted in a strong acceleration of photon emission starting at day+1 after HCT indicating a high T cell responsiveness followed by proliferation (Figure 4.16B). In comparison to B6 recipients RIP-mOva mice showed a slight signal increase starting at day+3 after HCT. At day+6 after HCT in βa-Ova donor T cell distribution apparently span the whole body while in RIP-mOVA mice the BLI signal seemed to project to the thymus but no further reliable information on specific organ infiltration could be gathered. Hence, we euthanized the recipients and performed *ex vivo* BLI to further evaluate organ infiltration by donor T cells at day+6 after HCT. The imaging of the resected organs (cLNs, thymus, heart, lung, kidneys, iLNs, liver, spleen, pancreas, and gastrointestinal tract) provided higher resolution of selective signal distribution and revealed an overall organ infiltration of OT-I T cells in βa-Ova recipients (Figure 4.16D). In RIP-mOva mice we found photon emission by donor T cells in the spleen, the mLNs, to some extend in the small bowel and mainly in the thymus and the pancreas. In B6 recipients that do not express ovalbumin at all, BLI revealed OT-I T cells only in the spleen and partially in the small bowel (here probably within PPs). Measurements of the mean flux (photon emission/ second/ cm^2) per organ confirmed an overall organ infiltration of OT-I T cells within βa-Ova recipients (Figure 4.16E). All organs of βa-Ova mice showed higher OT-I cell infiltration than organs of RIP-mOva or B6 recipients. We found especially high mean flux values per organ in SLOs (spleen, cLN, iLN, and mLN), thymus, lung, and pancreas that exceeded 1×10^5 photons/sec/cm^2. Compared to B6 recipients RIP-mOva mice showed a significant higher OT-I cell infiltration only in the thymus, lung, and pancreas whereas in liver, small bowel, spleen, and mLNs only little higher flux was detectable.

After BLI the resected organs were either snap frozen or stored in 4% PFA for histopathological analysis. Immunhistochemistry staining of CD90.1 revealed donor OT-I T cells distribution in diverse organs of different recipients (Figure 4.17). While donor OT-I T cells scattered throughout the whole spleen of βa-Ova recipients, in RIP-mOva and B6 recipients they mainly adhered to the red pulp (Figure 4.17A, spleen). The pancreas of βa-Ova recipients was heavily infiltrated by OT-I T cells while no OT-I T cells were found in B6 recipients. Remarkably, in pancreas of RIP-mOva recipients OT-I donor T cell infiltration was almost exclusively restricted to the islets (Figure 4.17A,B). Similar to other organs the large bowel and liver of βa-Ova recipients were severely infiltrated by OT-I T cells. In comparison, only few OT-I T cells could be identified in the large bowel but not in the liver of RIP-mOva recipients and no OT-I T cells were detectable in B6 recipients. The histopathological GVHD scoring of typical GVHD target-tissues from βa-Ova revealed grade 2 GVHD in the large

bowel, grade 1 GVHD in the liver, while no symptoms of GVHD was detectable in the skin by day+6 after HCT (Figure 4.17C). No signs of GVHD were detectable in GIT, liver or skin of RIP-mOva and B6 recipients.
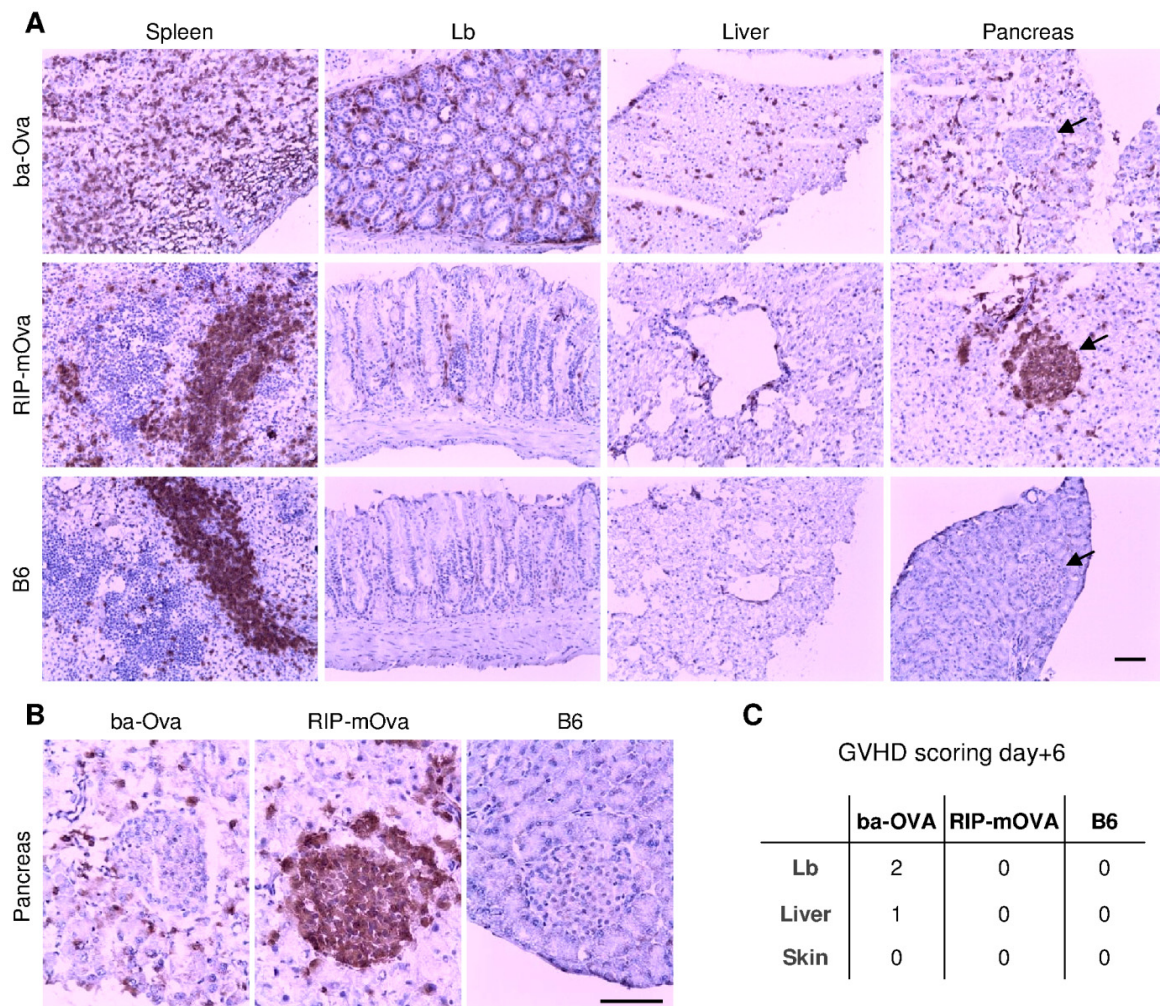
Figure 4.17: Histopathological analysis of CD90.1[+] donor OT-I cell infiltration of different recipient tissues. (A) At day+6 after single antigen mismatch allo-HCT of 2×10^6 OT-I T cells, recipients tissues, such as spleen large bowel (Lb), liver, and pancreas were investigated after immunhistochemistry staining. Pancreatic islets, indicated with arrows, **(B)** are shown with higher magnification. **(C)** GVHD scoring at day+6 after allo-HCT was performed by an experienced pathologist (Stephan Schulz).

We repeated the experiment with the same conditions, by using male donors and recipients. The results of this experiment are shown in Figure 4.18 and confirmed previous findings. Since more mice per group were available (n ≥ 8 mice/group) we additionally assessed survival of remaining mice after sacrificing 3 mice/group for *ex vivo* BLI at day+6 after HCT. Until day+3 all OT-I T cell recipients as well as BM control and irradiation control lost about 10% of their initial body weight (Figure 4.18A). While βa-Ova recipients lost up to 20% of weight until day+6 after HCT all other recipients regained weight. Again, initially all mice lost body weight until day+3, while βa-Ova recipients lost weight until day+6 after HCT. At day+6 βa-Ova recipients crouched with a hunchback and displayed clinical GVHD symptoms after OT-I T cell transplantation. Surprisingly, shortly thereafter those mice regained rapidly weight

61

and by day+14 after HCT reached more than 110% of their initial body weight. Bone marrow control mice as well as B6 recipients of OT-I T cells regained weight already after day+3 and weighed more than 100% at day+25 after HCT. In contrast, RIP-mOva recipients started again losing weight at day+6 after HCT. Two of three RIP-mOva mice died at day+8 and the last mouse died 14 days after HCT.

C

	Donor cells / 10 HPFs (mean ± SD)		
	ba-Ova	RIP-mOva	B6
Kidney	290.7± 8.4	3.3 ± 3.0	0 ± 0
Lb	332.7 ± 39.8	12.7 ± 2.1	1.7 ± 1.5
Sb	252.3 ± 15.0	29.7 ± 9.3	8.3 ± 0.6
Pancreas	244 ± 48.7	120.3 ± 69.7	0 ± 0
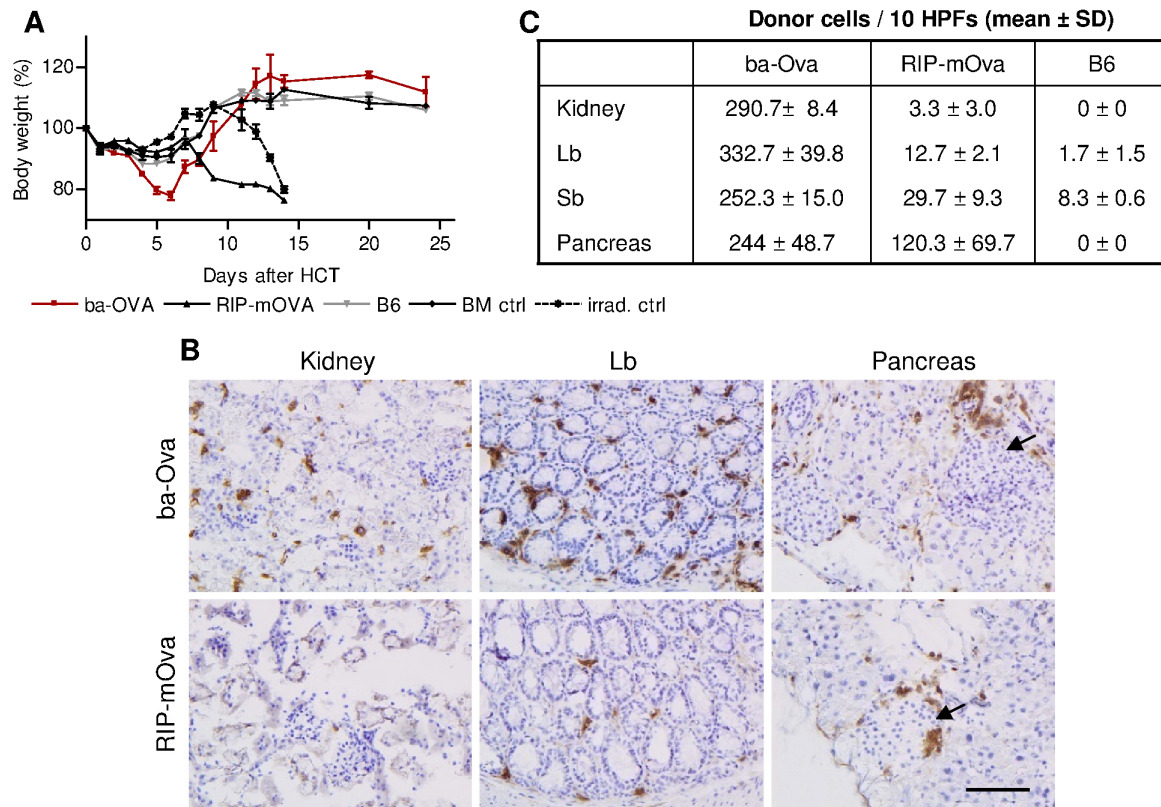
Figure 4.18: Cognate antigen expressing tissue is infiltrated by OT-I T cells after single antigen mismatch HCT. (A) Body weight change of different recipients after allo-HCT of OT-I T cells. **(B)** Immunhistochemistry staining of CD90.1[+] OT-I T cells in kidney, large bowel (Lb) and pancreatic tissue of βa-Ova and RIP-mOva recipients at day+6 after allo-HCT. Arrows indicating pancreatic islets (Scale: 100 µm). **(C)** CD90.1[+] OT-I T cells were counted in 10 representative high power fields (HPFs) of kidney, large bowel (Lb), small bowel (Sb) and pancreas and mean values ± standard deviations are listed.

Immunohistochemistry staining revealed CD90.1[+] donor OT-I T cells in selected tissues of different recipients. We counted donor T cells per 10 high power fields (HPFs) and found similar numbers in different organs of βa-Ova recipients, ranging from 244 ± 48.7 (Mean ± SD) OT-I T cells within the pancreas to 332.7 ± 39.8 (mean ± SD/ HPF) OT-I T cells in the large bowel. In contrast, RIP-mOva mice had only very few OT-I T cells in the kidney 3.3 ± 3.0 (mean ± SD / HPF) some more OT-I T cells were found in the large bowel (29.7 ± 9.3, mean ± SD / HPF) and many OT-I T cells could be detected in the pancreas (120.3 ± 69.7, mean ± SD / HPF). Although BLI signal intensity of large bowel and small bowel of RIP-mOva and B6 recipients were comparable, little less OT-I T cells were found in B6 recipients using immunohistochemistry. However, no OT-I T cells were found in kidney or pancreas of B6 recipients.

4.2.2 Effective T cell mediated destruction of single alloantigen expressing target tissues

In contrast to previous studies that reported about insufficiency of single antigen disparity to cause GVHD (Fontaine et al., 2001) Toubai et al. (2012) found that a single H-Y antigen disparity can cause GVHD, when transferring sufficient numbers of alloreactive precursor cells. In our experiments we found donor T cells effectively infiltrating alloantigen expressing tissues on day+6 after allo-HCT. This implies that the transferred number of T cells was sufficient to evoke an alloantigen response, including effective T cell priming, proliferation and migration to the alloantigen expressing tissues.

To test whether the specific infiltration of alloantigen expressing tissues is dependent on high numbers of alloreactive precursor cells, we next decreased the numbers of transferred T cells. Therefore, we FACS sorted OT-I CD45.1$^+$luciferase$^+$ cells (CD8$^+$ post sort purity: 99.5%) and transplanted either 1 x 10^6, 1 x 10^5, 1 x 10^4 or 1 x 10^3 T cells together with 5 x 10^6 C57Bl/6 bone marrow cells either into irradiated βa-Ova (n = 4 mice/group) or RIP-mOva (n = 5 mice/group). As syngeneic control we transplanted 1 x 10^5 OT-I T cells together with 5 x 10^6 C57Bl/6 bone marrow cells into C57Bl/6 recipients. We analyzed luciferase$^+$ T cell proliferation using BLI, measured blood glucose and assessed weight change and survival. We imaged RIP-mOva with BLI on day+6 after allo-HCT and detected T cell proliferation in mice receiving 1 x 10^6 or 1 x 10^5 OT-I T cells and to lesser extent in recipients of fewer OT-I T cells (Figure 4.19A). We stopped imaging at this time since several RIP-mOva recipients already showed first signs of sickness (ruffled fur, weight loss). Almost all recipients of 1 x 10^6 and 1 x 10^5 OT-I T cells had high blood glucose levels at day+8, indicating a dramatic destruction of islets by OT-I T cells by this time, and died within 15 days after allo-HCT. Blood glucose levels of 1 x 10^4 OT-I T cells recipients were high at day+10 and at day+12 recipients of 1 x 10^3 OT-I T cells had high glucose levels (Figure 4.19B). All mice died within 24 days after allo-HCT (Figure 4.19C,D). These results suggested that alloantigen recognition, as well as the specific alloantigen expressing tissue infiltration by CD8$^+$ T cells after allo-HCT was very efficient as 1 x 10^4 OT-I T cells were enough to cause severe islet destruction.
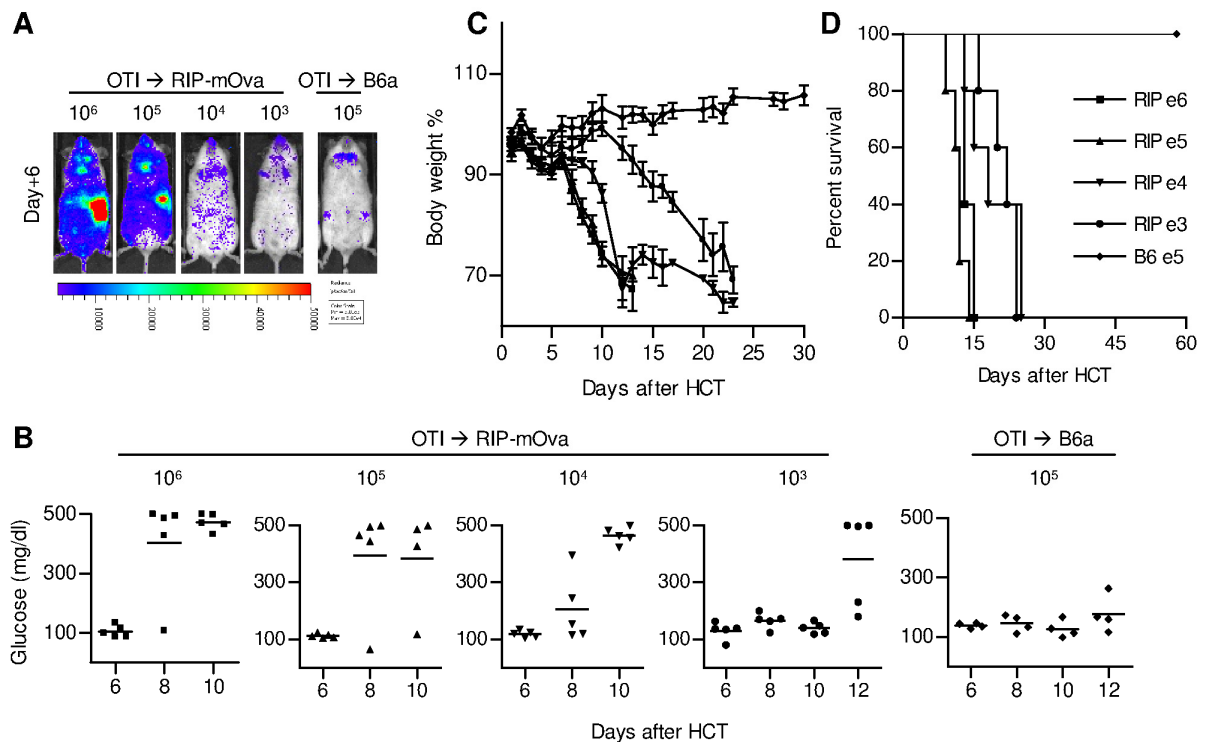
Figure 4.19: Effective T cell mediated destruction of cognate antigen expressing target tissues after single antigen mismatch allo-HCT of OT-I T cells into RIP-mOva recipients. (**A**) BLI at day+6 after allo-HCT of different cell numbers of luciferase[+] OT-I T cells together with 5 x 10^6 BM cells from a B6 donor into B6a.RIP-mOva or B6a recipients. Administered OT-I cell numbers are indicated (e.g. 10^6 or e6 indicates recipients of 1 x 10^6 OT-I T cells). (**B**) Blood glucose measurement is indicating critical time points of islet destruction (each dot represents an analyzed recipient and mice with levels above 300 mg/dl were considered diabetic). (**C**) Weight change and (**D**) Kaplan-Meier survival curves after allo-HCT of decreasing OT-I cell numbers.

In contrast, the survival of βa-Ova recipients was dependent on transplanted OT-I cell numbers (cell number / survival: 1 x 10^6 / 25%; 1 x 10^5 or 1 x 10^4 / 75% and 1 x 10^3 / 100%). Using BLI we detected a strong proliferation of luciferase^{+} T cells in recipients of 1 x 10^6 and 1 x 10^5 OT-I T cells between day+3 and day+6 (Figure 4.20A,B). No βa-Ova recipient died after day+15 (Figure 4.20D,C) and none of the βa-Ova recipient had high blood glucose levels (data not shown).
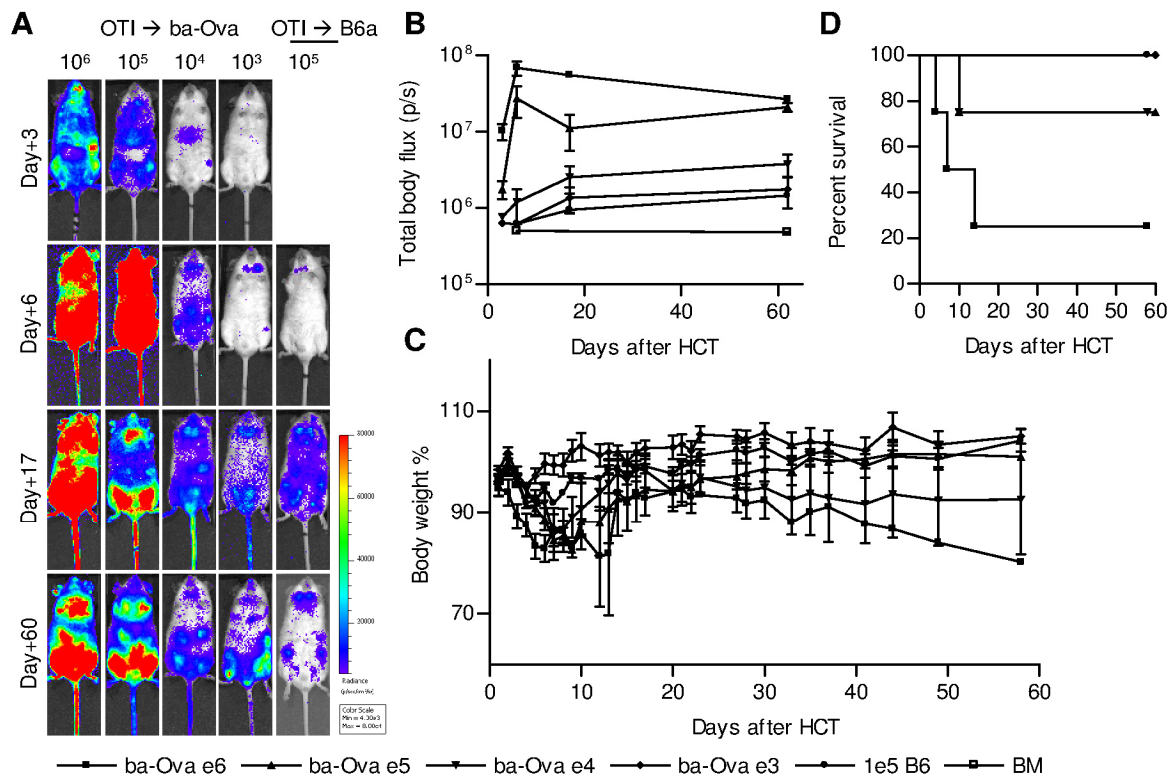
Figure 4.20: Survival of βa-Ova recipients is dependent on OT-I cell numbers of allo-HCT. (**A**) BLI and (**B**) quantification after allo-HCT of different luciferase[+] OT-I cell numbers together with 5 x 10^6 BM cells from a B6 donor into B6a.βa-Ova or B6a recipients. Administered OT-I cell numbers are indicated (e.g. 10^6 or e6 indicates recipients of 1 x 10^6 OT-I T cells). (**C**) Weight change and (**D**) survival was assessed until day+60 after allo-HCT of decreasing OT-I cell numbers.

4.2.3 Quantification of organ infiltrating OT-I T cells with flow cytometry

We analyzed tissues of different recipients with flow cytometry to determine infiltrating OT-I cell-numbers at defined time points.

For single antigen mismatch allo-HCT we transferred 1.2 x 10^6 OT-I CD45.1^{+} cells (CD8^{+} purity: approx. 80%) together with 5 x 10^6 C57Bl/6 bone marrow cells into irradiated B6a.βa-Ova, B6a.RIP-mOva or B6a recipients (n = 6 mice/group). At day+4 and at day+6 mice were euthanized and we collected spleen, kidney, pancreas, lung, liver, small bowel (sb), and large bowel (lb). Importantly, all organs were collected in regard of comparable sizes to achieve comparable volumetric enumeration (left kidney and left lung, whole spleen and pancreas excluding pancreatic LNs by visual encounter), one representative lobe of the liver, exactly 4 cm of sb or lb without PPs). For cell dissociation, but for the spleen all organs were cut in small pieces followed by enzymatic digestion. Cells were suspended and analyzed in defined volumes to calculate donor OT-I cell numbers. We identified donor T cells by CD45.1^{+} and CD8^{+} staining as indicated in Figure 4.21.
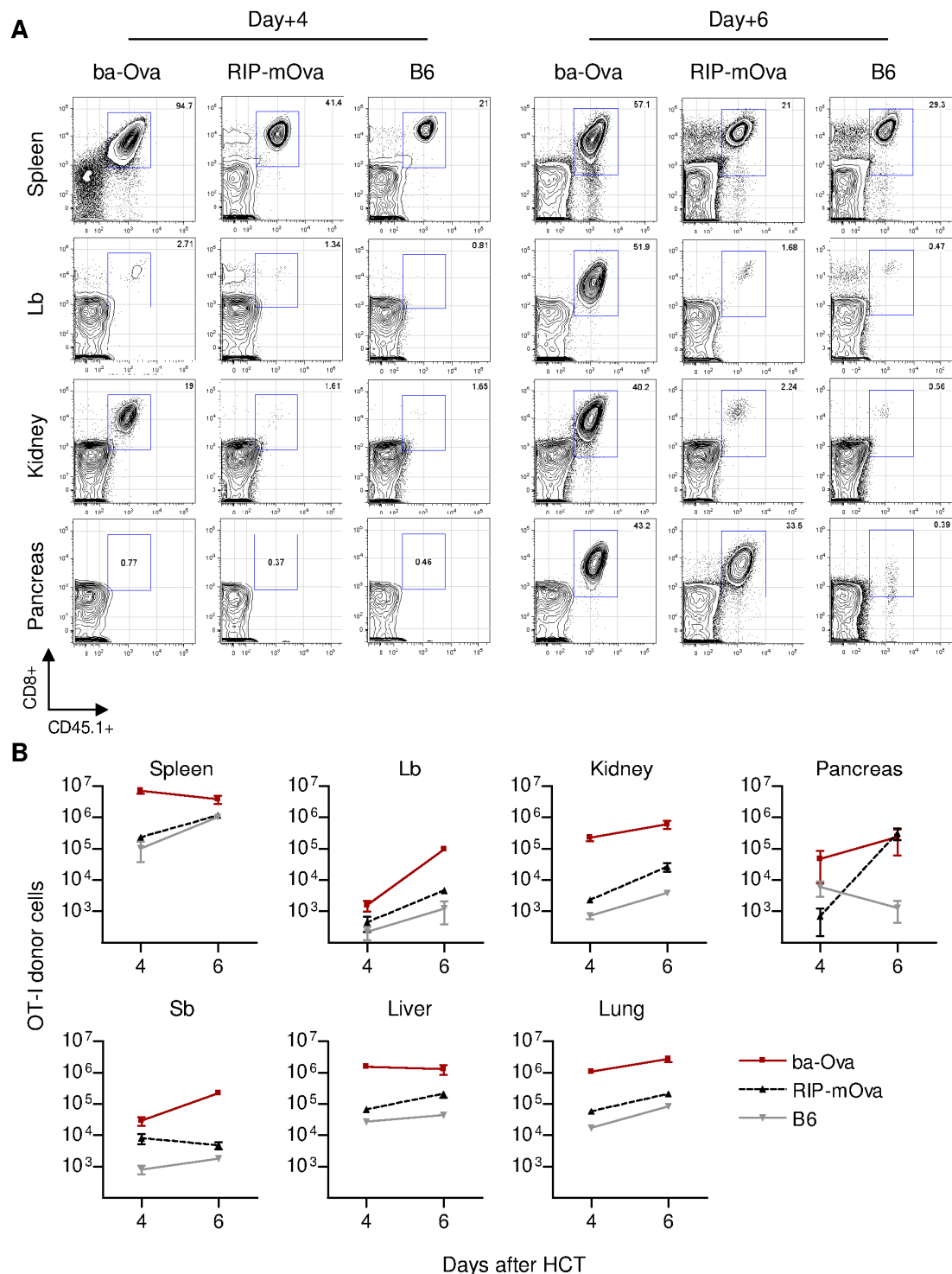
Figure 4.21: Enumeration of organ infiltrating OT-I T cells using FACS. Conditioned recipients of βa-Ova, RIP-mOva or B6 were injected with MACS enriched 1.2 x 10^6 CD45.1[+] OT-I T cells together with 5 x 10^6 BM cells from a C57BL/6 donor. At day+4 and day+6 after allo-HCT, tissues were removed and cell suspensions were prepared for flow cytometry. **(A)** Representative FACS plots and gating on CD45.1[+] OT-I T cells, isolated from recipients. **(B)** Quantification of OT-I donor cells (n = 3 mice/group).

In βa-Ova mice we identified at day+4 large numbers of OT-I T cells in spleen, kidney, (Figure 4.21) liver, and lung. In these recipients OT-I cell numbers in spleen and liver decreased between day+4 and day+6, but increased in all other investigated organs. In RIP-mOva and B6 recipients we could only identify large numbers of OT-I T cells in the spleen 4

days after allo-HCT (Figure 4.21A). Until day+6 we detected a slight increase of OT-I T cells in tissues of B6 recipients, except within the pancreas (Figure 4.21B). Here we found decreasing cell numbers, which might be explained by blood circulating OT-I T cells on day+4. Similarly, we detected a slight increase of OT-I T cells in tissues of RIP-mOva recipients and slightly decreasing OT-I cell number in the small bowel. However, in these recipients pancreas infiltration by OT-I T cells increased by more than 100 fold between day+4 and day+6, strongly indicating a specific accumulation of donor OT-I T cells.

4.2.4   Identification of organ infiltrating OT-I T cells with LSFM

As described above (Chapter 4.1) we have demonstrated that LSFM is a reliable method to visualize and quantify high numbers of donor T cells after HCT as well as detecting rare cellular events within various adult mouse organs. Consequently, we employed this technique to study the kinetic of alloantigen dependent tissue infiltration by alloreactive T cells.

To guarantee the detection of T cells infiltrating the pancreatic islets, we first established the imaging of large areas deep within the intact pancreas. The clearing of pancreatic tissue resulted in optically transparent samples. Subsequently, to effectively detect first donor T cells infiltrating islets of ovalbumin expressing beta cells we established an anti-insulin antibody staining to visualize insulin producing islets in the pancreas (Figure 4.22A). Islets itself were already identifiable due to a higher autofluorescence in the green channel compared to the surrounding pancreatic tissue. Again, in an allo-HCT we transferred 1.2 x 10^6 OT-I CD45.1$^+$ cells (CD8$^+$ purity: approx. 80%) together with 5 x 10^6 C57Bl/6 bone marrow cells into irradiated B6a.RIP-mOva recipients. At indicated time points we perfused mice with PFA and prepared organs for LSFM imaging. By scanning large tissue volumes we detected first few pancreatic islets infiltrating OT-I T cells the earliest by day+4 after allo-HCT followed by a massive T cell migration to the pancreas within the following 24 h (Figure 22B-D). In comparison we found only few cells in other peripheral organs, such as the liver or large bowel.
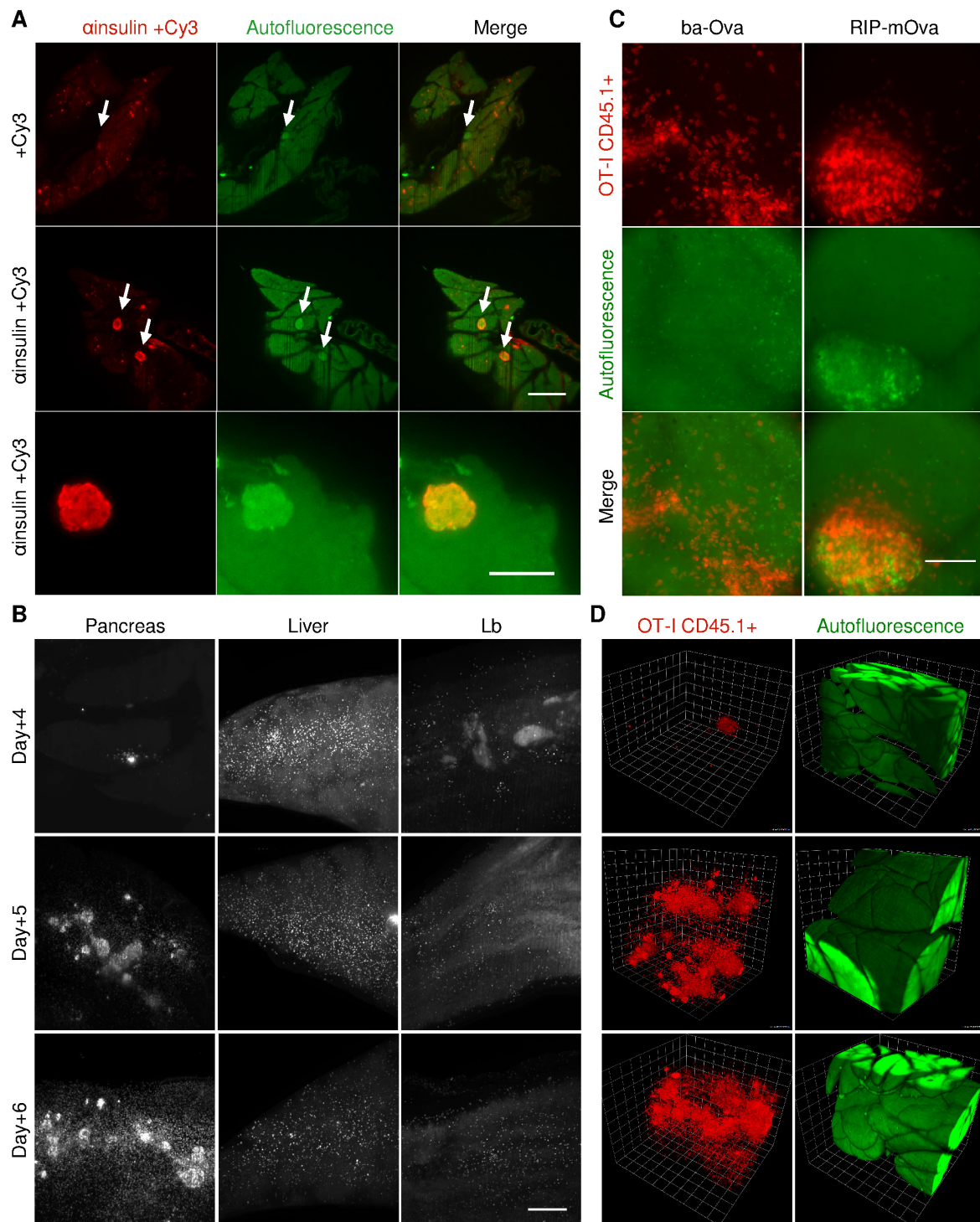
Figure 4.22: Identification of organ infiltrating OT-I T cells using LSFM. (**A**) Pancreatic tissue imaging: autofluorescence in the green channel already revealed pancreatic islets (indicated by an arrow). Staining of α-insulin colocalized with the enhanced islet autofluorescence (scale upper panels 500 μm, lower panel 200 μm). (**B**) CD45.1[+] OT-I cell infiltration in tissues of RIP-Ova recipients at indicated time points after single antigen mismatch allo-HCT (z-Projections, scale 500μm). (**C**) Detailed comparison of CD45.1[+] OT-I cell in pancreatic tissue of βa-Ova and RIP-mOva mice at day+4 after allo-HCT (z-Projections, scale 200 μm). (**D**) 3D reconstruction of pancreatic island infiltration of RIP-Ova mice by CD45.1[+] OT-I T cells at indicated time points after allo-HCT.

4.2.5 Antigen expression by either hematopoietic, or by parenchymal cells only result in alloreactive T cell organ infiltration

Next, we asked whether the expression and presentation of cognate antigens on the hematopoietic or exclusively non-hematopoietic host cells would affect the tissue distribution of TCR transgenic CD8$^+$ T cells after allo-HCT.

Therefore, we generated B6 → B6a (B6/B6) or βa-Ova → B6a (βa-Ova/B6) chimeras such that the ovalbumin antigen is encoded only by host hematopoietic cells and not by non-hematopoietic target tissues. After three months the chimerism in the blood was 93.4% ± 3.7% (n = 14). The chimeras were then used as allo-HCT recipients, injected with 5 x 10^6 C57Bl/6 bone marrow cells plus 2 x 10^6 OT-I T cells (purity after MACS enrichment > 85% CD8$^+$). Only dim bioluminescence signals were detectable in B6/B6 recipients and luciferase$^+$ signal of OT-I T cells mainly projected to the SLOs at day+6, suggesting homeostatic proliferation (Figure 4.23A-C). In contrast, we found massive proliferation of OT-I T cells in βa-Ova/B6 recipients as indicated by BLI. At day+3, bioluminescence signals of OT-I T cells mainly projected to the liver and SLOs such as cLN, iLN, and spleen. Already 24 h later the cells left the liver and spread within the recipient. At day+6 after allo-HCT *ex vivo* BLI revealed a whole organ distribution of OT-I T cells in βa-Ova/B6 recipients (Figure 4.23D,E). At this time point we found increased levels of MCP-1 and IFN-γ in βa-Ova/B6 recipients (Figure 4.23F).

Next we generated βa-Ova → βa-Ova (βa-Ova /βa-Ova) and B6 → βa-Ova (B6/βa-Ova) chimeras such that the ovalbumin antigen is encoded only by non-hematopoietic target tissues and not by hematopoietic cells (B6/βa-Ova), or encoded by both (βa-Ova /βa-Ova). Again, we waited three months (chimerism > 95%) before chimeric mice were used as single antigen mismatch allo-HCT recipients, injected with 5 x 10^6 C57Bl/6 bone marrow cells plus 2 x 10^6 OT-I T cells (purity after MACS enrichment > 78% CD8$^+$). At day+6 after allo-HCT BLI revealed that all organs were infiltrated in a similar pattern with similar levels of OT-I cell proliferation and organ infiltration, irrespectively whether the antigen was expressed only by non-hematopoietic target tissues, only by hematopoietic cells, or expressed by both (Figure 4.24).
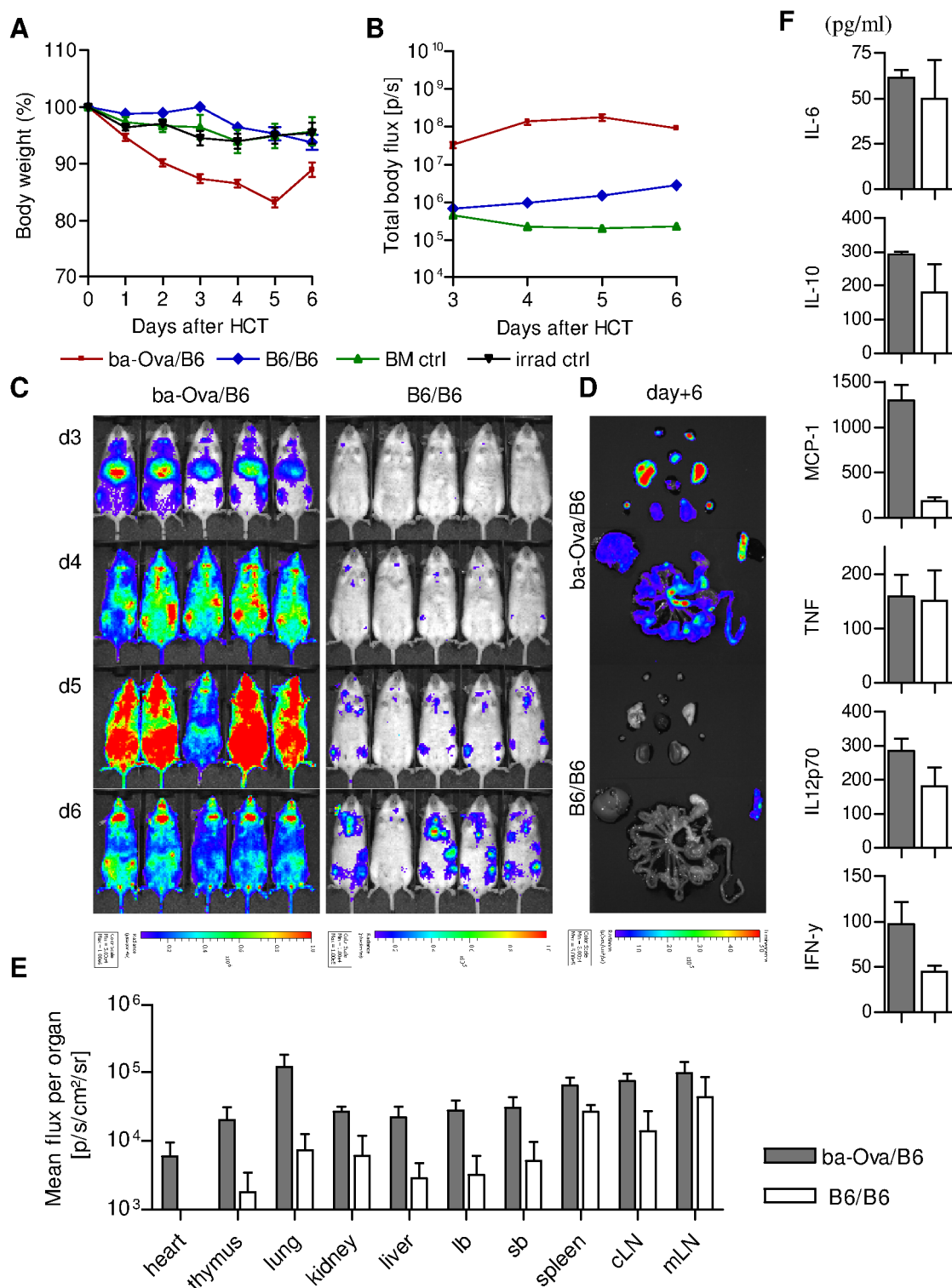
Figure 4.23: Cognate antigen expression by hematopoietic cells results in an overall organ infiltration by alloreactive T cells. Chimeras were generated, so that ovalbumin is either expressed only on hematopoietic-derived cells (βa-Ova/B6) or is not expressed at all (B6/B6). These chimeras were then irradiated and transplanted with 2 x 10⁶ luciferase⁺ OT-I T cells together with 5 x 10⁶ BM cells from a C57BL/6 donor. **(A)** Body weight change after allo-HCT was assessed until day+6. **(B,C)** *In vivo* BLI of recipients revealed OT-I cell proliferation and migration. **(D)** At day+6 after allo-HCT *ex vivo* BLI revealed T cell distribution and **(E)** quantification of organ infiltration. (**F**) Serum levels of IL-6, IL-10, MCP-1, TNF, IL12p70 and IFN-y at day+6 after all-HCT.
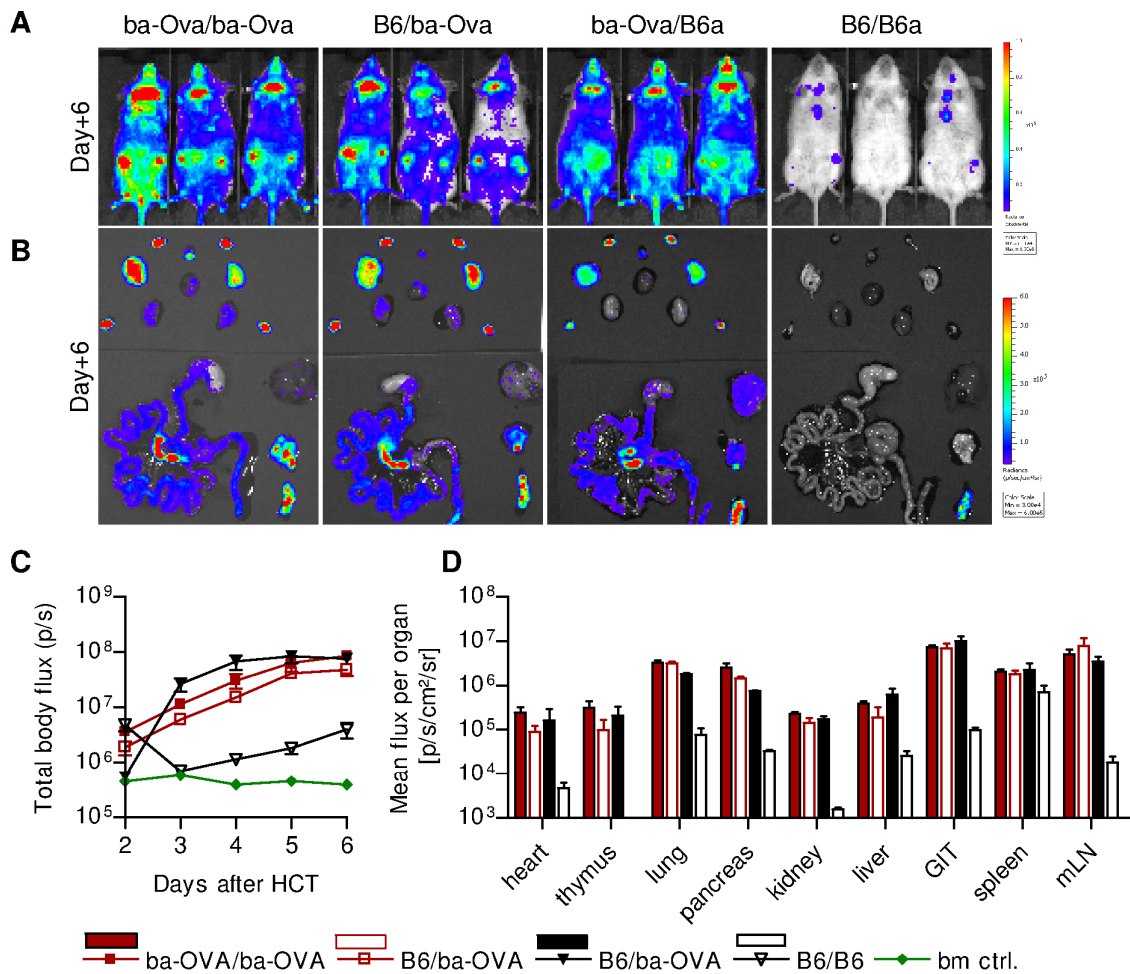
Figure 4.24: Cognate antigen expression solely by non-hematopoietic target tissues only results in an overall organ infiltration by alloreactive T cells. Chimeras were generated, so that ovalbumin is either expressed by non-hematopoietic target tissues and hematopoietic-derived cells (βa-Ova/βa-Ova), only by non-hematopoietic target tissues (B6/βa-Ova), only on hematopoietic-derived cells (βa-Ova/B6),or is not expressed at all (B6/B6). These chimeras were then irradiated and transplanted with 2 x 10^6 luciferase$^+$ OT-I T cells together with 5 x 10^6 BM cells from a C57BL/6 donor. (**A**) *In vivo* BLI and (**B**) *ex vivo* BLI at day+6 after allo-HCT revealed OT-I cell proliferation and migration. (**C**) Quantification of *in vivo* BLI and (**D**) *ex vivo* BLI demonstrated similar pattern of OT-I cell proliferation and organ infiltration in βa-Ova/βa-Ova, B6/βa-Ova and βa-Ova/B6 recipients and only homeostatic proliferation in B6/B6 recipients.

4.2.6   OT-I proliferation ability and IFN-γ production *in vitro*

As we had found high levels of IFN-γ in the serum of OT-I recipients that expressed ovalbumin (βa-Ova, βa- Ova-chimeras and RIP-mOva) we asked whether the IFN-γ production might be induced by donor T cells. Therefore, we analyzed the ability of OT-I cell proliferation as well as IFN-γ production upon antigen presentation *in vitro*. Therefore, we isolated OT-I T cells from spleens of donor mice and labeled them with CFSE. Naïve OT-I T cells were stimulated either with an alloantigen independent TCR stimulation by adding CD3$^+$ antibody together with IL-2 or with irradiated splenocytes from βa-Ova mice (target cells).

After 3 days of stimulation, the effector OT-I T cells were either re-confronted with target cells or were not re-challenged. After 5 h of re-stimulation we analyzed IL-2 and IFN-γ production of OT-I T cells by intracellular staining and FACS. OT-I T cells showed great
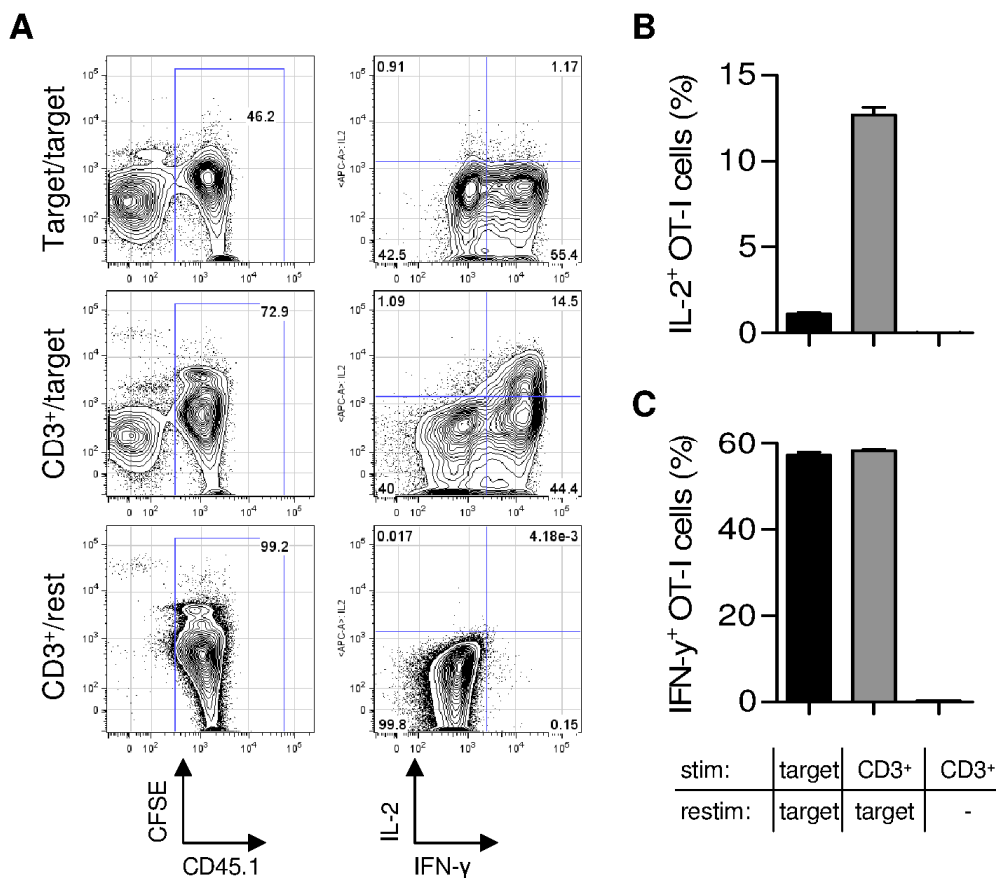
Figure 4.25: OT-I cell proliferation and IFN-γ production *in vitro*. CD45.1$^+$ OT-I T cells were stimulated either with CD3$^+$ antibody (CD3$^+$) or with irradiated spleen cells from βa-Ova mice (target) and were subsequently either re-stimulated with βa-Ova cells or not exposed to an antigen again (rest). **(A)** Representative FACS plots and gating of CD45.1$^+$ effector cells as well as intracellular staining of IL-2 and IFN-γ. Quantification of **(B)** IL-2$^+$ and **(C)** IFN-γ$^+$ OT-I T cells after stimulation and re-stimulation (n = 6/treatment).

proliferation capacity upon CD3+IL-2-stimulation or target cell stimulation as indicated by CFSE dilution (Figure 4.25A, first panel). OT-I T cells stimulated with target cells and re-stimulated with target cells (target/target) showed some IL-2 production (Figure 4.25A,B mean: 1.1%, n = 5). In comparison, OT-I T cells stimulated with CD3+IL-2 and re-stimulated with target cells (CD3/target) showed much higher IL-2 production (CD3/target, mean: 12.65%, n = 3). This high numbers of IL-2 producing OT-I T cells could not be found when CD3+IL-2 stimulated cells were not re-stimulated with target cells (CD3/resting mean: 0.0%, n = 5). We found a dramatic IFN-γ production of effector OT-I T cells when re-stimulating with target cells (target/target, mean: 45.6%, n = 5; CD3/target, mean: 42,2%, n = 3). We could

not observe IFN-γ production of effector OT-I T cells that were not re-stimulated after priming (CD3/resting, mean: n = 3).

Hence, OT-I T cells showed great potential of proliferation upon alloantigen presentation *in vitro*, leading to dramatic IFN-γ and to a lesser extent to IL-2 production upon re-encounter with the cognate alloantigen.

4.2.7 Cognate antigen recognition of TCR transgenic CD4$^+$ T cells - proliferation and migration of OT-II cells

To rule out whether alloantigen dependent tissue infiltration, as observed for CD8$^+$ T cells at day+6 after OT-I allo-HCT, might also occur after allo-HCT of CD4$^+$ T cells that depend on MHC II recognition, we employed TCR transgenic OT-II T cells in an allo-HCT setting. Consequently, we transplanted either 1 or 2 x 10^6 FACS sorted luciferase$^+$ CD4$^+$ T cells from B6.L2G85.OT-II.Ragko.CD45.1 donors (purity: > 98% CD4$^+$) together with 5 x 10^6 BM cells from C57BL/6 mice into myeloablatively irradiated (9 Gy) B6a.βa-Ova or B6a.RIP-Ova recipients, that matched in age and sex. We used *in vivo* BLI to analyze T cell proliferation and migration after transplantation.

In βa-Ova recipients of OT-II T cells, we found a strong acceleration of photon emission starting at day+2 after HCT indicating a high T cell responsiveness followed by proliferation (Figure 4.26A,B). At this time point BLI signal mainly projected to cervical LNs as well as spleen, suggesting an effective homing to and priming in SLOs. *In vivo* BLI indicated that by day+3 after HCT the first OT-II T cells migrated from SLOs to peripheral organs such as the GIT. In contrast, in RIP-mOva recipients that had received 1 x 10^6 (n = 3) OT-II T or 2 x 10^6 (n = 1) OT-II T cells, donor T cells were not detectable by day+6 after HCT using BLI (Figure 4.26A). At day+6 after HCT we performed *ex vivo* BLI to evaluate organ infiltration by donor T cells in more detail. *Ex vivo* imaging of organs from βa-Ova recipients revealed an overall organ infiltration of OT-II cells, while no luciferase signal was detectable in RIP-mOva recipients (Figure 4.26C,D).
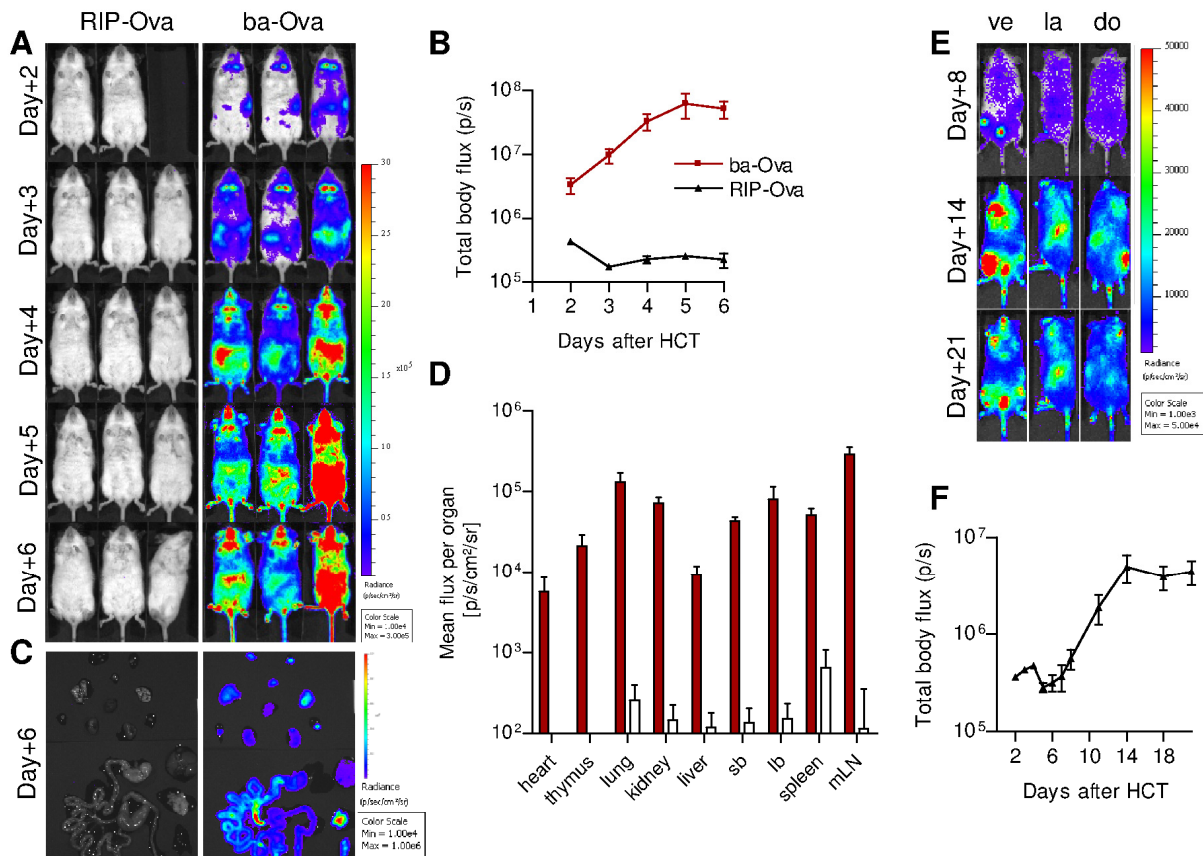
Figure 4.26: Cognate antigen recognition of TCR transgenic CD4$^+$ T cells – proliferation and migration of OT-II cells.
(**A, B**) 1 x 10^6 CD4$^+$ FACS sorted luciferase$^+$ OT-II cells together with 5 x 10^6 BM cells of a C57Bl/6 donor were injected into irradiated RIP-Ova and βa-Ova mice and T cell expansion and migration was analyzed with BLI. (**C,D**) At day+6 after allo-HCT *ex vivo* BLI revealed massive luciferase$^+$ T cell distribution in all organs of βa-Ova recipients, but not in RIP-mOva. (**E,F**) BLI revealed that transplanted luciferase$^+$ OT-II cells in RIP-mOva were partly located in the bone marrow compartments and slightly expanded until day+14 (ve, ventral; la, lateral; do, dorsal).

Hence, we repeated single antigen mismatch allo-HCT of OT-II (post FACS purity 97.8% CD4$^+$) into RIP-mOva recipients (n = 8). Again we could barely detect luciferase$^+$ donor cells before day+6 after HCT. At day+6 focal spots, projecting to bone marrow compartments such as spine or femur, appeared and increased in signal intensity until day+14 after-HCT (Figure 4.26E,F). However, when we examined the recipients until day+21 after single antigen mismatch allo-HCT we neither observed further OT-II donor cell proliferation nor any clinical signs of acute GVHD.

5 Discussion

5.1 Mapping immunological processes in intact organs using LSFM

The vertebrate immune system exhibits an enormous complexity that requires the approach of employing new imaging technologies to study structural and functional processes in its biological context. Molecular 3D imaging techniques are very instrumental in revealing cellular events in tissues and organs (Ludewig et al., 2012). Another benefit of molecular imaging is that the images provide quantitative data, while preserving the intact structure of the experimental subject (Massoud and Gambhir, 2003). To this end, we established a novel convenient and versatile technique of optical light sheet illumination microscopy that allows visualizing and automatizing of single cell analysis within whole organs in multiple colors.

5.1.1 A virtual journey through intact tissues by advanced multicolor LSFM

A self-built prototype multicolor LSFM enabled us to investigate multiple tissues based on the principal of optical sectioning, a procedure of tissue clearing for optimal light penetration and computational 3D reconstruction. In my thesis project, we demonstrated for the first time that this technique is suitable to analyze complex immune processes in whole secondary lymphoid organs (e.g. PPs and mLNs) and showed its application to diverse murine and human tissues including lung, liver, heart, skin, and testicles. Importantly, we also established deep-tissue staining protocols for multicolor display of individual cell distribution, achieved subcellular sensitivity and quantified absolute cellular infiltrates by employing a single microscopy setup.

Multicolor LSFM fills a gap between microscopic imaging techniques like confocal microscopy and macroscopic imaging techniques as magnetic resonance imaging (MRI) and computer tomography (CT), or bioluminescence imaging (in experimental models). Hereby, LSFM circumvents the obstacle of alternative 3D imaging methods such as optical projection tomography (OPT) that suffer from the requirement of time-consuming backprojection (Sharpe et al., 2002). A clear advantage of LSFM is that optical sectioning allows the rapid screening for rare events in mesoscopic specimens without requiring any image calculation. Therefore, areas of interest can be identified immediately during the acquisition process which allows for more focused investigation at higher magnifications.

5.1.2   Application of LSFM in multiple tissues of mice and human

Labeling of intact tissues with multiple fluorescent antibodies for 3D imaging opens a broad range of biomedical applications. The utilization of antibodies is highly flexible because any molecule of interest can be stained, while fluorescent proteins are inapplicable for human tissues or wild type animal models. In cleared samples high tissue autofluorescence particularly in the green color channel, caused by formalin fixation (Leischner et al., 2010), allows the display of detailed microanatomical features in various organs. This proved advantageous to locate specific fluorescently labeled cell populations within their anatomical context. However, this strong autofluorescent background noise also poses certain limitations to utilize green fluorophores and therefore, we recommend reliance on fluorophores in the red or near-infrared color spectrum, as demonstrated in this study. Fluorescent proteins have been proven to be beneficial for many biological applications and were used for various imaging techniques in the past decade (e.g. Betzig et al., 2006; Hoffman and Yang, 2006). Especially the development of new available fluorescent proteins promises many innovative tools for biological imaging (Shaner et al., 2004, 2005). Thus, we also aimed to track donor T cells expressing fluorescent proteins with LSFM after HCT, but in our hands were not able to detect them after the clearing procedure. However, other groups demonstrated the suitability of fluorescent proteins in imaging motor neurons expressing DsRed-Express (Ermolayev et al., 2009a, 2009b) or neurons expressing GFP (Dodt et al., 2007), after the samples have been incubated with clearing solution. More recently, several protocols have been established to retain the stability of certain fluorescent proteins in restricted tissues by avoiding the use of clearing solution (Ertürk et al., 2011, 2012; Hama et al., 2011).

To further improve LSFM we envision to implement several alterations that promise to further increase contrast, generate less image artifacts, and provide even higher resolution such as illumination from two sides (Dodt et al., 2007), scanning the light sheet (Huisken and Stainier, 2007; Keller et al., 2008), structured-illumination (Keller et al., 2010), Bessel beam plane illumination (Planchon et al., 2011) or even combination of LSFM with STED microscopy (Friedrich et al., 2011). Recent improvements to optimize clearing procedures rendering organs transparent, as shown for the central nervous system (Ertürk et al., 2011; Hama et al., 2011) will further assist to reduce background fluorescence and enhance fluorescent protein stability.

5.1.3 Quantification of immune processes in entire organs using a murine GVHD model

After we established multicolor LSFM staining protocols and tissue analysis methods we applied this technique to monitor dynamic changes within PPs during acute GVHD. Here, especially the combination of BLI with LSFM proofed to be very effective for whole body T cell tracking *in vivo* to a detailed single cell imaging (*ex situ*). BLI is a well established method to effectively explore and evaluate complex immunological processes such as GVHD and GVL reactions (Edinger et al., 2003; Cao et al., 2004, 2005; Beilhack et al., 2005). Thereby the sensitivity of BLI is sufficient to detect 100–1.000 lymphoma cells (Edinger et al., 2003) or even 10 T cells (Rabinovich et al., 2008) *in vivo* and the ability to serially track cell populations non-invasively allows for the identification of key time points and locations for further analysis (Negrin and Contag, 2006). Further optical imaging techniques, including fluorescence imaging, exist to generate whole-body images of HCT recipients (Panoskaltsis-Mortari et al., 2004) and might be helpful in combination with LSFM.

Imaging whole PPs of recipients that underwent HCT with LSFM we found a dramatic upregulation of MAdCAM-1 on HEVs and within follicular areas. It is well established that MAdCAM-1 is an important regulator in lymphocyte homing to PPs via HEVs (Hamann et al., 1991) but is also expressed on marginal reticular cells and follicular dendritic cells (Szabo et al., 1997) and thus is thought to potentially contribute to lymphocyte motility (Boscacci et al., 2010). In accordance with our findings, Szabo et al. (1997) found an enhanced MAdCAM-1 expression within peripheral lymph nodes and spleen in response to antigenic stimulation. However, the exact function of this dynamic MAdCAM-1 regulation in follicular areas still needs to be further elucidated. Furthermore, in my thesisproject, we successfully quantified donor T cell numbers in the entire PPs. The dense clustering of the T cells impeded automated cell counting and we calculated cell numbers by using the mean value of the measured cell volume. Because of the limited number of fluorescent channels available we did not stain for the nuclei. Nuclear staining in combination with surface molecule staining may have facilitate automated cell count as demonstrated previously (Bolte and Cordelières, 2006). However, with solely optical sectioning by LSFM, these quantifications were not prone to artifacts that occur on cut surfaces. This turned out to be particularly advantageous when reliable counting of rare cellular events is required and hundreds of serial cryo-sections may become overly challenging.

5.1.4 Visualizing and counting rare events with LSFM

We investigated the fate of individual CD4$^+$ T cell subsets that either induce (T$_N$ and T$_{CM}$) or do not induce (T$_{EM}$) lethal GVHD after allo-HCT (Anderson et al., 2003; Chen et al., 2004; Beilhack et al., 2005; Dutt et al., 2007; Zheng et al., 2008). The mechanisms why T$_{EM}$ fail to cause GVHD remains unclear. One controversial hypothesis proposes differences in migration and priming (Beilhack et al., 2005; Anderson et al., 2008), since T$_{EM}$ do not express CD62L and CCR7, and are therefore relatively excluded from lymph nodes (Gunn et al., 1998). In line with this, when scanning whole SLOs in high resolution we quantified low numbers of CD4$^+$ T$_{EM}$ cells homing to T cell areas of PPs and mLNs. Hence, LSFM gave us new insights in migration and dispersal of different T cell subtypes after HCT and will prove useful to optimize cellular therapies. The ability to detect and automatically count rare events in micrometer resolution within large tissue samples, suggests LSFM as an effective tool to study single hematopoietic stem cells (Wagers et al., 2002), tumor-draining lymph node infiltrating immune cells (Kohrt et al., 2005) or even to identify cancer stem cells (Al-Hajj et al., 2003).

In conclusion, we have shown multicolor LSFM as advantageous for multiple research applications in biomedicine and immunology, particularly in inflammatory processes, such as GVHD, to track clonal cell distribution throughout the body. Due to the speed and its automatable operation, LSFM may advance systematic and comprehensive large-scale studies of cell migration and interaction within various tissues, in experimental animal models as well as human tissue biopsies. Biomedical research, that translates scientific progress into clinical approaches will highly benefit from the application of this high resolution and high throughput technology. Therefore, 3D multicolor LSFM holds the promise to complement classical histopathological diagnosis.

5.2 Relevance of tissue alloantigen expression for the selective GVHD organ manifestation

5.2.1 Alloantigen expression determines organ infiltration of TCR transgenic CD8⁺ T cells after single antigen mismatch allo-HCT

Alloantigen expression on host epithelium is crucial for the induction of acute GVHD in MHC-matched, minor histocompatibility antigen–mismatched (miHAg-mismatched) models of HCT (Jones et al., 2003). Here we used a TCR transgenic model of GVHD that target a single peptide antigen and therefore resembles a MHC-matched single antigen mismatched miHAg-mismatched HCT. We investigated the importance of alloantigen expression for the selective organ manifestation after HCT into conditioned hosts that either express the peptide antigen ovalbumin ubiquitously or selectively in the pancreas, an organ that is normally not affected by acute GVHD. At day+6 after HCT we found that TCR transgenic CD8⁺ T cell infiltrated either all organs (βa-Ova) or only the pancreas (RIP-mOva) respectively to the site of antigen expression. Hence, in this mouse model of MHC class I dependent antigen recognition we could identify an alloantigen dependent organ infiltration of OT-I T cells after HCT.

Although MHC I molecules have a broad tissue expression pattern (Shlomchik, 2007), alloreactive T cells mainly affect gut, liver, and skin following MHC-mismatched HCT. In contrast miHAgs can differ in their range and distribution of tissue expression. Furthermore in a MHC matched, miHAg mismatched HCT a direct target-cell–T-cell contact is required for CD8⁺ T-cell-mediated acute GVHD and therefore the tissue expression pattern of miHAgs could reflect which organs are involved in the disease, as demonstrated in our experiments. This would imply that certain acute GVHD relevant miHAgs are predominantly or even exclusively expressed in the target organs of acute GVHD. However, recently Toubai et al. (2012) experimentally demonstrated that an ubiquitously expressed clinically relevant H-Y miHAg antigen can cause acute GVHD, by using H-Y specific TCR transgenic CD8⁺ T cells (Matahari). After HCT they assessed acute GVHD by monitoring survival and amongst other parameters also analyzed GVHD target organs histopathologically, but did not investigate the fate of further peripheral organs that are typically non-target during acute GVHD, such as pancreas or kidneys. Nonetheless, when alloantigen expression on host epithelium is necessary for the induction of tissue selective acute GVHD, further mechanisms preventing tissue infiltration in non-target must exist. Strikingly, we found non-target organ infiltration after HCT when the organs expressed the cognate alloantigen.

In a MHC-matched, multiple miHAg-mismatched mouse model it was demonstrated that CD8$^+$ T cell mediated acute GVHD required direct interactions between TCRs on donor CD8$^+$ T cells and MHC I on target tissues (Matte-Martone et al., 2008). In this study, recipient mice were chimeras that express MHC I on hematopoietic cells, allowing the activation of alloreactive CD8$^+$ T cells, but allo-antigen was not expressed on parenchymal cells as chimeric mice were deficient for MHC I (wt → β2M$^{-/-}$ chimeric mice). Importantly, Matte-Martone et al. (2008) did not detect tissue infiltrating T cells, highlighting the importance of parenchymal alloantigen expression for donor CD8$^+$ T cell infiltration. This observation is in accordance with our findings, that the parenchymal alloantigen expression determined the organ infiltration after allo-HCT. The hampered infiltration might be explained by the inability of CD8$^+$ T cells to mediate tissue damage that might either promote an accumulation of further donor CD8$^+$ T cells by local retention and survival of T cells after entering target tissues, or result in an increased T-cell recruitment from the blood (Matte-Martone et al., 2008). Although this suggestion might explain the importance of parenchymal antigen presentation in T cell infiltration of certain tissues after HCT, it could not clarify the tissue selective organ infiltration in acute GVHD. Non-target organs of acute GVHD, that normally also express parenchymal antigen, are not affected by T cell infiltration after allogeneic HCT. When we transplanted OT-I T cells into established chimeras expressing the antigen ovalbumin only by hematopoietic cells we found an organ infiltration, although the parenchymal tissue did not express the alloantigen. However, in contrast to the experiments by Matte-Martone et al. (2008) in our experiments the recipients were not impaired in presenting peptides via MHC I and thus the alloantigen might be released from apoptotic hematopoietic cells and cross-presented by parenchymal cells, as discussed later in chapter 5.2.5.

In HCT of OVA specific T cells, βa-Ova recipients were chosen to mimic a clinically relevant model of ubiquitously cognate antigen expression, a situation that one might anticipate for allorecognition if single alloreactive T cells recognize ubiquitously expressed allogeneic MHC complexes. However, in contrast to the observed selective GVHD target-tissue manifestation of other acute GVHD models, we found, after a massive proliferation phase, ubiquitous organ infiltration by antigen specific T cells followed by 50% survival. Also, previous studies employing defined alloreactive TCR transgenic T cell clones observed only limited acute GVHD manifestation in allo-HCT recipients. HCT of TCR transgenic CD8$^+$ T cells into antigen expressing recipients resulted in a short burst of T cell expansion, followed by apoptosis or anergy (Rocha et al., 1995; Yu et al., 1999). However, using 2C (Yu et al., 2006) or H-Y (Toubai et al., 2012) TCR transgenic CD8$^+$ T cells clinical models of acute GVHD with target organ infiltration and mortality could be established. Interestingly, 2C CD8$^+$ TCR transgenic cells were more pathogenic in recipients with an intermediate-affinity alloantigen than in

those with a high-affinity alloantigen (Yu et al., 2006). However, alloantigen affinity in both, βa-Ova and RIP-mOva mice is equal, but only caused in the latter recipients high mortality. Nonetheless, there is a discrepancy in the priming of TCR transgenic CD8$^+$ T cells between RIP-mOVA and βa-Ova recipients. In RIP-mOVA recipients ovalbumin is mainly restricted to pancreatic β cells and TCR transgenic CD8$^+$ T cells are primed via cross-presentation. In contrast, all cells of βa-Ova recipients express ovalbumin, including APCs, allowing for direct priming of TCR transgenic CD8$^+$ T cells.

In previous studies OT-I T cells were adoptively transferred into RIP-OVA (Kurts et al., 1996) or iFABP-OVA transgenic mice (Vezys et al., 2000) and activation and proliferation was observed in lymph nodes draining the ovalbumin expressing tissues. However, in these studies tissue destruction was not observed (Kurts et al., 1996; Vezys et al., 2000) and transferred OT-I T cells either became anergic (Vezys et al, 2000) or were deleted (Kurts et al., 1997b, 1999), except if more than 5 x 10^6 OT-I T cells were transferred (Kurts et al., 1997a). Concordantly, 5 x 10^6 OT-I T cells adoptively transferred into K14-mOVA transgenic mice regularly induced GVHD-like inflammatory skin inflammation and tissue damage, whereas less cells did not induce significant inflammatory reactions (Shibaki et al., 2004). Analysis of RIP-mOVA mice that were adoptively transferred with less than 5 x 10^6 OT-I T cells suggested that the TCR transgenic CD8$^+$ T cells were lost, probably due to deletion, after entry in the peripheral tissues (Kurts et al., 1997b). In most mouse models of transgenic self-antigen presentation an additional inflammatory signal such as viral infection (Oldstone et al., 1991; Vezys et al., 2000) or sublethal irradiation (Azukizawa et al., 2003) was generally required to initiate disease. Most mouse models of acute GVHD involve myeloablative irradiation for host conditioning and, therefore, to model allo-HCT we also used this conditioning regimen before transfer of OT-I T cells into RIP-mOva recipients.

In contrast to the restriction to gut, liver, and skin in acute GVHD, we found that after HCT also other organs had been infiltrated in an antigen dependent manner. However, it must be kept in mind that we used transgenic mouse models and therefore results have to be interpreted with caution. Monoclonal TCR transgenic CD8$^+$ T cells, such as OT-I T cells, possess a relatively high-avidity for antigen (Heath et al., 1993). Furthermore the nature of precursor frequency of alloreactivity in this TCR transgenic T cell model amounts to 100% and thus differs from polyclonal T cell responses in multiple miHAg-mismatched allo-HCT.

5.2.2 Effective T cell mediated destruction of alloantigen expressing target tissues

We had hypothesized that the high numbers of proliferating OT-I T cells may compete for resources and survival factors, such as IL2, and therefore failed to cause lethal tissue

damage in βa-Ova recipients. However, we found that HCT of lower OT-I cell numbers into βa-Ova recipients led to a higher survival rate, which did not support our initial hypothesis.

In RIP-mOva mice, Kurts et al. (1997a) demonstrated that in the absence of irradiation the transfer of high OT-I T cell numbers ($> 5 \times 10^6$) is sufficient to effectively cause diabetes. We found that after irradiation the transfer of as little as 100 OT-I T cells sufficed to effectively cause diabetes with 100% mortality. In comparison to RIP-mOva recipients that had received high OT-I cell numbers ($1 \times 10^5 - 1 \times 10^6$), recipients of lower numbers developed diabetes later, that was followed by a delayed mortality. Cell number dependent course and outcome of an autoimmune disease is observed in many experimental mouse models of acute GVHD (Schroeder and DiPersio, 2011) and diabetes (Kurts et al., 1997a). Yet, we could demonstrate that the alloantigen recognition of OT-I T cells is highly effective and even very few cells were sufficient for localization and destruction of alloantigen expressing cells. Hence, also the expression of a single miHAg should be sufficient to cause acute GVHD even when the precursor frequency is very low.

5.2.3 Quantification of organ infiltrating OT-I T cells with FACS

To directly determine and compare numbers of organ infiltrating OVA specific CD8$^+$ T cells after HCT we analyzed tissues of different recipients with FACS at defined time points. In βa-Ova recipients we detected high OT-I T cell numbers already at day+4 after HCT, demonstrating a massive T cell proliferation and accumulation in peripheral tissues. In contrast, at day+4 we found in RIP-mOva as well as in B6 recipients very few OT-I T cells in almost all peripheral organs. This few early migrating T cells could probe peripheral tissues for cognate antigen. At sites of alloantigen recognition probing T cells could engage in their effector mechanisms, including direct target cell killing and cytokine production and consequently directly or indirectly attract further T cells to this site. Accordingly, from day+4 to day+6 we detected a slight increase of OT-I T cells, similar between organs of RIP-mOva and B6 recipients, but for the pancreas. In the pancreas of RIP-mOva recipients OT-I T cells increased by more than 100 fold, suggesting a specific trafficking or recruitment of donor OT-I T cells.

In infections, pathogen-induced tissue inflammation might specifically dictate effector T cell migration. Mouse models of acute GVHD rely on total body irradiation for recipient conditioning, inducing a systemic inflammation rather than a tissue specific irritation. One would hypothesize that without any tissue specific signal the activated antigen specific T cells should randomly migrate from SLOs to peripheral organs where they might encounter by chance their cognate antigen when entering a tissue. We observed a specific accumulation

of donor OT-I T cells in the pancreas of RIP-mOva mice. This phenomenon might be explained either by direct T cell guiding mechanisms such as recruitment by selective endothelial antigen presentation in the pancreas, or by clues released by early probing T cells that had randomly encountered cognate antigen. Yet, remarkably, organ manifestation in acute GVHD was restricted to selective tissues that neither in mouse models nor in patients involve the pancreas.

5.2.4   Identification of organ infiltrating OT-I T cells with LSFM

As we could demonstrate that LSFM is an effective tool for detecting single cells in large specimen, we applied this versatile technique to screen large tissue samples of intact organs, with the goal of detecting first organ infiltrating OT-I T cells after HCT. To reveal the kinetics of T cell migration and organ infiltration following HCT we applied repeated sampling. Remarkably, in RIP-mOva recipients we found very low numbers of first islet infiltrating T cells on day+4 after HCT followed by a massive T cell migration to the pancreas within the following 24h. The kinetic of this T cell migration suggests a targeted recruitment to the tissue of alloantigen expression. Importantly, although we found few OT-I T cells in various other organs of RIP-mOva recipients between day+3 and day+6 after HCT, such a massive T cell migration only occurred to the pancreas. Thus we postulate that the first target antigen recognizing OT-I T cells might directly or indirectly contribute to attract further T cells to the pancreas.

In a mouse model of vaginal HSV-2 infection, Nakanishi et al. (2009) found that CD4$^+$ effector T cells enter the infected vaginal mucosa prior to CD8$^+$ effector T cells. They demonstrated that these early infiltrating CD4$^+$ T cells secrete IFN-γ, presumably upon antigen contact, and stimulated the vaginal epithelium to secrete CXCL9 and CXCL10, guiding the CD8$^+$ T cells migration into the infected tissues (Nakanishi et al., 2009). The CD4$^+$ T cell migration to the infected tissues itself, might already be promoted by the IFN-γ secreting natural killer (NK) cells that are involved early after vaginal HSV-2 infection (Nakanishi et al., 2009). Nonetheless, in this model of HSV-2 infection, CD4$^+$ T cells appear to serve as the pathfinder for an effective CD8$^+$ T cell recruitment. In our study we transferred TCR transgenic OVA specific CD8$^+$ T cells only, excluding the involvement of antigen specific donor CD4$^+$ T cells that may have facilitated an effective CD8$^+$ T cell recruitment. Vaginal HSV-2 infection causes a tissue selective inflammation, promoting tissue specific innate immune processes that in turn might facilitate adaptive immune responses. In contrast, in our experiments that mimic the clinical scenario of HCT the recipients underwent total body irradiation, causing systemic inflammation. It is possible that in this scenario the very early migrating effector T cells randomly scan all organs and upon cognate antigen encountering subsequently facilitate an

effective recruitment by the bulk of activated effector T cells. Such a hypothetical model would be in accordance with our observation that we found few OT-I T cells in various organs of RIP-mOva recipients at day+4 after HCT. Only in the ovalbumin-expressing pancreas we found a subsequent steep increase of infiltrating antigen specific OT-I T cells. Hence, we postulate that first target antigen recognizing OT-I T cells may act as pathfinder that directly or indirectly trigger a signal cascade, e.g. via the release of cytokines or chemokines to induce further T cell attraction to the pancreas. These signals may include IFN-γ and CCL2 as we detected high levels of these cytokines at day+6 after HCT of OT-I T cells into ovalbumin expressing recipients.

5.2.5 Antigen expression by either hematopoietic, or by parenchymal cells only result in alloreactive T cell organ infiltration

In the setting of HCT alloantigens are expressed on hematopoietic cells, GVHD target epithelium and leukemia cells (Asakura et al., 2010). We transplanted antigen specific OT-I T cells into established chimeras expressing the antigen ovalbumin either by hematopoietic cells or by parenchymal cells only. Interestingly, we found that OT-I T cells infiltrated all organs at day+6 after HCT, irrespective of alloantigen expression by hematopoietic cells or parenchymal cells. However, in both cases the alloantigen might be released from apoptotic cells, caused by conditioning. Cross-presentation by endothelial cells might allow to selectively recruit antigen specific CTLs (Kurts et al., 2010). Furthermore, liver endothelial cells have been reported to efficiently present exogenous antigens to CD8$^+$ T cells (Limmer et al., 2000). In a mouse model of diabetes Savinov et al. (2003) demonstrated that cross-presentation of the specific antigen by pancreatic endothelium allows for the homing of insulin-specific CD8 T cells to the islet. They suggested that endothelial cells may play a prominent role in the trafficking of activated T cells, at least for secreted proteins as insulin (Savinov et al., 2003). That non-secreted antigens can be cross-presented by endothelial cells was also suggested by studies of tissue transplantation models (Kreisel et al., 2002; Valujskikh et al., 2002). In light of peptide cross-presentation, endothelial cells can participate in the effector phase of T cell-mediated inflammatory responses such as autoimmunity, anti-tumor immunity, and transplant rejection (Bagai et al., 2005) without the necessity of organ specific alloantigen expression by parenchymal cells.

Another possible mechanism allowing an antigen specific T cell regulation in absence of parenchymal alloantigen expression would be cross-presentation of tissue residential DCs. CD103$^+$ DCs have been identified to uptake and cross-present tissue antigens after migrating into draining lymph nodes (Bedoui et al., 2009). If these DCs can cross-present antigens also in peripheral tissues remains unclear and, thus, the ability of DCs in regulating effector CTLs

in an antigen-specific manner is unknown (Kurts et al., 2010). Recently, mucosal resident CX3CR1⁺ DCs have been identified to effectively cross-present circulatory or luminal antigens and control CD8⁺ T cell activation (Chang et al., 2013). Nonetheless, DC cross-presentation cannot elicit epithelial damage that is triggered during acute GVHD, because CD8⁺ T cells require a direct contact to a target-cell to promote killing (Trapani and Smyth, 2002). However, this contact may induce danger signals or stimulate the T cell for cytokine release, followed by further T cell attraction.

5.2.6   OT-I T cell proliferation ability and IFN-γ production *in vitro*

We found high levels of IFN-γ in the serum of ovalbumin expressing recipients (βa-Ova, βa-Ova-chimeras and RIP-mOva) of OT-I T cells at day+6 after HCT, indicating an involvement of this cytokine in antigen specific OT-I T cell mediated pathology. *In vitro* activated OT-I T cells responded with the production of IFN-γ upon antigen re-encounter. We postulate that IFN-γ might be relevant in the alloantigen dependent organ infiltration of antigen specific CD8⁺ T cell infiltration after HCT.

IFN-γ is a key cytokine in innate and adaptive immune responses by having multiple functions on macrophages, NK cells, and T cells (Hu and Ivashkiv, 2009). In acute GVHD IFN-γ has the ability to either promote or attenuate the development of disease (Welniak et al., 2000; Asavaroengchai et al., 2007; Lu and Waller, 2009; Wang et al., 2009). IFN-γ is considered to induce the production of chemokines in target organs during the initial phase of GVHD (Schroeder and DiPersio, 2011). Especially the timing of IFN-γ production might influence the development and severity of acute GVHD, as immediately after HCT IFN-γ is described to mediate immunosuppressive effects but during the GVHD effector phase can also amplify GVHD pathology due to its pro-inflammatory properties (Lu and Waller, 2009; Blazar et al., 2012). During the pathogenesis of acute GVHD IFN-γ further induces chemokines as well as inflammatory responses, enhancing the migration of effector T cells to the sites of inflammation (Mapara et al., 2006). Similarly, IFN-γ release is also required for inducing further chemokine-production to promote CD8⁺ T cell entry in the herpes virus infected vaginal mucosa (Nakanishi et al., 2009). In a mouse model of diabetes IFN-γ, among others, plays an important role in the control of the homing of activated diabetogenic T cells to the islets (Savinov et al., 2001).

5.2.7 Antigen recognition of alloreactive TCR transgenic CD4^{+} T cells - proliferation and migration of OT-II cells

When we transplanted TCR transgenic CD4^{+} T cells (OT II cells) into conditioned βa-Ova recipients we observed similarly to OT-I T cell HCT, an effective proliferation and an overall organ infiltration at day+6 after HCT, suggesting also an antigen dependent T cell distribution.

MHC II presented peptides derive from extracellular antigens or cytosolic proteins that are degraded through autophagy (Crotzer and Blum, 2010; Neefjes et al., 2011). MHC-II expression and therefore also antigen presentation is restricted to APCs, such as DCs, B cells or macrophages. Also epithelial cells within the gastrointestinal tract have been reported to present antigens via MHC II molecules during inflammation (Beers et al., 2005). Recently, it could be shown that non-hematopoietic antigen-presenting cells of HCT recipients alone are sufficient to induce a CD4^{+} T cell mediated lethal acute GVHD (Koyama et al., 2011). If the migration of OT-II cells depends on the access to alloantigens, both, the site of antigen expression and the presentation by APCs could dictate the tissue tropism. Hence, in this case the tissue specific distribution of APCs as well as tissue dependent efficiency of antigen presentation might influence CD4^{+} T cell migration.

In contrast to OVA-specific CD8^{+} T cells that have to be cross-primed when transferred to RIP-mOva recipients, OT-II cells rely on the presentation of peptides in the context of MHC-II via professional APCs for activation. After HCT into RIP-mOva recipients OT-II cells did not efficiently proliferate and therefore we could not detect migrating antigen specific T cells to peripheral tissues, such as the pancreas at day+6. Accordingly, in adoptive transfer experiments of OT-II cells into RIP-mOva recipients, Kurts et al. (1997a) found that even high numbers of 10×10^6 OVA-specific CD4 T cells failed to induce diabetes. Nevertheless, they demonstrated that the coinjection of OVA-specific CD4 helper T cells together with small numbers of OVA-specific CD8 T cells increased the incidence of diabetes. This enhancing effect of OT-II cells was neither explained by an increased proliferation of OT-I T cells nor by an effector function to the pancreatic islet cells, but by an impaired survival of CD8^{+} T cells (Kurts et al., 1997a). Whether CD4^{+} T cell help was provided in the draining LNs or at the site of antigen-expression, was not investigated in this study.

In conclusion, here we demonstrated the importance of alloantigen expression for the organ infiltration of CD8^{+} T cells after HCT. We found that, depending on the tissue antigen expression, also GVHD non-target organs can be infiltrated by alloreactive T cells. At an early time point after HCT we found few donor cells distributing in all organs followed by a specific recruitment to the alloantigen expressing tissue. This finding might highlight the

importance of alloantigen dependent signaling for the further recruitment and accumulation of additional CD8$^+$ effector T cells.

We hypothesize that the selective organ manifestation during GVHD is initiated by first T cells that recognize their cognate antigen in peripheral tissues, produce cytokines and thus further recruit additional donor T cells. We conjecture that the activation of alloreactive T cells in mucosal associated SLOs as well as peripheral antigen presentation may favor the initial donor T cell infiltration of the gastrointestinal tract after allo-HCT. However, peripheral alloantigen expression directs the organ specific T cell infiltration and the absence of cognate antigen from the typical GVHD target tissues can result in an altered organ manifestation as demonstrated by our experiments.

References

Al-Hajj, M., Wicha, M.S., Benito-Hernandez, A., Morrison, S.J., and Clarke, M.F. (2003). Prospective identification of tumorigenic breast cancer cells. Proc. Natl. Acad. Sci. U.S.A. *100*, 3983–3988.

Anderson, B.E., Mcniff, J., Yan, J., Doyle, H., Mamula, M., Shlomchik, M.J., and Shlomchik, W.D. (2003). Memory CD4 + T cells do not induce graft-versus-host disease. J Clin Invest. *112*, 101–108.

Anderson, B.E., Taylor, P. a, McNiff, J.M., Jain, D., Demetris, A.J., Panoskaltsis-Mortari, A., Ager, A., Blazar, B.R., Shlomchik, W.D., and Shlomchik, M.J. (2008). Effects of donor T-cell trafficking and priming site on graft-versus-host disease induction by naive and memory phenotype CD4 T cells. Blood *111*, 5242–5251.

Asakura, S., Hashimoto, D., Takashima, S., Sugiyama, H., Maeda, Y., Akashi, K., Tanimoto, M., and Teshima, T. (2010). Alloantigen expression on non-hematopoietic cells reduces graft-versus-leukemia effects in mice. *120*,.

Asavaroengchai, W., Wang, H., Wang, S., Wang, L., Bronson, R., Sykes, M., and Yang, Y.-G. (2007). An Essential Role for IFN-γ in Regulation of Alloreactive CD8 T Cells Following Allogeneic Hematopoietic Cell Transplantation. Biol Blood Marrow Transplant *13*, 46–55.

Azukizawa, H., Kosaka, H., Sano, S., Heath, W.R., Takahashi, I., Gao, X.-H., Sumikawa, Y., Okabe, M., Yoshikawa, K., and Itami, S. (2003). Induction of T-cell-mediated skin disease specific for antigen transgenically expressed in keratinocytes. European Journal of Immunology *33*, 1879–1888.

Bagai, R., Valujskikh, A., Canaday, D.H., Bailey, E., Lalli, P.N., Harding, C. V, and Heeger, P.S. (2005). Mouse endothelial cells cross-present lymphocyte-derived antigen on class I MHC via a TAP1- and proteasome-dependent pathway. Journal of Immunology *174*, 7711–7715.

Banchereau, J., Briere, F., Caux, C., Davoust, J., Lebecque, S., Liu, Y., Pulendran, B., and Palucka, K. (2000). Immunobiology of Dendritic Cells. Annu Rev Immunol. *18*, 767–811.

Bedoui, S., Whitney, P.G., Waithman, J., Eidsmo, L., Wakim, L., Caminschi, I., Allan, R.S., Wojtasiak, M., Shortman, K., Carbone, F.R., et al. (2009). Cross-presentation of viral and self antigens by skin-derived CD103+ dendritic cells. Nat Immunol *10*, 488–495.

Beers, C., Burich, A., Kleijmeer, M.J., Griffith, J.M., Wong, P., Alexander, Y., and Rudensky, A.Y. (2005). Cathepsin S Controls MHC Class II-mediated Antigen Presentation by Epithelial Cells In Vivo. J Immunol *174*, 1205–1212.

Beilhack, A., Schulz, S., Baker, J., Beilhack, G.F., Nishimura, R., Baker, E.M., Landan, G., Herman, E.I., Butcher, E.C., Contag, C.H., et al. (2008). Prevention of acute graft-versus-host disease by blocking T-cell entry to secondary lymphoid organs. Blood *111*, 2919–2928.

Beilhack, A., Schulz, S., Baker, J., Beilhack, G.F., Wieland, C.B., Herman, E.I., Baker, E.M., Cao, Y.-A., Contag, C.H., and Negrin, R.S. (2005). In vivo analyses of early events in acute graft-versus-host disease reveal sequential infiltration of T-cell subsets. Blood *106*, 1113–1122.

Van Bekkum, D., and Knaan, S. (1977). Role of bacterial microflora in development of intestinal lesions from graft-versus-host reaction. J Natl Cancer Inst. *58*, 787–790.

Betzig, E., Patterson, G.H., Sougrat, R., Lindwasser, O.W., Olenych, S., Bonifacino, J.S., Davidson, M.W., Lippincott-Schwartz, J., and Hess, H.F. (2006). Imaging Intracellular Fluorescent Proteins at Nanometer Resolution. Science *313* , 1642–1645.

Billingham, R.E. (1966). The biology of graft-versus-host reactions. Harvey Lect. *62*, 21–78.

Blazar, B.R., Murphy, W.J., and Abedi, M. (2012). Advances in graft-versus-host disease biology and therapy. Nature Reviews. Immunology *12*, 443–458.

Bleakley, M., and Riddell, S.R. (2004). Molecules and mechanisms of the graft-versus-leukaemia effect. Nature Reviews. Cancer *4*, 371–380.

Bolte, S., and Cordelières, F.P. (2006). A guided tour into subcellular colocalization analysis in light microscopy. Journal of Microscopy *224*, 213–232.

Boppart, S.A., Brezinski, M.E., Bouma, B.E., Tearney, G.J., and Fujimoto, J.G. (1996). Investigation of Developing Embryonic Morphology Using Optical Coherence Tomography. Dev. Biol. *63*, 54 –63.

Boscacci, T., Pfeiffer, F., Gollmer, K., Isabel, A., Sevilla, C., Martin, A.M., Soriano, S.F., Natale, D., Henrickson, S., Andrian, U.H. Von, et al. (2010). Comprehensive analysis of lymph node stroma-expressed Ig superfamily members reveals redundant and nonredundant roles for ICAM-1, ICAM-2, and VCAM-1 in lymphocyte homing. Blood *116*, 915–925.

Bour, H., Horvath, C., Lurquin, C., Cerottini, J.C., and MacDonald, H.R. (1998). Differential requirement for CD4 help in the development of an antigen-specific CD8+ T cell response depending on the route of immunization. Journal of Immunology *160*, 5522–5529.

De Bueger, M., Bakker, A., Van Rood, J., Van der Woude, F., and Goulmy, E. (1992). Tissue distribution of human minor histocompatibility antigens. Ubiquitous versus restricted tissue distribution indicates heterogeneity among human cytotoxic T lymphocyte-defined non-MHC antigens. determined. J Immunol. *149*, 1788–1794.

Campbell, D.J., and Butcher, E.C. (2002). Rapid Acquisition of Tissue-specific Homing Phenotypes by CD4 2 T Cells Activated in Cutaneous or Mucosal Lymphoid Tissues. *195*, 135–142.

Cao, Y.-A., Bachmann, M.H., Beilhack, A., Yang, Y., Tanaka, M., Swijnenburg, R.-J., Reeves, R., Taylor-Edwards, C., Schulz, S., Doyle, T.C., et al. (2005). Molecular Imaging Using Labeled Donor Tissues Reveals Patterns of Engraftment, Rejection, and Survival in Transplantation. Transplantation *80*, 134–139.

Cao, Y.-A., Wagers, A.J., Beilhack, A., Dusich, J., Bachmann, M.H., Negrin, R.S., Weissman, I.L., and Contag, C.H. (2004). Shifting foci of hematopoiesis during reconstitution from single stem cells. Proc. Natl. Acad. Sci. U.S.A. *101*, 221–226.

Carbone, F.R., Kurts, C., Bennett, S.R.M., Miller, J.F.A.P., and Heath, W.R. (1998). Cross-presentation: a general mechanism for CTL immunity and tolerance. Immunology Today *19*, 368–373.

Chakraverty, R., Côté, D., Buchli, J., Cotter, P., Hsu, R., Zhao, G., Sachs, T., Pitsillides, C.M., Bronson, R., Means, T., et al. (2006). An inflammatory checkpoint regulates recruitment of graft-versus-host reactive T cells to peripheral tissues. The Journal of Experimental Medicine *203*, 2021–2031.

Chang, S.-Y., Song, J.-H., Guleng, B., Cotoner, C.A., Arihiro, S., Zhao, Y., Chiang, H.-S., O'Keeffe, M., Liao, G., Karp, C.L., et al. (2013). Circulatory Antigen Processing by Mucosal Dendritic Cells Controls CD8+ T Cell Activation. Immunity *38*, 153–165.

Chen, B.J., Cui, X., Sempowski, G.D., Liu, C., and Chao, N.J. (2004). Transfer of allogeneic CD62L- memory T cells without graft-versus-host disease. Blood *103*, 1534–1541.

Coghill, J.M., Sarantopoulos, S., Moran, T.P., Murphy, W.J., Blazar, B.R., and Serody, J.S. (2011). Effector CD4+ T cells, the cytokines they generate, and GVHD: something old and something new. Blood *117*, 3268–3276.

Cooke, K.R., Gerbitz, a, Crawford, J.M., Teshima, T., Hill, G.R., Tesolin, a, Rossignol, D.P., and Ferrara, J.L. (2001). LPS antagonism reduces graft-versus-host disease and preserves graft-versus-leukemia activity after experimental bone marrow transplantation. The Journal of Clinical Investigation *107*, 1581–1589.

Crotzer, V.L., and Blum, J.S. (2010). Autophagy and adaptive immunity. Immunology *131*, 9–17.

Csencsits, K.L., and Bishop, D.K. (2003). Contrasting alloreactive CD4+ and CD8+ T cells: there's more to it than MHC restriction. American Journal of Transplantation : Official Journal of the American Society of Transplantation and the American Society of Transplant Surgeons *3*, 107–115.

Cyster, J.G. (2005). Chemokines, sphingosine-1-phosphate, and cell migration in secondary lymphoid organs. Annual Review of Immunology *23*, 127–159.

Damdinsuren, B., Zhang, Y., Khalil, A., Wood, W.H., Becker, K.G., Shlomchik, M.J., and Sen, R. (2010). Single round of antigen receptor signaling programs naive B cells to receive T cell help. Immunity *32*, 355–366.

Davenport, M.P., Grimm, M.C., and Lloyd, a R. (2000). A homing selection hypothesis for T-cell trafficking. Immunology Today *21*, 315–317.

Dodt, H.-U., Ulrich Leischner, Anja Schierloh, Nina Jährling, C.P.M., Katrin Deininger, Jan Michael Deussing, Matthias Eder, W.Z., and Becker, K. (2007). Ultramicroscopy: three-dimensional visualization of neuronal networks in the whole mouse brain. Nat. Methods *4*, 331–336.

Drexler, W., and Fujimoto, J.G. (2008). State-of-the-art retinal optical coherence tomography. Prog. Retin. Eye Res. *27*, 45–88.

Dutt, S., Tseng, D., Ermann, J., George, T.I., Liu, Y.P., Davis, C.R., Fathman, C.G., and Strober, S. (2007). Naive and Memory T Cells Induce Different Types of Types of Graft-versus-Host Disease. J Immunol. *179*, 6547–6554.

Edinger, M., Cao, Y.-A., Verneris, M.R., Bachmann, M.H., Contag, C.H., and Negrin, R.S. (2003). Revealing lymphoma growth and the efficacy of immune cell therapies using in vivo bioluminescence imaging. Blood *101*, 640–648.

Ermolayev, V., Cathomen, T., Merk, J., Friedrich, M., Härtig, W., Harms, G.S., Klein, M. a, and Flechsig, E. (2009a). Impaired axonal transport in motor neurons correlates with clinical prion disease. PLoS Pathogens *5*, e1000558.

Ermolayev, V., Friedrich, M., Nozadze, R., Cathomen, T., Klein, M. a, Harms, G.S., and Flechsig, E. (2009b). Ultramicroscopy reveals axonal transport impairments in cortical motor neurons at prion disease. Biophys. J. *96*, 3390–3398.

Ertürk, A., Becker, K., Jährling, N., Mauch, C.P., Hojer, C.D., Egen, J.G., Hellal, F., Bradke, F., Sheng, M., and Dodt, H.-U. (2012). Three-dimensional imaging of solvent-cleared organs using 3DISCO. Nature Protocols *7*, 1983–1995.

Ertürk, A., Mauch, C.P., Hellal, F., Förstner, F., Keck, T., Becker, K., Jährling, N., Steffens, H., Richter, M., Hübener, M., et al. (2011). Three-dimensional imaging of the unsectioned adult spinal cord to assess axon regeneration and glial responses after injury. Nat. Med. *18*, 166–172.

Ferrara, J.L., Levy, R., and Chao, N.J. (1999). Pathophysiologic mechanisms of acute graft-vs.-host disease. Biology of Blood and Marrow Transplantation : Journal of the American Society for Blood and Marrow Transplantation *5*, 347–356.

Ferrara, J.L.M., and Krenger, W. (1998). Graft-versus-host disease: The influence of type 1 and type 2 T cell cytokines. Transfusion Medicine Reviews *12*, 1–17.

Ferrara, J.L.M., and Reddy, P. (2006). Pathophysiology of Graft-Versus-Host Disease. Seminars in Hematology *43*, 3–10.

Fontaine, P., Roy-Proulx, G., Knafo, L., Baron, C., Roy, D.C., and Perreault, C. (2001). Adoptive transfer of minor histocompatibility antigen-specific T lymphocytes eradicates leukemia cells without causing graft-versus-host disease. Nature Medicine *7*, 789–794.

Friedrich, M., Gan, Q., Ermolayev, V., and Harms, G.S. (2011). STED-SPIM : Stimulated Emission Depletion Improves Sheet Illumination Microscopy Resolution. Biophys. J. *100*, L43–L45.

Gonzalez, M., Quezada, S. a, Blazar, B.R., Panoskaltsis-Mortari, A., Rudensky, A.Y., and Noelle, R.J. (2002). The balance between donor T cell anergy and suppression versus lethal graft-versus-host disease is determined by host conditioning. Journal of Immunology *169*, 5581–5589.

Graser, R.T., DiLorenzo, T.P., Wang, F., Christianson, G.J., Chapman, H.D., Roopenian, D.C., Nathenson, S.G., and Serreze, D. V (2000). Identification of a CD8 T cell that can independently mediate autoimmune diabetes development in the complete absence of CD4 T cell helper functions. Journal of Immunology *164*, 3913–3918.

Gross, S., Moss, B.L., and Piwnica-Worms, D. (2007). Veni, vidi, vici: in vivo molecular imaging of immune response. Immunity *27*, 533–538.

Guermonprez, P., Saveanu, L., Kleijmeer, M., Davoust, J., Van Endert, P., and Amigorena, S. (2003). ER-phagosome fusion defines an MHC class I cross-presentation compartment in dendritic cells. Nature *425*, 397–402.

Gunn, M.D., Tangemann, K., Tam, C., Cyster, J.G., Rosen, S.D., and Williams, L.T. (1998). A chemokine expressed in lymphoid high endothelial venules promotes the adhesion and chemotaxis of naive T lymphocytes. Proc. Natl. Acad. Sci. U.S.A. *95*, 258–263.

Gyurkocza, B., Storb, R., Storer, B.E., Chauncey, T.R., Lange, T., Shizuru, J. a, Langston, A. a, Pulsipher, M. a, Bredeson, C.N., Maziarz, R.T., et al. (2010). Nonmyeloablative allogeneic hematopoietic cell transplantation in patients with acute myeloid leukemia. Journal of Clinical Oncology : Official Journal of the American Society of Clinical Oncology *28*, 2859–2867.

Hama, H., Kurokawa, H., Kawano, H., Ando, R., Shimogori, T., Noda, H., Fukami, K., Sakaue-Sawano, A., and Miyawaki, A. (2011). Scale: a chemical approach for fluorescence imaging and reconstruction of transparent mouse brain. Nat. Neurosci. *14*, 1481–1488.

Hamann, A., Jablonski-Westrich, D., Jonas, P., and Thiele, H.G. (1991). Homing receptors reexamined: mouse LECAM-1 (MEL-14 antigen) is involved in lymphocyte migration into gut-associated lymphoid tissue. Eur. J. Immunol. *21*, 2925–2929.

Harning, R., Mainolfi, E., Bystryn, J., Henn, M., Merluzzi, V.J., and Rothlein, R. (1991). Serum Levels of Circulating Intercellular Adhesion Molecule 1 in Human Malignant Melanoma. Cancer Research 5003–5005.

He, S., Cao, Q., Qiu, Y., Mi, J., Zhang, J.Z., Jin, M., Ge, H., Emerson, S.G., Zhang, Y., and Zhang, Y. (2008). A new approach to the blocking of alloreactive T cell-mediated graft-versus-

host disease by in vivo administration of anti-CXCR3 neutralizing antibody. The Journal of Immunology *181*, 7581–7592.

Heath, W.R., Kjer-Nielsen, L., and Hoffmann, M.W. (1993). Avidity for antigen can influence the helper dependence of CD8+ T lymphocytes. Journal of Immunology *151*, 5993–6001.

Herzenberg, L.A., Tung, J., Moore, W.A., Herzenberg, L.A., and Parks, D.R. (2006). Interpreting flow cytometry data: a guide for the perplexed. Nature Immunology *7*, 681–685.

Heymann, F., Meyer-schwesinger, C., Hamilton-williams, E.E., Hammerich, L., Panzer, U., Kaden, S., Quaggin, S.E., Floege, J., Gröne, H., and Kurts, C. (2009). Kidney dendritic cell activation is required for progression of renal disease in a mouse model of glomerular injury. *119*,.

Hildebrandt, G.C., Duffner, U. a, Olkiewicz, K.M., Corrion, L. a, Willmarth, N.E., Williams, D.L., Clouthier, S.G., Hogaboam, C.M., Reddy, P.R., Moore, B.B., et al. (2004). A critical role for CCR2/MCP-1 interactions in the development of idiopathic pneumonia syndrome after allogeneic bone marrow transplantation. Blood *103*, 2417–2426.

Hill, G.R., Crawford, J.M., Cooke, K.R., Brinson, Y.S., Pan, L., and Ferrara, J.L. (1997). Total body irradiation and acute graft-versus-host disease: the role of gastrointestinal damage and inflammatory cytokines. Blood *90*, 3204–3213.

Hoffman, R.M., and Yang, M. (2006). Whole-body imaging with fluorescent proteins. Nat. Protocols *1*, 1429–1438.

Hu, X., and Ivashkiv, L.B. (2009). Cross-regulation of signaling pathways by interferon-gamma: implications for immune responses and autoimmune diseases. Immunity *31*, 539–550.

Huisken, J., and Stainier, D.Y.R. (2007). Even fluorescence excitation by multidirectional selective plane illumination microscopy (mSPIM). Opt. Lett. *32*, 2608–2610.

Huisken, J., Swoger, J., Del Bene, F., Wittbrodt, J., and Stelzer, E.H.K. (2004). Optical sectioning deep inside live embryos by selective plane illumination microscopy. Science *305*, 1007–1009.

Hänninen, A., Nurmela, R., Maksimow, M., Heino, J., Jalkanen, S., and Kurts, C. (2007). Islet beta-cell-specific T cells can use different homing mechanisms to infiltrate and destroy pancreatic islets. The American Journal of Pathology *170*, 240–250.

Jaksch, M., and Mattsson, J. (2005). The pathophysiology of acute graft-versus-host disease. Scandinavian Journal of Immunology *61*, 398–409.

Jennings, S.R., Bonneau, R.H., Smith, P.M., Wolcott, R.M., and Chervenak, R. (1991). CD4-positive T lymphocytes are required for the generation of the primary but not the secondary CD8-positive cytolytic T lymphocyte response to herpes simplex virus in C57BL/6 mice. Cellular Immunology *133*, 234–252.

Jones, S.C., Murphy, G.F., Friedman, T.M., and Korngold, R. (2003). Importance of minor histocompatibility antigen expression by nonhematopoietic tissues in a CD4 + T cell – mediated graft-versus-host disease model. The Journal of Clinical Investigation *112*, 1880–1886.

Kaplan, D.H., Anderson, B.E., McNiff, J.M., Jain, D., Shlomchik, M.J., and Shlomchik, W.D. (2004). Target antigens determine graft-versus-host disease phenotype. Journal of Immunology *173*, 5467–5475.

Keller, P.J., Schmidt, A.D., Santella, A., Khairy, K., Bao, Z., Wittbrodt, J., and Stelzer, E.H.K. (2010). Fast, high-contrast imaging of animal development with scanned light sheet-based structured-illumination microscopy. Nat. Methods *7*, 637–642.

Keller, P.J., Schmidt, A.D., Wittbrodt, J., and Stelzer, E.H.K. (2008). Reconstruction of Zebrafish Early Light Sheet Microscopy. Science *322*, 1065–1069.

Kittan, N., and Hildebrandt, G. (2010). The Chemokine System: A Possible Therapeutic Target in Acute Graft Versus Host Disease. In The Chemokine System in Experimental and Clinical Hematology SE - 23, O. Bruserud, ed. (Springer Berlin Heidelberg), pp. 97–120 LA – English.

Kohrt, H.E., Nouri, N., Nowels, K., Johnson, D., Holmes, S., and Lee, P.P. (2005). Profile of immune cells in axillary lymph nodes predicts disease-free survival in breast cancer. PLoS Medicine *2*, e284.

Korytowski, W., and Sarna, T. (1990). Bleaching of melanin pigments. Role of copper ions and hydrogen peroxide in autooxidation and photooxidation of synthetic dopa-melanin. The Journal of Bological Chemestry *265*, 12410–12416.

Koyama, M., Kuns, R.D., Olver, S.D., Raffelt, N.C., Wilson, Y. a, Don, A.L.J., Lineburg, K.E., Cheong, M., Robb, R.J., Markey, K. a, et al. (2011). Recipient nonhematopoietic antigen-

presenting cells are sufficient to induce lethal acute graft-versus-host disease. Nature Medicine *18*,.

Kreisel, D., Krupnick, A.S., Gelman, A.E., Engels, F.H., Popma, S.H., Krasinskas, A.M., Balsara, K.R., Szeto, W.Y., Turka, L. a, and Rosengard, B.R. (2002). Non-hematopoietic allograft cells directly activate CD8+ T cells and trigger acute rejection: an alternative mechanism of allorecognition. Nature Medicine *8*, 233–239.

Kumar, V., Scandella, E., Danuser, R., Onder, L., Nitschké, M., Fukui, Y., Halin, C., Ludewig, B., and Stein, J. V (2010). Global lymphoid tissue remodeling during a viral infection is orchestrated by a B cell-lymphotoxin-dependent pathway. Blood *115*, 4725–4733.

Kurts, B.C., Carbone, F.R., Barnden, M., Blanas, E., Allison, J., Heath, W.R., and Miller, J.F.A.P. (1997a). CD4+ T Cell Help Impairs CD8+ T Cell Deletion Induced by Cross-presentation of Self-Antigens and Favors Autoimmunity. The Journal of Experimental Medicine *186*, 2057–2062.

Kurts, B.C., Heath, W., Carbone, F., Allison, J., Miller, J.F.A.R., and Kosaka, H. (1996). Constitutive class I-restricted exogenou spresentation of self antigens in vivo. The Journal of Experimental Medicine *184*, 923–930.

Kurts, C., Kosaka, H., Carbone, F.R., Miller, J.F.A.P., and Heath, W.R. (1997b). Class I – restricted Cross-Presentation of Exogenous Self-Antigens Leads to Deletion of Autoreactive. The Journal of Experimental Medicine *186*, 239–245.

Kurts, C., Robinson, B.W.S., and Knolle, P. a. (2010). Cross-priming in health and disease. Nature Reviews Immunology *10*, 403–414.

Kurts, C., Sutherland, R.M., Davey, G., Li, M., Lew, a M., Blanas, E., Carbone, F.R., Miller, J.F., and Heath, W.R. (1999). CD8 T cell ignorance or tolerance to islet antigens depends on antigen dose. Proceedings of the National Academy of Sciences of the United States of America *96*, 12703–12707.

Lampert, I.A., Suitters, A.J., and Chisholm, P.M. (1981). Expression of Ia antigen on epidermal keratinocytes in graft-versus-host disease. Nature *293*, 149–150.

Leischner, U., Schierloh, A., Zieglgänsberger, W., and Dodt, H.-U. (2010). Formalin-induced fluorescence reveals cell shape and morphology in biological tissue samples. PloS One *5*, e10391.

Leventhal, J., Huang, Y., Xu, H., Goode, I., and Ildstad, S.T. (2012). Novel regulatory therapies for prevention of Graft-versus-host disease. BMC Medicine *10*, 48.

Limmer, A., Ohl, J., Kurts, C., Ljunggren, H.G., Reiss, Y., Groettrup, M., Momburg, F., Arnold, B., and Knolle, P. a (2000). Efficient presentation of exogenous antigen by liver endothelial cells to CD8+ T cells results in antigen-specific T-cell tolerance. Nature Medicine *6*, 1348–1354.

Lu, Y., and Waller, E.K. (2009). Dichotomous role of interferon-γ in allogeneic bone marrow transplant. Biol. Blood Marrow Transplant. *15*, 1347–1353.

Ludewig, B., Stein, J. V, Sharpe, J., Cervantes-Barragan, L., Thiel, V., and Bocharov, G. (2012). A global "imaging" view on systems approaches in immunology. European Journal of Immunology *42*, 3116–3125.

Machnik, A., Neuhofer, W., Jantsch, J., Dahlmann, A., Tammela, T., Machura, K., Park, J.-K., Beck, F.-X., Müller, D.N., Derer, W., et al. (2009). Macrophages regulate salt-dependent volume and blood pressure by a vascular endothelial growth factor-C-dependent buffering mechanism. Nat. Med. *15*, 545–552.

Mackay, C.R. (2001). Chemokines : immunology ' s high impact factors. Nat Immunol. *2*, 95–101.

Mapara, M.Y., Leng, C., Kim, Y.-M., Bronson, R., Lokshin, A., Luster, A., and Sykes, M. (2006). Expression of chemokines in GVHD target organs is influenced by conditioning and genetic factors and amplified by GVHR. Biology of Blood and Marrow Transplantation : Journal of the American Society for Blood and Marrow Transplantation *12*, 623–634.

Masopust, D., Vezys, V., Marzo, a L., and Lefrançois, L. (2001). Preferential localization of effector memory cells in nonlymphoid tissue. Science *291*, 2413–2417.

Massoud, T.F., and Gambhir, S.S. (2003). Molecular imaging in living subjects: seeing fundamental biological processes in a new light. Genes & Development *17*, 545–580.

Matte, C.C., Liu, J., Cormier, J., Anderson, B.E., Athanasiadis, I., Jain, D., McNiff, J., and Shlomchik, W.D. (2004). Donor APCs are required for maximal GVHD but not for GVL. Nature Medicine *10*, 987–992.

Matte-Martone, C., Liu, J., Jain, D., McNiff, J., and Shlomchik, W.D. (2008). CD8+ but not CD4+ T cells require cognate interactions with target tissues to mediate GVHD across only

minor H antigens, whereas both CD4+ and CD8+ T cells require direct leukemic contact to mediate GVL. Blood *111*, 3884–3892.

Mora, J.R., Bono, M.R., and Manjunath, N. (2003). Selective imprinting of gut-homing T cells by Peyer's patch dendritic cells. Nature *424*, 7–12.

Moser, B., Wolf, M., Walz, A., and Loetscher, P. (2004). Chemokines: multiple levels of leukocyte migration control. Trends in Immunology *25*, 75–84.

Murai, M., Yoneyama, H., Ezaki, T., Suematsu, M., Terashima, Y., Harada, A., Hamada, H., Asakura, H., Ishikawa, H., and Matsushima, K. (2003). Peyer's patch is the essential site in initiating murine acute and lethal graft-versus-host reaction. Nature Immunology *4*, 154–160.

Murai, M., Yoneyama, H., Harada, a, Yi, Z., Vestergaard, C., Guo, B., Suzuki, K., Asakura, H., and Matsushima, K. (1999). Active participation of CCR5(+)CD8(+) T lymphocytes in the pathogenesis of liver injury in graft-versus-host disease. The Journal of Clinical Investigation *104*, 49–57.

Nakanishi, Y., Lu, B., Gerard, C., and Iwasaki, A. (2009). CD8(+) T lymphocyte mobilization to virus-infected tissue requires CD4(+) T-cell help. Nature *462*, 510–513.

Neefjes, J., Jongsma, M.L.M., Paul, P., and Bakke, O. (2011). Towards a systems understanding of MHC class I and MHC class II antigen presentation. Nature Reviews. Immunology *11*, 823–836.

Negrin, R.S., and Contag, C.H. (2006). In vivo imaging using bioluminescence: a tool for probing graft-versus-host disease. Nature Reviews. Immunology *6*, 484–490.

Oldstone, M.B.A., Nerenberg, M., Southern, P., Price, J., and Lewicki, H. (1991). Virus infection triggers insulin-dependent diabetes mellitus in a transgenic model: Role of anti-self (virus) immune response. Cell *65*, 319–331.

Panoskaltsis-Mortari, a, Hermanson, J.R., Haddad, I.Y., Wangensteen, O.D., and Blazar, B.R. (2001). Intercellular adhesion molecule-I (ICAM-I, CD54) deficiency segregates the unique pathophysiological requirements for generating idiopathic pneumonia syndrome (IPS) versus graft-versus-host disease following allogeneic murine bone marrow transplantation. Biology of Blood and Marrow Transplantation : Journal of the American Society for Blood and Marrow Transplantation *7*, 368–377.

Panoskaltsis-Mortari, A., Price, A., Hermanson, J.R., Taras, E., Lees, C., Serody, J.S., and Blazar, B.R. (2004). In vivo imaging of graft-versus-host-disease in mice. Blood *103*, 3590–3598.

Petrovic, A., Alpdogan, O., Willis, L.M., Eng, J.M., Greenberg, A.S., Kappel, B.J., Liu, C., Murphy, G.J., Heller, G., and Van den Brink, M.R.M. (2004). LPAM (alpha 4 beta 7 integrin) is an important homing integrin on alloreactive T cells in the development of intestinal graft-versus-host disease. Blood *103*, 1542–1547.

Planchon, T.A., Gao, L., Milkie, D.E., Davidson, M.W., Galbraith, J.A., Galbraith, C.G., and Betzig, E. (2011). Rapid three-dimensional isotropic imaging of living cells using Bessel beam plane illumination. Nat. Methods *8*, 417–423.

Rabinovich, B. a, Ye, Y., Etto, T., Chen, J.Q., Levitsky, H.I., Overwijk, W.W., Cooper, L.J.N., Gelovani, J., and Hwu, P. (2008). Visualizing fewer than 10 mouse T cells with an enhanced firefly luciferase in immunocompetent mouse models of cancer. Proc. Natl. Acad. Sci. U.S.A. *105*, 14342–14346.

Reddy, P., Arora, M., Guimond, M., Mackal, C.L., and Weisdorf, D. (2009). GVHD: a continuing barrier to the safety of allogeneic transplantation. Biol Blood Marrow Transplant *15*, 162–168.

Reddy, P., and Ferrara, J.L.M. (2003). Immunobiology of acute graft-versus-host disease. Blood Reviews *17*, 187–194.

Reddy, P., and Ferrara, J.L.M. (2009). Mouse models of graft-versus-host disease. StemBook 1–23.

Reinhardt, R.L., Khoruts, a, Merica, R., Zell, T., and Jenkins, M.K. (2001). Visualizing the generation of memory CD4 T cells in the whole body. Nature *410*, 101–105.

Rocha, B., Grandien, A., and Freitas, A.A. (1995). Anergy and Exhaustion Are Independent Mechanisms of Peripheral T Cell Tolerance. The Journal of Experimental Medicine *181*, 993–1003.

Rollins, B.J. (1997). Chemokines. Blood *90*, 909–928.

Rot, A., and Von Andrian, U.H. (2004). Chemokines in innate and adaptive host defense: basic chemokinese grammar for immune cells. Annual Review of Immunology *22*, 891–928.

Sallusto, F., Lenig, D., Förster, R., Lipp, M., and Lanzavecchia, a (1999). Two subsets of memory T lymphocytes with distinct homing potentials and effector functions. Nature *401*, 708–712.

Santi, P. a, Johnson, S.B., Hillenbrand, M., GrandPre, P.Z., Glass, T.J., and Leger, J.R. (2009). Thin-sheet laser imaging microscopy for optical sectioning of thick tissues. Biotechniques *46*, 287–294.

Savinov, A.Y., Wong, F.S., and Chervonsky, A. V (2001). IFN-gamma affects homing of diabetogenic T cells. Journal of Immunology *167*, 6637–6643.

Savinov, A.Y., Wong, F.S., Stonebraker, A.C., and Chervonsky, A. V. (2003). Presentation of Antigen by Endothelial Cells and Chemoattraction Are Required for Homing of Insulin-specific CD8+ T Cells. Journal of Experimental Medicine *197*, 643–656.

Schroeder, M.A., and DiPersio, J.F. (2011). Mouse models of graft-versus-host disease: advances and limitations. Disease Models & Mechanisms *4*, 318–333.

Serody, J.S., Burkett, S.E., Panoskaltsis-mortari, A., Ng-cashin, J., Matsushima, G.K., Lira, S.A., Cook, D.N., Blazar, B.R., Dc, W., and Mcmahon, E. (2000). T-lymphocyte production of macrophage inflammatory protein-1a is critical to the recruitment of CD8 + T cells to the liver , lung , and spleen during graft-versus-host disease. Blood *96*, 2973–2980.

Shaner, N.C., Campbell, R.E., Steinbach, P.A., Giepmans, B.N.G., Palmer, A.E., and Tsien, R.Y. (2004). Improved monomeric red, orange and yellow fluorescent proteins derived from Discosoma sp. red fluorescent protein. Nat Biotech *22*, 1567–1572.

Shaner, N.C., Steinbach, P.A., and Tsien, R.Y. (2005). A guide to choosing fluorescent proteins. Nat Meth *2*, 905–909.

Sharpe, J., Ahlgren, U., Perry, P., Hill, B., Ross, A., Hecksher-Sørensen, J., Baldock, R., and Davidson, D. (2002). Optical projection tomography as a tool for 3D microscopy and gene expression studies. Science *296*, 541–545.

Shibaki, A., Sato, A., Vogel, J.C., Miyagawa, F., and Katz, S.I. (2004). Induction of GVHD-like skin disease by passively transferred CD8(+) T-cell receptor transgenic T cells into keratin 14-ovalbumin transgenic mice. The Journal of Investigative Dermatology *123*, 109–115.

Shlomchik, W.D. (2007). Graft-versus-host disease. Nature Reviews. Immunology *7*, 340–352.

Shlomchik, W.D., Couzens, M.S., Tang, C.B., McNiff, J., Robert, M.E., Liu, J., Shlomshik, Mark, J., and Emerson, S.G. (1999). Prevention of Graft Versus Host Disease by Inactivation of Host Antigen-Presenting Cells. Science *285*, 412–415.

Siedentopf, H., and Zsigmondy, R. (1903). Über Sichtbarmachung und Größenbestimmung ultramikroskopischer Teilchen, mit besonderer Anwendung auf Goldrubingläser. Annalen Der Physik *10*, 1–39.

Spalteholz, W. (1914). Über das Durchsichtigmachen von menschlichen und tierischen Präparaten. (Leipzig: S. Hierzel).

Stenstad, H., Ericsson, A., Johansson-Lindbom, B., Svensson, M., Marsal, J., Mack, M., Picarella, D., Soler, D., Marquez, G., Briskin, M., et al. (2006). Gut-associated lymphoid tissue-primed CD4+ T cells display CCR9-dependent and -independent homing to the small intestine. Blood *107*, 3447–3454.

Sullivan, K. (2004). Graft-vs.-host disease. In Blume KG, Forman SJ, Appelbaum FR, Eds. Thomas' Hematopoietic Cell Transplantation., (Oxford, United Kingdom: Blackwell Publishing Ltd), pp. 635–664.

Swoger, J., Huisken, J., and Stelzer, E.H.K. (2003). Multiple imaging axis microscopy improves resolution for thick-sample applications. Optics Letters *28*, 1654–1656.

Swoger, J., Verveer, P., Greger, K., Huisken, J., and Stelzer, E.H.K. (2007). Multi-view image fusion improves resolution in three-dimensional microscopy. Optics Express *15*, 8029–8042.

Szabo, M.C., Butcher, E.C., and Mcevoy, L.M. (1997). Specialization of Mucosal Follicular Dendritic Cells Revealed by Mucosal Addressin-Cell Adhesion Molecule-1 Display. J. Immunol. *158*, 5584–5588.

Teshima, T., Ordemann, R., Reddy, P., Gagin, S., Liu, C., Cooke, K.R., and Ferrara, J.L.M. (2002). Acute graft-versus-host disease does not require alloantigen expression on host epithelium. Nature Medicine *8*, 575–581.

Toubai, T., Tawara, I., Sun, Y., Liu, C., Nieves, E., Evers, R., Friedman, T., Korngold, R., and Reddy, P. (2012). Induction of acute GVHD by sex-mismatched H-Y antigens in the absence of functional radiosensitive host hematopoietic-derived antigen-presenting cells. Blood *119*, 3844–3853.

Trapani, J. a, and Smyth, M.J. (2002). Functional significance of the perforin/granzyme cell death pathway. Nature Reviews. Immunology *2*, 735–747.

Tung, J.W., Parks, D.R., Moore, W.A., Herzenberg, L.A., and Herzenberg, L.A. (2004). New approaches to fluorescence compensation and visualization of FACS data. Clinical Immunology (Orlando, Fla.) *110*, 277–283.

Valujskikh, A., Lantz, O., Celli, S., Matzinger, P., and Heeger, P.S. (2002). Cross-primed CD8(+) T cells mediate graft rejection via a distinct effector pathway. Nature Immunology *3*, 844–851.

Vezys, V., Olson, S., and Lefranc, L. (2000). Expression of Intestine-Specific Antigen Reveals Novel Pathways of CD8 T Cell Tolerance Induction. Immunity *12*, 505–514.

Wagers, A.J., Sherwood, R.I., Christensen, J.L., and Weissman, I.L. (2002). Little evidence for developmental plasticity of adult hematopoietic stem cells. Science *297*, 2256–2259.

Wang, B., Norbury, C.C., Greenwood, R., Bennink, J.R., Yewdell, J.W., and Frelinger, J. a (2001). Multiple paths for activation of naive CD8+ T cells: CD4-independent help. Journal of Immunology *167*, 1283–1289.

Wang, H., Asavaroengchai, W., Yeap, B.Y., Wang, M.-G., Wang, S., Sykes, M., and Yang, Y.-G. (2009). Paradoxical effects of IFN-gamma in graft-versus-host disease reflect promotion of lymphohematopoietic graft-versus-host reactions and inhibition of epithelial tissue injury. Blood *113*, 3612–3619.

Wang, X., Li, H., Matte-Martone, C., Cui, W., Li, N., Tan, H.S., Roopenian, D., and Shlomchik, W.D. (2011). Mechanisms of antigen presentation to T cells in murine graft-versus-host disease: cross-presentation and the appearance of cross-presentation. Blood *118*, 6426–6437.

Welniak, L. a, Kuprash, D. V, Tumanov, A. V, Panoskaltsis-Mortari, A., Blazar, B.R., Sun, K., Nedospasov, S. a, and Murphy, W.J. (2006). Peyer patches are not required for acute graft-versus-host disease after myeloablative conditioning and murine allogeneic bone marrow transplantation. Blood *107*, 410–412.

Welniak, L.A., Blazar, B.R., Anver, M.R., Wiltrout, R.H., and Murphy, W.J. (2000). Opposing roles of interferon-gamma on CD4+ T cell-mediated graft-versus-host disease: Effects of conditioning. Biology of Blood and Marrow Transplantation *6*, 604–612.

Williams, M. a, and Bevan, M.J. (2007). Effector and memory CTL differentiation. Annual Review of Immunology *25*, 171–192.

Wysocki, C. a, Burkett, S.B., Panoskaltsis-Mortari, A., Kirby, S.L., Luster, A.D., McKinnon, K., Blazar, B.R., and Serody, J.S. (2004). Differential roles for CCR5 expression on donor T cells during graft-versus-host disease based on pretransplant conditioning. Journal of Immunology *173*, 845–854.

Wysocki, C. a, Panoskaltsis-Mortari, A., Blazar, B.R., and Serody, J.S. (2005). Leukocyte migration and graft-versus-host disease. Blood *105*, 4191–4199.

Yamazaki, K., Nguyen, T., and Podack, E.R. (1999). Cutting edge: tumor secreted heat shock-fusion protein elicits CD8 cells for rejection. Journal of Immunology *163*, 5178–5182.

YI, S., Feng, X., Hawthorne, W., Patel, A., Walters, S., and O'Connell, P.J. (2000). CD8+ T Cells Are Capable of Rejecting Pancreatic Islet Xenografts. Transplantation *70*,.

Yi, T., Zhao, D., Lin, C.-L., Zhang, C., Chen, Y., Todorov, I., LeBon, T., Kandeel, F., Forman, S., and Zeng, D. (2008). Absence of donor Th17 leads to augmented Th1 differentiation and exacerbated acute graft-versus-host disease. Blood *112*, 2101–2110.

Yu, X., Albert, M.H., and Anasetti, C. (2006). Alloantigen Affinity and CD4 Help Determine Severity of Graft-versus-Host Disease Mediated by CD8 Donor T Cells. The Journal of Immunology *176*, 3383–3390.

Yu, X.Z., Bidwell, S., Martin, P.J., and Anasetti, C. (1999). Visualization, fate, and pathogenicity of antigen-specific CD8+ T cells in the graft-versus-host reaction. Journal of Immunology *163*, 4780–4787.

Zhao, X.-Y., Xu, L.-L., Lu, S.-Y., and Huang, X.-J. (2011). IL-17-producing T cells contribute to acute graft-versus-host disease in patients undergoing unmanipulated blood and marrow transplantation. European Journal of Immunology *41*, 514–526.

Zheng, H., Matte-Martone, C., Li, H., Anderson, B.E., Venketesan, S., Sheng Tan, H., Jain, D., McNiff, J., and Shlomchik, W.D. (2008). Effector memory CD4+ T cells mediate graft-versus-leukemia without inducing graft-versus-host disease. Blood *111*, 2476–2484.

Acknowledgments

Curriculum vitae

PERSONAL DATA

Name	Christian Brede
Place and date of birth	Kassel, Germany, March 17th, 1982
Nationality	German
Marital Status	Single

EDUCATION

2008 – Present	University of Würzburg, Germany
	PhD student (Experimental stem cell transplantation)
2001 – 2007	Study of Biology (diploma)
	University of Bayreuth, Germany, pre-diploma received 2003
	University of Würzburg, Germany, diploma received 2007
1992 – 2001	High School: König Heinrich-Schule, Fritzlar, Germany
	university-entrance diploma („Abitur") 06/2001
1988 – 1992	Primary School: Louise-Schröder Schule, Niedenstein, Germany

SCIENTIFIC WORK ABROAD

05/2005 – 08/2005	Benin (West Africa) practical
07/2006 – 09/2006	Benin (West Africa) diploma-thesis
07/2007 – 09/2007	Guinea/Liberia (West Africa) scientific researcher
09/2008 – 10/2008	Guinea (West Africa) consultant, amphibian survey
07/2010 – 08/2010	Guinea (West Africa) consultant, amphibian survey

LANGUAGE SKILLS

German	Native Language
English	Fluent in writing and orally
French	Basic competency

PUBLICATIONS

Brede C, Friedrich M, von Krosigk V, Jordán-Garrote AL, Riedel SS, Bäuerlein CA, Heinze K, Bopp T, Schulz S, Mottok A, Rosenwald A, Einsele H, Negrin RS, Harms GS, Beilhack A. (2012) Mapping immune processes in intact tissues at cellular resolution. The Journal of Clinical Investigation, 122 (12), 4439-4446.

Riedel, S.S., Mottok, A., **Brede, C.**, Bäuerlein, C. A., Jordán Garrote, A.-L., Ritz, M., Mattenheimer, K., Rosenwald, A., Einsele, H., Bogen, B. & A. Beilhack (2012). Non-Invasive Imaging Provides Spatiotemporal Information on Disease Progression and Response to Therapy in a Murine Model of Multiple Myeloma. PLoS ONE, e52398.

Chopra M., Riedel S.S., Biehl M., Krieger S., von Krosigk V., Bäuerlein C. A., **Brede C**., Jordan Garrote A.-L., Kraus S., Schäfer V., Ritz M., Mattenheimer K., Degla A., Mottok A., Einsele H., Wajant H. and Beilhack A. (2013) Tumor necrosis factor receptor 2-dependent homeostasis of regulatory T cells as a player in TNF-induced experimental metastasis. Carcinogenesis.

Bäuerlein C.A., Riedel S.S., Baker J., **Brede C.**, Jordán Garrote A.-L, Chopra M., Ritz M., Beilhack G.F, Schulz S., Zeiser R., Schlegel P.G., Einsele H., Negrin R.S. and Beilhack A. (2013) A diagnostic window for the treatment of acute GVHD prior to visible clinical symptoms in a murine model. BMC Medicine. In press.

Rödel, M.-O., A. Hillers, A.D. Leaché, N.G. Kouamé, C. Ofori-Boateng, N.E. Assemian, B. Tohé, J. Penner, M.F. Barej, M. Hirschfeld, J.Doumbia, L.N. Gonwouo, J. Nopper, **C. Brede**, R. Diaz, M.K. Jujita, M. Gil, B.H. Seniagbeto, R. Ernst & L. Sandberger (2012) The genus Astylosternus in the Upper Guinea rainforests, West Africa, with the description of a new species (Amphibia: Anura: Arthroleptidae). Zootaxa 3245:1-29.

Böhme, W., Rödel, M.-O., **C. Brede** & P. Wagner (2011): The reptiles (Testudines, Squamata, Crocodylia) of the forested southeast of the Republic of Guinea (Guinée forestière), with a country-wide checklist. Bonn zoological Bulletin 60(1): 35-61.

Rödel, M.-O., M. Hirschfeld & **C. Brede** (2010): Le Phrynomantis vit avec les fourmis et les scorpions / Phrynomantis lives with ants and scorpiones. Pp: 223-225, in: Konaté, S. & D. Kampmann (2010, eds.): Atlas de la biodiversité de l'Afrique de l'Ouest, / Biodiversity atlas of West Africa, Tome / Volume III: Côte d'Ivoire. Abidjan & Frankfurt/M.

Sandberger, L., A. Hillers, J. Doumbia, N.-S. Loua, **C. Brede** & M.-O. Rödel (2010): Rediscovery of the Liberian Nimba toad, Nimbaphrynoides liberiensis (Xavier, 1978) (Amphibia: Anura: Bufonidae), and reassessment of its taxonomic status. Zootaxa.

Rödel, M.-O., **C. Brede**, P. Schiefenhövel, J. Penner, B. Sinsin & S.G.A. Nago (2007): The amphibians of the Lokoli Forest, a permanently inundated rainforest in the Dahomey Gap, Benin. Salamandra, 43: 231-238.

SCIENTIFIC CONFERENCES

5- 8 December 2009	51st ASH annual Meeting, New Orleans, USA
	Talk: Three-dimensional visualization of immunological processes of entire organs in subcellular resolution; Travel Award Winner
21 – 24 March 2010	36th Annual Meeting of the EBMT (contributions to O130, P487, P493)
2- 5 October 2010	DGHO Anual Meeting, Berlin, Germany
	Talk: Visualization of dynamic shifts in mucosa associated initiation sites of acute graft-versus-host disease (GVHD)

SCHOLARSHIPS AND AWARDS

2005	Stipend by the Bavarian State Ministry of Science, Research and the Arts
2008	Stipend by the Interdisciplinary Centre for Clinical Research (IZKF), Würzburg University
2009	ASH Travel Award

Würzburg, May 2013

Christian Brede

Affidavit (Eidesstattliche Erklärung)

I hereby confirm that my thesis entitled "Peripheral alloantigen expression directs the organ specific T cell infiltration after hematopoietic cell transplantation" is the result of my own work. I did not receive any help or support from commercial consultants. All sources and / or materials applied are listed and specified in the thesis.

Furthermore, I confirm that this thesis has not yet been submitted as part of another examination process neither in identical nor in similar form.

Hiermit erkläre ich an Eides statt, die Dissertation „Die Expression von Alloantigenen in peripheren Geweben beeinflusst die selektive Organinfiltration durch T Zellen nach hämatopoetischer Stammzelltransplantation" eigenständig, d.h. insbesondere selbstständig und ohne Hilfe eines kommerziellen Promotionsberaters, angefertigt und keine anderen als die von mir angegebenen Quellen und Hilfsmittel verwendet zu haben.

Ich erkläre außerdem, dass die Dissertation weder in gleicher noch in ähnlicher Form bereits in einem anderen Prüfungsverfahren vorgelegen hat.

Würzburg, May 2013

Christian Brede